Nano-Micro Letters

ISSN 2311-6706
e-ISSN 2150-5551
CN 31-2103/TB

REVIEW

https://doi.org/10.1007/s40820-021-00674-8

Cite as
Nano-Micro Lett.
(2021) 13:154

Received: 17 April 2021
Accepted: 31 May 2021

A Review on Metal- and Metal Oxide-Based Nanozymes: Properties, Mechanisms, and Applications

Qianwen Liu[1,2], Amin Zhang[1,2] ✉, Ruhao Wang[1,2], Qian Zhang[1,2], Daxiang Cui[1,2] ✉

HIGHLIGHTS

- The characteristics of metal- and metal oxide-based nanozymes with diverse construction are dissertated.
- The intrinsic properties and catalytic mechanism of metal- and metal oxide-based nanozymes are discussed.
- The recent applications of metal- and metal oxide-based nanozymes in biological analysis, relieving inflammation, antibacterial, and cancer therapy are reviewed.

ABSTRACT Since the ferromagnetic (Fe_3O_4) nanoparticles were firstly reported to exert enzyme-like activity in 2007, extensive research progress in nanozymes has been made with deep investigation of diverse nanozymes and rapid development of related nanotechnologies. As promising alternatives for natural enzymes, nanozymes have broadened the way toward clinical medicine, food safety, environmental monitoring, and chemical production. The past decade has witnessed the rapid development of metal- and metal oxide-based nanozymes owing to their remarkable physicochemical properties in parallel with low cost, high stability, and easy storage. It is widely known that the deep study of catalytic activities and mechanism sheds significant influence on the applications of nanozymes. This review digs into the characteristics and intrinsic properties of metal- and metal oxide-based nanozymes, especially emphasizing their catalytic mechanism and recent applications in biological analysis, relieving inflammation, antibacterial, and cancer therapy. We also conclude the present challenges and provide insights into the future research of nanozymes constituted of metal and metal oxide nanomaterials.

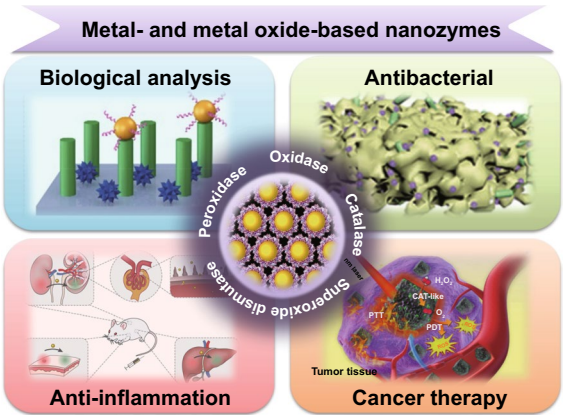

KEYWORDS Metal- and metal oxide-based nanozymes; Intrinsic properties; Catalytic mechanism; Applications

✉ Amin Zhang, zhangamin@sjtu.edu.cn; Daxiang Cui, dxcui@sjtu.edu.cn
[1] Institute of Nano Biomedicine and Engineering, Shanghai Engineering Research Center for Intelligent Diagnosis and Treatment Instrument, Department of Instrument Science and Engineering, School of Electronic Information and Electrical Engineering, Shanghai Jiao Tong University, 800 Dongchuan RD, Shanghai 200240, People's Republic of China
[2] Institute of Nano Biomedicine, National Engineering Research Center for Nanotechnology, 28 Jiangchuan Easternroad, Shanghai 200241, People's Republic of China

Published online: 09 July 2021

Abbreviations

AA	Ascorbic acid
ABTS	2,2'-Azino-bis(3-ethylbenzothiazoline-6-sulfonic acid)
3-AT	3-Amino-1,2,4-Triazole
ATP	Adenosine triphosphate
BSA	Bovine serum albumin
CAT	Catalase
CDT	Chemodynamic therapy
Ce6	Chlorine e6
CEA	Carcinoembryonic antigen
CO	Carbon monoxide
CT	Computed tomography
CTP	Cytidine triphosphate
L-Cys	L-Cysteine
EPR	Enhanced permeation and retention
ESR	Electron spin resonance
ELISA	Enzyme-linked immunosorbent assay
GA	Gallic acid
GOx	Glucose oxidase
GPx	Glutathione peroxidase
GSH	Glutathione
GTP	Guanosine triphosphate
H_2O_2	Hydrogen peroxide
His	Histidine
$HO_2^{\cdot}$	Hydroperoxyl radicals
HRP	Horseradish peroxidase
IBD	Inflammatory bowel disease
LFIA	Lateral flow immunoassay
MEDT	Microwave enhancing dynamic-therapy
MNPs	Magnetic nanoparticles
MRI	Magnetic resonance imaging
NCs	Nanoclusters
Neu	Neutrophils
NPs	Nanoparticles
NRs	Nanorods
NSs	Nanosheets
NTP	Nucleoside triphosphate
NWs	Nanowires
$O_2^{\cdot -}$	Oxygen superoxide anion
O_2^1	Singlet oxygen
$^{\cdot}OH$	Hydroxyl radical
OOH^-	Perhydroxyl anion
OPD	*o*-Phenylenediamine
OXD	Oxidase
PA	Photoacoustic
PDT	Photodynamic therapy
PEGylated	Polyethylene glycol
POD	Peroxidase
pNPP	*p*-Nitrophenyl phosphate
PSs	Photosensitizers
PTA	Photothermal agent
PTT	Photothermal therapy
PVP	Polyvinylpyrrolidone
RNS	Reactive nitrogen species
ROS	Reactive oxygen species
RONS	Reactive oxygen or/and nitrogen species
SDT	Sonodynamic therapy
SERS	Raman scattering
SOD	Superoxide dismutase
SPR	Surface plasmon resonance
SuOx	Sulfite oxidase
TA	Tannic acid
TAM	Tumor-associated macrophage
TBI	Traumatic brain injury
TMB	3,3′,5,5′-Tetramethylbenzidine
TME	Tumor microenvironment
TNF-α	Tumor necrosis factor-α
US	Ultrasound
UTP	Uridine triphosphate
XPS	X-ray photoelectron spectroscopy

1 Introduction

Enzymes are environmentally friendly biomaterials with remarkable catalytic efficiency and substrate specificity produced by living cells [1, 2]. Most of the natural enzymes are proteins, while a small part are RNA. The past decades have witnessed the extensive progress of biological enzymes in biology, medicine, chemistry, and industrial science [3]. Nevertheless, the complicated preparation procedure, unstable catalytical activity and intrinsic environmental sensitivity have restricted the scalable utilization of natural enzymes [4, 5]. Therefore, the exploration of alternative artificial enzymes to overcome shortcomings of natural catalysts has become an issue of increasing concern.

The evolution of nanotechnology and biology provides a bridge toward novel artificial enzymes. After the pioneering work of Gao et al. [6] reporting ferromagnetic (Fe_3O_4) nanoparticles (NPs) with enzyme-mimicking property in 2007, a bunch of nanozymes have been demonstrated as natural catalysts mimics. For instance, Au@Co–Fe hybrid NPs [7], $CuCo_2S_4$ NPs [8], MnO_2 nanowires (NWs) [9], Pt nanoclusters (NCs) [10], Au@Pt nanorods (NRs) [11], and carboxyl-modified graphene oxide (GO–COOH) [12] have been reported as peroxidase (POD) mimics. Nanozymes with multi-enzyme-type activities (e.g., $Co(OH)_2$/FeOOH/WO_3 ternary nanoflowers [13], AuNPs [14, 15], Co_3O_4 NPs

https://doi.org/10.1007/s40820-021-00674-8

[16], AgPt NPs [17], N-doped sponge-like carbon spheres [18], Mn_3O_4 NPs [19]) have been exploited in diverse investigation. Up to date, more than 540 types of nanozymes have been synthesized by over 350 research laboratories from 30 countries [20]. Generally, existing nanozymes are affiliated with two categories, namely oxidoreductase family and hydrolase family. Carbon-based materials, metal, and transition metal compounds are the most common nanozyme composition materials [21]. Wu et al. reviewed the history of nanozyme and draw a brief timeline for the evolution of artificial enzymes and natural enzymes (Fig. 1) [22]. With extensive efforts devoted to the investigation of artificial enzymes and nanotechnology, creative breakthroughs have been made steadily on the catalytic mechanisms and intrinsic properties of nanozymes, as well as the application field. In the past two years, the investigation on single-atom nanozyme (SAN) has aroused numerous attention due to their outstanding activity and selectivity [23, 24]. In the research of Kim et al. [25], the Fe–N–rGO SAN showed the best catalytic efficiency for different substrates among various classical POD mimics and natural HRP. Niu et al. [26] reported that the Fe–N–C SAN not only possessed excellent enzymatic activities, but also exerted splendid stability and robustness within a broad temperature and pH range.

Since nanozymes are recognized as a class of functional nanomaterials, they possess both the unique nature of nanomaterials and enzyme-like activity [27]. The surfaces of metal and metal oxide nanomaterials are covered with a large amount of charge, which was responsible for their superb electron properties [28]. Consequently, metal- and metal oxide-based nanozymes stand out in the area of electrocatalysis, sensing and fuel cells [29, 30]. Furthermore, as promising alternatives for natural biocatalysts, they commonly retained better stability and robustness under extreme conditions than natural enzymes [5]. The prominent physicochemical properties (e.g., high surface energy, superior optical, and photothermal conversion properties), as well as simplicity in preparation and storage also broaden their applications [31]. Interestingly, the catalytic performance and physicochemical properties of metal and metal oxide nanomaterials could be easily regulated according to the practical demand [32, 33]. For instance, surface modification has been revealed as a promising strategy to increase the biocompatibility of these nanozymes [34–36]. The structure design associated with the catalytic efficiency is flexible through suitable control of synthetic conditions [37]. Given the above ascendency, the research fields of metal- and metal oxide-related nanozymes have gradually extended from environment to chemical industry, food, agriculture, biomedicine, medicine, and so forth [38–40]. Even though tremendous efforts were devoted, further promotion of this kind of nanozymes is still facing difficulties. For example, the enhancement of catalytic activity and selectivity, closely associated with the sensitivity and specificity of nanozyme-based biosensors, remains a challenge [25, 41]. In addition, the strengthened physiological stability and biological safety is vital for the spread application of nanozymes in clinical medicine [42]. Therefore, novel nanozymes and biotechnology are urgently needed to make up these defects.

Dozens of excellent reviews concerned with nanozymes have been published in recent years. Some of the reviews involved the research progress of nanozymes in a particular

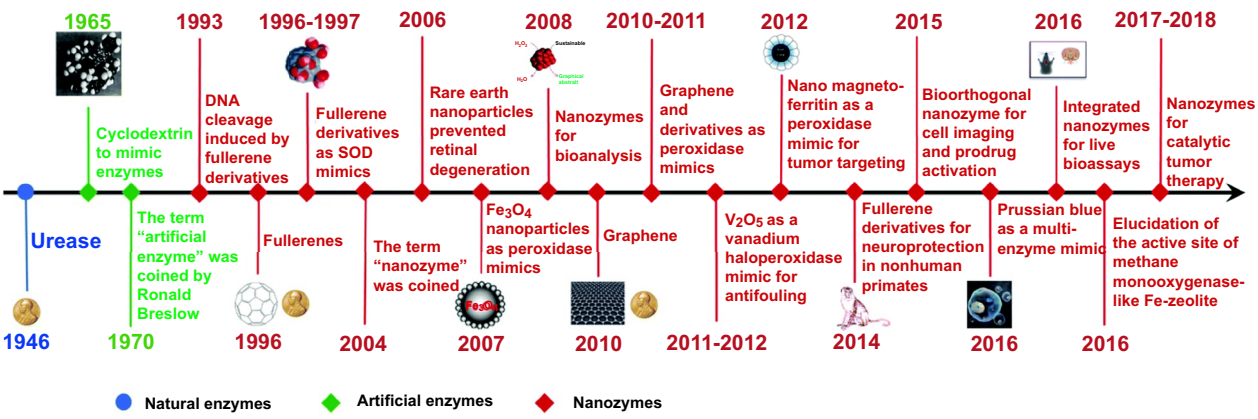

Fig. 1 A brief timeline for the evolution of artificial enzymes and natural enzymes. Reproduced from Ref. [22] with permission

field [5, 21, 27, 43, 44]. Some researchers organized and revealed the natural activities and working mechanisms of specific nanozymes [45–49]. In 2019, Huang et al. [50] systematically discussed the classification, intrinsic nature, enzymatic mechanisms and potential applications of nanozymes for the first time. However, a thorough overview for metal- and metal oxide-based nanozymes is still lacking. In this review, we firstly elucidate the characteristics and synthetic methods of metal- and metal oxide-based nanozymes. Then, we will dig into the catalytic mechanisms and property regulation of these nanozymes. After introducing their appliance in biological analysis, relieving inflammation, antibacterial and cancer therapy, we finally discuss the present challenges and give a future perspective for the research of nanozymes constituted of metal and metal oxide.

2 Preparing Diverse Nanozymes with Constructive Feature

Generally speaking, the existing metal- and metal oxide-based nanozymes can be roughly assorted into monometal [51], metal alloy [52–54], metal oxide [6, 55, 56], metallic core/shell nanostructure [57–59], and hybrid [60] nanomaterials in terms of constructive feature. Monometal nanozymes are usually noble metal nanomaterials possessing prominent chemical stability under natural conditions. They commonly possess facile conjugation sites to diverse biomolecule ligands and antibodies, remarkable surface plasmon resonance (SPR) properties, superior optical, and photothermal conversion properties [61–63]. However, bare monometal nanoparticles (e.g., Ag, Pt) tend to aggregate into nanoclusters, resulting in decreasing of catalytic activity [64]. What is worse, most bare noble metal nanozymes (except Au) have biological toxicity, thus limiting their application in clinical medicine. The structure, size, and morphology have been proved to influence the catalytic properties of these nanozymes [65–67]. Monometal nanozymes could be prepared through preformed-seed-mediated growth [68], high-temperature reduction method [2, 69–71], electrochemical synthesis, photochemical method, biosynthesis [72, 73], and spatially confined medium/template approach [74]. With different methods, various forms of noble metal nanomaterials (e.g., nanoparticles [14, 15], nanoclusters [10], nanorods [75], nanosheets [76], nanocubes) could be obtained. The preformed-seed-mediated growth is feasible for size control by changing the concentration and nature of seeds in the growth solution [77]. A variety of small molecules (e.g., tannic acid [71], citrate [78]) and macromolecular templates including DNA [79], dendrimers [80], and proteins (e.g., bovine serum albumin, human serum albumin, lactoferrin, pepsin, insulin) [2, 70] have been employed for monometal nanozymes synthesis via the high-temperature reduction procedure. The electrochemical strategy could modulate the size and morphology of noble metal nanomaterials through controlling electrodeposition parameters during the deposition process.

Metal alloy nanozymes, containing bimetal alloys and multimetallic alloys, could be obtained via common chemical synthesis such as the one-pot strategy [81], galvanic replacement reaction [82, 83], co-reduction method [84, 85], hydrothermal growth [86], and electrodeposition method [87, 88]. Besides, biological strategy [89] and bimetallic nanomaterials printing [90] have been present as favorable synthesis method as well. The biological strategy is widely known as a green synthesis method with biological elements as the reducing agents or growth template (e.g., leaf extract, plant extract, DNA) [91, 92]. Along with the preparation of diverse nanoalloys, researchers found that the composition as well as structure affected the enzymatic characteristic of metal alloy nanozymes [93, 94]. Therefore, adjusting the proportion of various metals, enlarging porosity and specific surface area of alloy nanomaterials have been recognized as effective approaches to regulate activity. Generally, the cost of metal alloy nanozymes is much lower than that of monometal nanomaterials as the incorporation of non-precious metals. Owing to the synergistic effect of the two components, bimetal nanoalloys tend to exhibit superiorly optical and chemical properties, as well as better catalytic performance compared with noble metal nanomaterials [95]. Furthermore, the introduction of magnetic metal (e.g., Co, Fe, and Ni) could endow alloys with magnetism besides optimizing their enzymatic properties [83, 84].

Possessing high surface energy and surface-to-volume ratio, metal oxide nanozymes have been considered as promising artificial enzymes for decades [96]. The most common metal oxide nanozymes like CeO_2, Fe_2O_3, Fe_3O_4, Co_3O_4, Mn_2O_3, and Mn_3O_4 nanomaterials have all been reported to possess multi-enzyme-like activities [97]. In addition, they exhibit plenty of unique properties such as magnetic, fluorescence quenching and dielectric properties [98]. Compared

 https://doi.org/10.1007/s40820-021-00674-8

with precious metal nanomaterials, metal oxide nanozymes commonly exert lower price and concise synthesis process [99]. Furthermore, the low biological toxicity and favorable accumulation in biological tissues have broadened their application toward biopharmaceutical [100]. Nevertheless, there are some disadvantages of unmodified metal oxide nanozymes in terms of biology. For instance, they might show awful stability and accelerate the generation of harmful free radicals under physiological conditions [101]. Additionally, the improper surface ligands coating would lead to the failure control of drug release [102]. In recent, diverse methods have been employed for metal oxide nanozymes preparation, including the hydrothermal [103, 104], solvothermal [105, 106], pulsed laser ablation [107], co-precipitation [108, 109], sol–gel [110], and thermal decomposition method [111].

The metallic core/shell (inorganic/inorganic) nanostructure-based nanozymes could be prepared through the hydrothermal reaction [112], solvothermal method [113], sol–gel approach [114], and atomic layer deposition [115]. By combining different materials and modifying structure, researchers could regulate the stability and functionality of core/shell structure-based nanozymes conveniently [116]. For example, the introduction of SiO_2 as coating significantly realized good stability and reduced bulk conductivity of the core particles [117]. The dispersion and biological safety of magnetite NPs encapsulated by silica could also be improved when existed in physiological environment [118]. In addition, the Au-coated nanostructure-based nanozymes have demonstrated to show enhanced chemical stability, biocompatibility, and optical properties [119, 120]. However, the accessibility between substrate and the active phase of nanozymes could be affected by coating materials [121]. Therefore, regulating coatings' thickness, porosity, and synthesis procedure was demanded to modulate enzyme-like capacity and other chemical properties of nanozymes.

The metal- and metal oxide-based hybrid nanozymes could be prepared with organic molecules or polymers modified on the surface of metal or metal oxide nanomaterials [122, 123]. The modifications on the surface of hybrid nanozymes are used to optimize the catalytic performance, instead of acting as stabilizer during the synthesis process [124]. Generally, the intrinsic properties of hybrid nanozymes might be ascribed to size, content, and components structure [125, 126]. For instance, polymer/metal nanozymes have been revealed to show stable catalytic capacity in which metal nanoparticles are evenly dispersed in polymer [127, 128]. In parallel with enhancing catalytic activity and selectivity, the incorporation of polymer or organic molecule endows hybrid nanozymes with amazing physical, chemical, and mechanical properties (e.g., adsorption [129], water solubility [130], biodegradability [131]), thereby expanding their application in miscellaneous fields [124].

The catalytic activities and efficiency of metal- and metal oxide-based nanozymes involved in the recent reports are listed in Table 1. These nanozymes mainly imitate four kinds of natural enzymes, namely POD, oxidase (OXD), catalase (CAT), and superoxide dismutase (SOD). The Michaelis–Menten constant (K_m) and maximal velocity (V_{max}) reflects the enzyme affinity with its substrate and maximal reaction velocity respectively [132]. And the K_{cat} is the maximum number of substrate molecules converted to product per enzyme molecule per second. The lower value of K_m and the higher value of V_{max} indicate the stronger catalytic activity of nanozymes.

3 Properties of Metal- and Metal Oxide-Based Nanozymes

3.1 Catalytic Mechanism

3.1.1 Catalase-Like Activity

CAT is a kind of binding enzyme with iron porphyrin as its prosthetic group [161]. CAT presents in the living tissues could catalyze hydrogen peroxide (H_2O_2) into oxygen and water, hence protecting tissues from excessive H_2O_2 [162]. Up to now, a series of metal-associated nanozymes, such as platinum (Pt) [51], gold (Au) [163], CeO_2 [164], Mn_3O_4 [19], have been demonstrated to show CAT-like activity. Although promising in anti-inflammatory, tumor treatment, biological detection and many other fields, considerable CAT mimics still constrained by the obscure mechanism [165, 166]. Li et al. [167] verified that the pre-adsorbed OH group on the surface of noble metal served as the active site for CAT-like catalytic reaction. Although most reported nanomaterial-based CAT mimics showed favorable catalysis ability in neutral and alkaline environment, Liu et al. [80] firstly reported that amine-terminated PAMAM dendrimer encapsulated gold nanoclusters (AuNCs-NH_2) displayed

Table 1 Intrinsic activity and catalytic efficiency of typical metal- and metal oxide-based nanozymes

Nanomaterial	Surface modification	Activity	Catalyst efficiency: k_{cat} (s^{-1}), substrate, K_m (mM), V_{max} (μM s^{-1})	References
Monometal				
Au NPs		GOx	18.52, glucose, 6.97, 0.63	[133]
Au NCs	Amine-terminated PAMAM dendrimer	POD,CAT,SOD	–, H_2O_2,16.0,0.452 (CAT)	[80]
Pt NPs	BSA	POD	–, TMB, 0.119, 0.21	[134]
			–, H_2O_2, 41.8, 0.167	
Pt NCs		POD	–, TMB, 0.096, 0.1414	[135]
			–, H_2O_2, 3.07, 0.1817	
Pd NPs	Carboxylated chitosan	POD	–, TMB,0.09, 0.177	[136]
			–, H_2O_2, 537.71, 0.112	
Ru NPs		HRP, OXD	–, TMB,0.234, 0.0825 (HRP)	[137]
			–, H_2O_2, 2.206, 0.583 (HRP)	
Cu NCs		POD	–, TMB, 0.648, 0.0596	[138]
			–, H_2O_2, 29.16, 0.0422	
Os NPs	Citrate	POD	1.72×10^3,TMB, 0.096, 0.412	[139]
			2.35×10^3, H_2O_2, 3.88, 0.565	
Ir NPs	Citrate	POD,CAT,OXD	5×10^2, TMB, 0.0906, 1.7 (POD)	[140]
			4.4×10^2, H_2O_2, 0.27, 1.5 (POD)	
			–, H_2O_2, 21.09, – (CAT)	
Rh NPs	Citrate	POD	3.87×10^2, TMB, 0.198, 0.0678	[141]
			1.38×10^3, H_2O_2, 0.38, 0.241	
Metal alloy				
Au_2Pt		CAT	–, H_2O_2, 7.7066, 0.9018	[142]
AgPt NPs	BSA	CAT,POD	0.751×10^3,OPD,0.129,89.71 (POD)	[17]
			1.075×10^3, H_2O_2,76.05, 128.49 (POD)	
			183.735×10^3, H_2O_2,54.30, 16.2 (CAT)	
Au–Pt NCs	Guanosine monophosphate (GMP)	OXD	–, TMB, 6.805, 2.538	[143]
			–, ABTS, 0.1321,0.1798	
Fe–Pt NPs		OXD	–, TMB, 0.030, 0.0142	[144]
Pd/Pt NWs		OXD	–, TMB, 0.058, 0.114	[33]
NiPd NPs		CAT,POD,OXD	–, TMB,0.11, 0.0152 (POD)	[83]
			–, H_2O_2, 0.66, 0.2618 (POD)	
Metal oxide				
MnO_2 NSs	HSA	OXD	–, TMB, 0.042,0.212	[145]
Mn_3O_4 NPs		OXD	–, TMB, 0.08, 0.4817	[146]
Fe_3O_4	histidine	POD	1.8256×10^5, TMB, 6.22, 0.157	[105]
			1.6965×10^5, H_2O_2, 10.58, 0.1459	
CeO_2 NPs		Phosphatase	–, pNPP, 0.74, 7.33×10^{-6}	[147]
CeO_2 NRs	SO_4^{2-}	OXD	16.55, TMB, 0.22, 0.48	[148]
Co_3O_4 NPs		CAT	1.63×10^4, H_2O_2, 34.3, 11.2	[103]
Co_3O_4 NPs		OXD	–, TMB, 0.051, 0.033	[104]
			–, ABTS, 0.037,0.032	
Co_3O_4 nanoflowers		POD,CAT, OXD,SOD	–, TMB, 0.2830, 0.1052 (POD)	[149]
			–, H_2O_2, 5.9322, 0.0985 (POD)	
			–, H_2O_2,839.85, 1466.66 (CAT)	
			–, TMB, 0.0469, 0.0459 (OXD)	

https://doi.org/10.1007/s40820-021-00674-8

Table 1 (continued)

Nanomaterial	Surface modification	Activity	Catalyst efficiency: k_{cat} (s^{-1}), substrate, K_m (mM), V_{max} (μM s^{-1})	References
NiO nanoflowers		SOD	2.6×10^{10}, $O_2^{\cdot-}$, 0.043,35	[106]
Core/shell nanostructure				
Au@Pt		POD	1.475×10^3,TMB, 0.00243, 0.04425	[150]
			2.004×10^3, H_2O_2, 0.00407, 0.06013	
Fe_3O_4@MoS_2		POD	–, TMB,0.25, 0.111	[151]
			–, H_2O_2, 1.39, 1.63	
Fe_3O_4@C NWs		POD	–, TMB,0.20, 0.0134	[152]
			–, H_2O_2, 0.23,0.0241	
Co@Fe_3O_4		POD	–, TMB,1.17, 0.379	[153]
			–, H_2O_2, 0.19,0.715	
Au/CeO_2 NPs		POD,CAT,SOD	–, TMB, 0.29, 0.039 (POD)	[154]
			–, H_2O_2, 44.69, 0.0223 (POD)	
Cu_2O@TiO_2 NWs		OXD	15.25, glucose, –, 0.915	[155]
Pd cube@CeO_2 NPs		OXD	–, TMB, 0.21, –	[156]
Hybrid nanozymes				
PVP/IrPt NPs		CAT,POD,OXD	–, TMB, 0.16, 2.25 (POD)	[157]
			–, H_2O_2, 0.75, 2.66 (POD)	
Fe_3O_4/CoFe-LDH		POD	–, TMB, 0.395, –	[158]
			–, H_2O_2, 10.24, –	
Co_3O_4@β-cyclodextrin NPs		POD	–, TMB, 0.17, 0.0281	[36]
			–, H_2O_2, 1.42, 0.0285	
HS-Pt NPs		OXD	–, TMB, 0.01012, –	[159]
His@AuNCs/RGO		OXD	–, TMB, 0.031, 0.0655	[160]

BSA bovine serum albumin, *PVP* polyvinylpyrrolidone, *PNPP* *p*-nitrophenyl phosphate, *LDH* layered double hydroxides, *HS* heparin sodium, *RGO* reduced graphene oxide, *His* histidine, *GOx* glucose oxidase, *HRP* horseradish peroxidase, *OPD* o-phenylenediamine, *NSs* nanosheets, *HSA* human serum albumin

CAT-mimicking property not only in acidic environment but also over physiological pH range (i.e., pH 4.8–7.4). They speculated that the protonation of tertiary amines from dendrimers in acidic solution could stimulate pre-adsorbing OH, thus providing active sites for H_2O_2 decomposition to generate oxygen and water.

In terms of metal oxide nanozymes, Celardo et al. put forward a possible catalytic model of CeO_2 NPs with CAT-mimicking properties in 2011 [168]. In the system, H_2O_2 was firstly bind to the $2Ce^{4+}$ binding site presented by the oxygen vacancy site of CeO_2 NPs (Fig. 2a①, ②). Then, the fully reduced oxygen vacancy site was formed as the protons released and two electrons transferred to the two Ce^{4+} (Fig. 2a③). The oxygen was generated from the reduced oxygen vacancy site (Fig. 2a④). Afterwards, another H_2O_2 molecule was bind to the $2Ce^{3+}$ site (Fig. 2a⑤). The homolysis of O–O bond happened with the transfer of two electrons and a uptake of two protons (Fig. 2a⑥). After H_2O molecules released, the initial Ce^{4+} sites were regenerated on nanoceria surface. Interestingly, Mu et al. reported that a larger concentration of the perhydroxyl anion (OOH^-) contained in H_2O_2 molecule were existed in the neutral and alkaline solution [103]. The OOH^- then might interact with metal centres of Co_3O_4 and form the $^{\cdot}O_2H$ due to its prominent nucleophilic ability compared with H_2O_2. With terephthalic acid as the fluorescent probe, it could be found that the production efficiency of the hydroxyl radical ($^{\cdot}OH$) depended on the Co_3O_4 concentration, indicating that the CAT-type property of Co_3O_4 NPs would influence the decomposition of H_2O_2 to $^{\cdot}OH$. Moreover, thermodynamic and kinetic analysis revealed that there might be more "active sites" on the surface of Co_3O_4 NPs than natural CAT owing to the stronger affinity between H_2O_2 and Co_3O_4 compared with natural CAT.

The existing hypothetical mechanisms for the CAT-like property of CeO_2 NPs and Co_3O_4 NPs mentioned above still

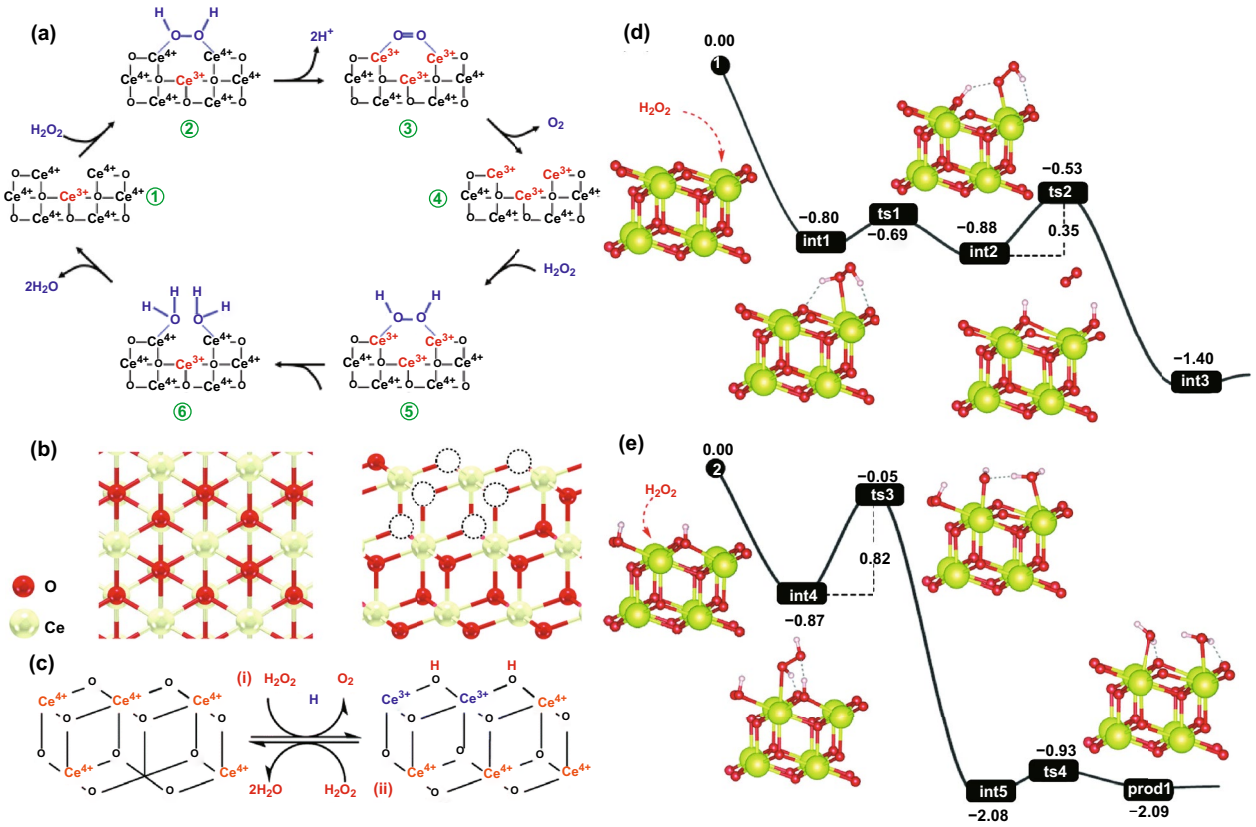

Fig. 2 **a** Electron transfer mechanism for the CAT-mimetic activity of CeO_2 NPs. **b** Top view (left) and side view (right) of the CeO_2 (111) structural model. **c** Atomistic-level catalytic mechanisms for the CAT-mimicking reactions of nanoceria. **d**, **e** Energy profiles for steps (1) and (2) for CeO_2 (111). Adapted from **a** Ref. [168], **b**–**e** [171] with permission

show certain limitations due to the neglect of the real structural features discussion [169]. Therefore, Guo et al. [170] investigated the possible catalytic mechanism of CAT-type activity at atomic or molecular level, involving the base-like dissociative, acid-like dissociative, and bi-hydrogen peroxide associative mechanisms. Based on the calculation of thermochemical energies and associated activation barriers, they reported that the bi-hydrogen peroxide associative mechanism was most viable for the CAT-mimicking catalytic recycle for Co_3O_4. Wang et al. deeply investigated the structural and electronic properties of nanoceria to propose the atomistic-level mechanisms (Fig. 2b, c) [171]. In their model, the CeO_2 (111) surface oxidized H_2O_2 molecule to form O_2 and a reduced H_2-CeO_2(111) surface. Then, anotehr H_2O_2 molecule would react with the H_2-CeO_2(111) surface to produce H_2O. As shown in Fig. 2d, the reaction between H_2O_2 and CeO_2 (111) surface was exoenergetic (energy difference $\Delta E = -1.40$ eV) with a small energy barrier (E_a) of 0.35 eV. Since $\Delta E = -2.09$ eV and $E_a = 0.82$ eV, the interaction between H_2-CeO_2(111) surface and H_2O_2 was also exoenergetic and kinetically favorable as well (Fig. 2e).

3.1.2 *Peroxidase-Like Activity*

Peroxidase, produced by microorganisms or plants, is closely related to the growth of animals and plants [172, 173]. The peroxidase family is very huge, and most peroxidases are heme enzymes with ferric protoporphyrin IX (protoheme) as the prosthetic group (e.g., horseradish peroxidase, lignin peroxidases, myeloperoxidase) [174–177]. Following the blooming exploration on enzymes, peroxidases with selenium (glutathione peroxidase, GPx), manganese (manganese peroxidase), and vanadium (bromoperoxidase) as active centers have been widely reported [178–180]. Peroxidase catalytically oxidizes organic substrates in which H_2O_2 acted as an electron acceptor, thereby decomposing H_2O_2 and effectively eliminating the toxicity of phenols

 https://doi.org/10.1007/s40820-021-00674-8

and amines. In 2007, GAO et al. discovered that magnetite (Fe_3O_4) nanoparticles had a special property that similar to HRP [6]. Since then, a series of nanomaterials have been unraveled to serve as POD mimics, including metal materials [181], metal oxides [182], conducting polymers [183], metal organic frameworks [184], carbon nanomaterials [185], single-atom catalysts [186] and so on.

The catalytic mechanisms of various nanomaterial-based POD mimics could generally be concluded as Fenton or Fenton-like reaction or the electron transfer process [117]. Wang et al. [187] prepared Fe_3O_4 magnetic nanoparticles (Fe_3O_4 MNPs) via a reverse co-precipitation method under ultrasonic irradiation. The possible catalytic mechanism of Fe_3O_4 MNPs with POD-type activity was displayed in Fig. 3a. The bound Fe^{2+} and Fe^{3+} activated H_2O_2 molecules that adsorbed on the surface of Fe_3O_4 MNPs to produce $^{\cdot}OH$ and oxygen superoxide anion ($O_2^{\cdot-}$)/hydroperoxyl radicals ($HO_2^{\cdot}$). Then, the $^{\cdot}OH$ and $O_2^{\cdot-}/HO_2^{\cdot}$ radicals would induce the subsequent degradation and mineralization of Rhodamine B (RhB). However, Maxim et al. [188] put forward different opinions about the generation of $^{\cdot}OH$ under conditions of the biologically relevant superoxide-driven Fenton reaction. Based on the spin-trapping electron paramagnetic resonance (EPR) experiments, they discovered that the reactions (Eqs. 1–3) at the nanoparticles' surface rather than the metal ions released by the nanoparticles were responsible for the POD-mimicking property of γ-Fe_2O_3 and Fe_3O_4 NPs (Fig. 3b). What is more, the production effect of the catalytic centers on the surface of γ-Fe_2O_3 was demonstrated to be at least 50-fold higher than that of the dissolved metal ions.

$$Fe^{3+} + O_2^{\cdot-} \rightarrow Fe^{2+} + O_2 \quad (1)$$

$$2O_2^{\cdot-} + 2H^+ \rightarrow H_2O_2 + O_2 \quad (2)$$

$$Fe^{2+} + H_2O_2 \rightarrow Fe^{3+} + OH^- + {}^{\cdot}OH \quad (3)$$

The nanocrystalline structure of nanozymes was also considered to make contribution to the H_2O_2-activating ability. André et al. reported that the intrinsic POD-like activity of V_2O_5 nanowires was attributed to surficial properties of the nanozymes instead of free orthovanadate anions [189]. They proposed a likely reaction mechanism based on analyzing the layered V_2O_5 orthorhombic structure (Fig. 3c). The (001) surface and the (110) surface were predominantly connected to the selective oxidation of hydrocarbons and total oxidation, respectively. The surface sites on the exposed (010) lattice planes of V_2O_5 NWs was assumed to be related to their enzyme-like property. The V atoms in the (010) plane and the electron lone pairs of the bridging oxygen atoms, respectively, acted as Lewis acid and base sites. Consequently, an intermediate peroxo species was produced after the reaction between V_2O_5 NWs and H_2O_2 (Fig. 3d). Afterward, the ABTS was bind to the vanadium peroxo species via a nucleophilic attack and then oxidized into ABTS^{*+} species. The regeneration of the V_2O_5 NWs required another ABTS molecule since H_2O_2 is a two-electron oxidant.

In recent years, the electron transfer-related mechanism was applied to a bunch of POD mimics such as IrO_2/rGO nanocomposites [123], FePt-Au hybrid NPs [190], Co_3O_4 NPs [191], and AuNPs@CDs nanocomposites [122]. Han et al. [9] obtained recyclable biotemplate-based MnO_2 nanowires with genetically engineered filamentous phages M13 as template. As illustrated in Fig. 3e, an electron transfer model was proposed for the reaction mechanism. With an electron transferred to MnO_2 NWs, the first substrate ABTS was oxidized. Then, another electron would transfer from MnO_2 to H_2O_2 and hence produced H_2O molecules. According to the chromogenic reaction and a series of control experiments, the enhanced POD-mimetic capacity of 1D M13-E4@MnO_2 nanozymes could be attributed to the surface effect, the small size effect and the homogeneous distribution of nanocrystals. When it comes to noble metal nanozymes, Cui et al. [71] speculated that Ir NPs could serve as the electron transfer mediators between H_2O_2 and 3,3′,5,5′-tetramethylbenzidine (TMB) (Fig. 3f). TMB adsorbed on the Ir surface provided lone-pair electrons from amino group to the Ir NPs, whose electron density was consequently increased. The electrons that transferred from the Ir NPs to peroxides would accelerate the oxidation of TMB and the reduction of H_2O_2.

3.1.3 Oxidase-Like Activity

Oxidases catalytically oxidize substrate (electron donor) and produce H_2O or H_2O_2 in the presence of oxygen, which is served as the electron acceptor. The oxidase family is classified according to the acting group of donors, including amino groups, CH-OH group (GOx), Ph-OH group

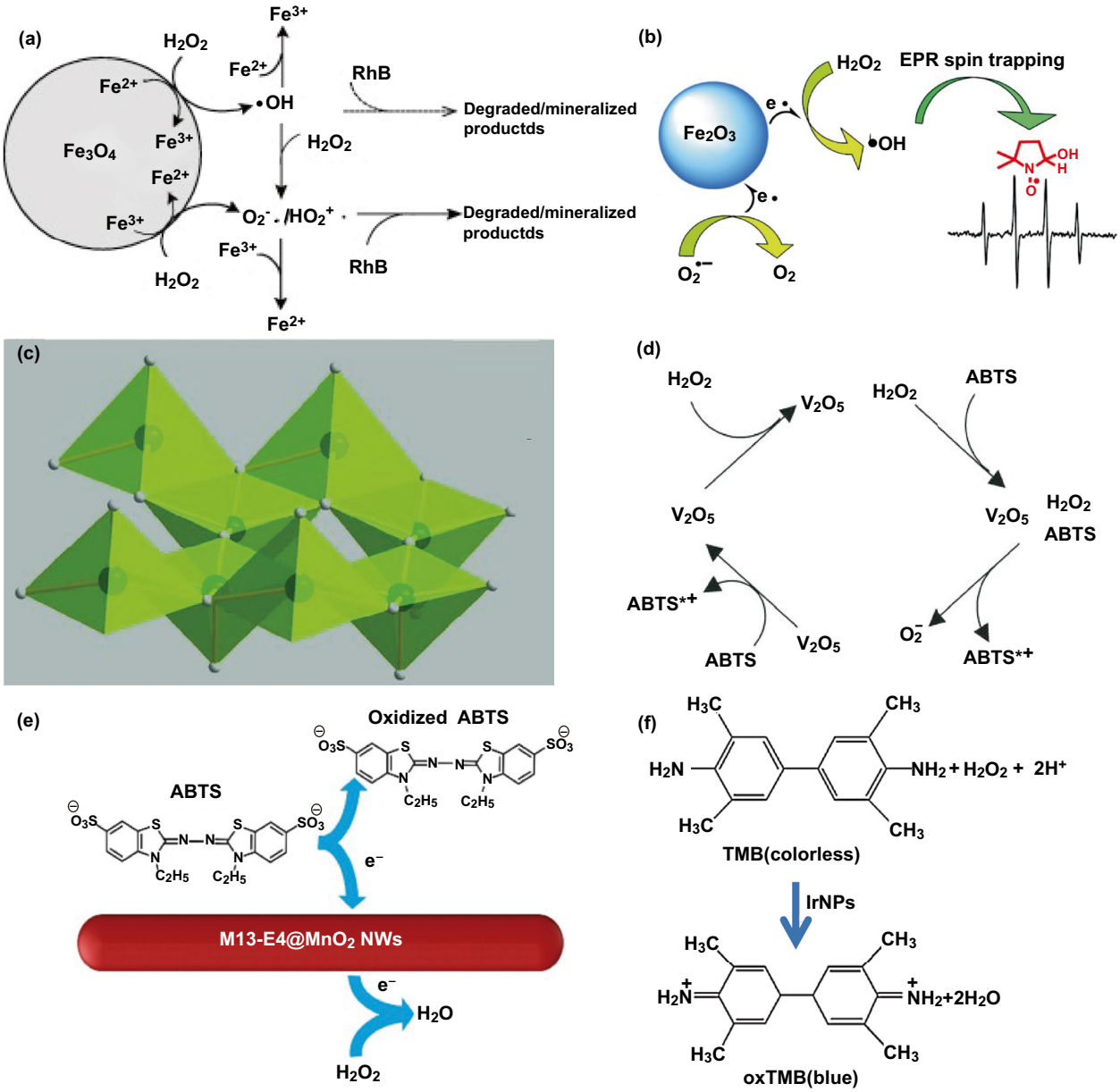

Fig. 3 **a** Mechanism for the POD-like activity of Fe_3O_4 MNPs in the degradation of organic pollutants. **b** Mechanism mediated by γ-Fe_2O_3 NPs. **c** View of Single layer from the V_2O_5 structure. **d** Possible mechanism for the catalytic reaction of the V_2O_5 NWs. **e** Catalytic mechanism of M13-E4@MnO_2 NWs with POD-type properties. **f** Corresponding reaction equation of TMB oxidized by H_2O_2 with the Ir NPs as POD mimics. *ABTS* (2,2'-azino-bis(3-ethylbenzothiazoline-6-sulfonic acid)). Adapted from **a** Ref. [187], **b** Ref. [188], **c**, **d** Ref. [189], **e** Ref. [9], **f** Ref. [71] with permission

(polyphenol oxidase), sulfur group (sulfite oxidase, SuOx), and ferrous ions (ferroxidase and cytochrome *c* oxidase) [192]. Among them, the OXD-mimetic nanozymes that acting on amino groups were widely investigated. Up to date, a large amount of metal-based and metal oxide-based oxidase mimics have been uncovered, such as CuO [193], $MnFe_2O_4$ [194], and Pt@MnO_2 [58]. The formation of intermediates (e.g., singlet oxygen, oxygen superoxide anion) and electron transfer process have been demonstrated to have important impacts on the OXD-type properties of these nanozymes [195]. The possible reaction mechanism of Mn_3O_4 NPs proposed by Zhang et al., which was illustrated in Fig. 4a

 https://doi.org/10.1007/s40820-021-00674-8

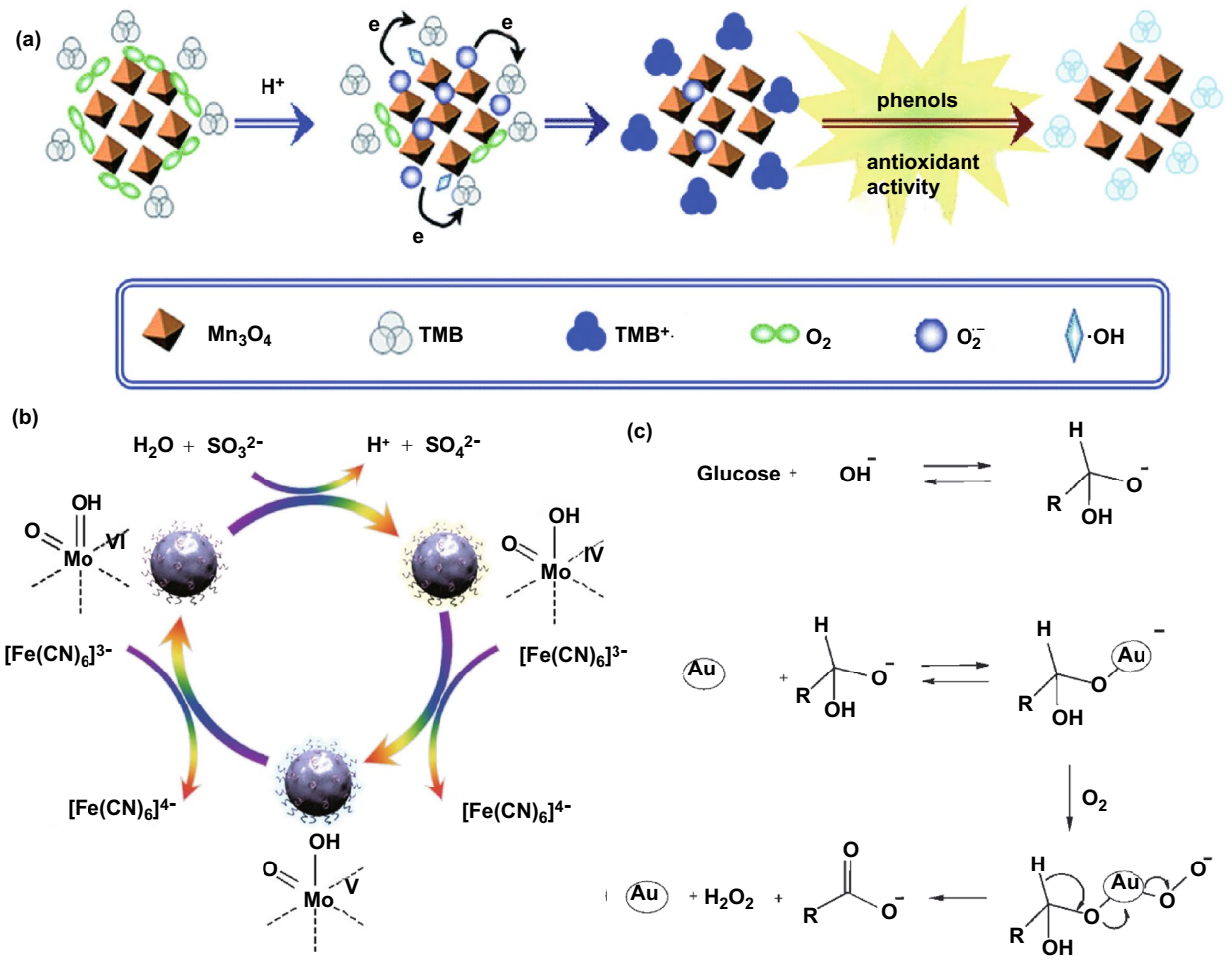

Fig. 4 **a** Reaction of the TMB oxidized by Mn_3O_4 NPs with OXD-like activity. **b** Possible reaction mechanism for the SuOx-type activity of P-MoO_{3-x} NPs in the presence of sulfite and $K_3[Fe(CN)_6]$. **c** Catalytic mechanism of Au NPs as GOx mimics. Adapted from **a** Ref. [196], **b** Ref. [198], **c** Ref. [199] with permission

[196]. The electrons that transferring from manganese to O_2 caused the formation of $O_2^{\cdot-}$, part of which was responsible for the generation of H_2O_2 and O_2 via non-enzymatic or SOD-catalyzed dismutation. Then, some of produced H_2O_2 would react with the dissolved Mn^{2+} and decomposed into $^{\cdot}OH$. Afterward, the intermediate $^{\cdot}OH/O_2^{\cdot-}$ and Mn^{3+} would oxidize the TMB, thus forming the TMB–Mn_3O_4 NP system. As a concerned nanomaterial, the CeO_2 has been demonstrated to exhibit multi-enzyme-mimicking activities. Cheng et al. probed into the O_2-dependent catalytic behavior of nanoceria and confirmed its OXD-type activity under the studied conditions [197]. In the reaction mechanism, the O_2 molecules were adsorbed onto defect sites of nanoceria and converted into $O_2^{\cdot-}$ under acidic conditions (Eq. 4). As the surface Ce^{4+} reduced to Ce^{3+}, the TMB was oxidized into TMB_{ox} (Eq. 6). As the main intermediate, the in situ produced $O_2^{\cdot-}$ finally regenerated Ce^{4+} via the oxidation of Ce^{3+}, accompanied by the generation of water (Eq. 7). Alternatively, the oxidation of TMB could be directly initiated by $O_2^{\cdot-}$ as well (Eq. 5).

$$O_2 + Ce^{3+}(CeO_2) \rightarrow O_2^{\cdot-} + Ce^{4+}(CeO_2) \quad (4)$$

$$O_2^{\cdot-} + TMB_{red} \rightarrow H_2O + TMB_{ox} \quad (5)$$

$$CeO_2 + TMB_{red} \rightarrow Ce_2O_3 + TMB_{ox} \quad (6)$$

$$Ce_2O_3 + O_2^{\cdot-} + 2H^+ \rightarrow CeO_2 + H_2O \quad (7)$$

Mechanism study on the nanozymes mimicking the other members of the oxidase family has made great progress as well. Following the exploration on the MoO_3 NPs as SuOx mimics [198], Chen et al. synthesized PEGylated (polyethylene glycol)-MoO_{3-x} nanoparticles (P-MoO_{3-x} NPs) that could catalytically oxidize sulfite. As shown in Fig. 4b, the sulfite was oxidized into sulfate with the two electron oxidative hydroxylation. Following the reduction of $[Fe(CN)_6]^{3-}$, one electron then transferred in succession to the Mo^{V} intermediate for the stabilization of the inactive Mo^{IV} state. In terms of nanozymes with GOx-like acticity, Comotti et al. put forward a two-electron mechanism to explain the intrinsic catalytic activity of the Au NPs (Fig. 4c) [199]. In their model, the hydrated glucose anions that formed in the presence of alkali were adsorbed on the surface of AuNPs. The gold surface atoms on the hydrated glucose then activated molecular oxygen and formed the dioxogold intermediate, which provided a bridge (Au^{+}–O_2^{-} or Au^{2+}–O_2^{2-} couples) for the electron transfer. After two electrons transferring from glucose to dioxygen, the gluconic acid and H_2O_2 were finally generated. Zhang et al. [200] prepared crown-jewel-structured Au/Pd nanoclusters with high reactivity. The anionic charge on the top Au atoms may directly contribute to the high GOx-like activity since a hydroperoxo-like species was formed during the electron transfer progress form the anionic top Au atoms to O_2. In addition, the PtCu NPs were reported to possess ferroxidase-like activity isolated from the impact of other ions based on the Fenton-like reaction [201]. Despite the obscure mechanism, the Pt NPs (as catechol oxidase mimics) [202], Au nanorod/ Pt nanodot structures (as ferroxidase mimics) [203], Cu_2O NPs (as cytochrome *c* oxidase mimics) [204] and many other metal- and metal oxide-based nanozymes have broaden the way toward the prosperity of OXD mimics.

3.1.4 Superoxide Dismutase-Like Activity

Superoxide dismutase is a kind of metalloenzyme that mainly distributed in microorganisms, plants and animals. Oxidative stress, involving the increasing concentration of reactive oxygen species (ROS), is considered to be an important factor in aging and disease [205]. ROS refers to the reduction products of oxygen in the body, including oxygen radicals (e.g., $O_2^{\cdot-}$, $^{\cdot}OH$, $HO_2^{\cdot}$) and certain nonradical oxidizing agents (e.g., ozone, H_2O_2, hypochlorous acid) [206]. SOD is selected as a favorable tool to anti-oxidation and anti-aging since it could transform superoxide anion radicals into H_2O_2 and O_2 [207]. Numerous nanomaterials have been proven as SOD mimics, such as Mn_3O_4 [208], Au[63], MnO_2 [209], and CeO_2 [210]. The coupled electron-transfers model was once accepted as a rational mechanism to explain the SOD mimetic property of CeO_2 NPs as shown in Fig. 5a [168]. Following the oxidative half-reaction (Fig. 5a①–④, same as that in Fig. 2a), a $O_2^{\cdot-}$ molecule would bind to the reduced oxygen vacancy site (Fig. 5a⑤). Then, H_2O_2 was released with the absorption of two protons and the transfer of electron from one Ce^{3+} (Fig. 5a⑥). The original nanoceria state would be regenerated by repeating this reaction with a second $O_2^{\cdot-}$ molecule (Fig. 5a⑦). However, this model was questioned since Cafun et al. demonstrated the absence of spin-unpaired Ce^{3+} sites in colloidal nanoceria via means of high-energy resolution hard X-ray spectroscopy [211]. Given profound consideration about the true structure and electronic characteristics of cerium oxide, Wang et al. proposed a polished catalytic cycle mechanism for nanoceria as SOD mimics [171]. The surface defect states were critical to the enzyme-like activity in this model. After the coadsorption of $HO_2^{\cdot}$ onto the surface of CeO_2, the intermediate was formed as shown in Fig. 5b. Then, the reaction between the intermediate and another $HO_2^{\cdot}$ radicals could release H_2O_2 and O_2, with the nanoceria restored to the initial state.

With the assistance of rigorous density functional theory and microkinetic modeling, Guo et al. investigated the Langmuir–Hinshelwood (LH) and Eley–Rideal (ER) mechanisms to describe the SOD-like activity of Co_3O_4 [170] and Fe_3O_4 [212] respectively. As illustrated in Fig. 5c, the ER mechanism is more viable for Co_3O_4 as the barriers involved through ER mechanism was lower than those along LH mechanism [170]. The $O_2^{\cdot-}$ molecule would capture a proton from water to form OH^{-} and $HO_2^{\cdot}$. The ER mechanism began with the chemisorption of $HO_2^{\cdot}$ on the surface of Co_3O_4 to generate the intermediate (INT1) and the adsorption energy was − 35.52 kcal mol^{-1}. Hereafter, INT1 would react with a second $HO_2^{\cdot}$ to release H_2O_2 and O_2, accompanied by the regeneration of Co_3O_4. The activation barrier of the elementary reaction passing through the transition state (TS1) was 19.02 kcal mol^{-1}. When it comes to Fe_3O_4, the LH mechanism is viable since the barrier along the LH mechanism is lower (Fig. 5d) [212]. Two $HO_2^{\cdot}$ molecules were absorbed on the surface of Fe_3O_4 to from the intermediate (INT2) with OOH* and HOO* species. Then, the O–H bond of OOH* species was split and the H atom

https://doi.org/10.1007/s40820-021-00674-8

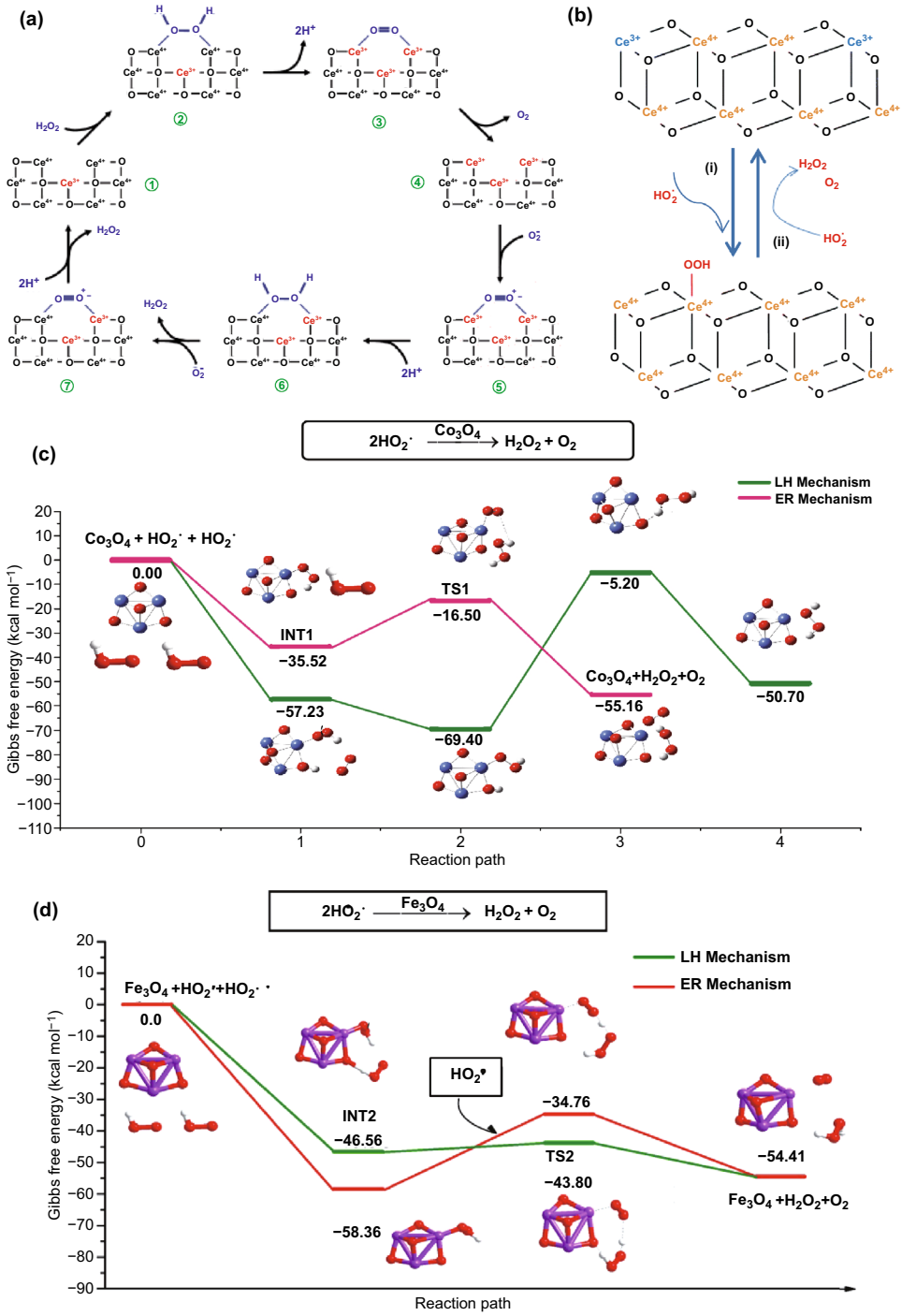

Fig. 5 **a** Electron transfer model for the oxidation of H_2O_2 by nanoceria as SOD mimics. **b** Reaction mechanism for the SOD mimetic activity of nanoceria. **c**, **d** Calculated reaction energy profiles for the SOD-mimic activity of Co_3O_4 and Fe_3O_4. Adapted from **a** Ref. [168], **b** Ref. [171], **c** Ref. [170], **d** [212] with permission

was combined with the nearby O atom of HOO* (TS2). The H_2O_2 and O_2 molecule were produced with the O_2 molecule binding to the Fe site. Finally, the H_2O_2 and O_2 molecule were released.

3.1.5 Others

Compared with oxidoreductive family, the reports about metal- and metal oxide-based nanomaterials with hydrolase mimetic activities are relatively rare. The peptide-functionalized monolayer protected gold clusters (Au MPCs) have been demonstrated as mimics of nuclease, esterase and silicatein [213–216]. The functional groups present on the protecting shells of Au MPCs were fundamental to their catalytic activities [217]. In addition, the CeNPs have been uncovered to show phosphatase-like property since they could cleave the phosphate ester bond of ATP, pNPP, and *o*-phospho-l-tyrosine [218–220]. The key to their catalytic phosphate ester bond cleavage lied on the availability of cerium(III) sites. Dhall et al. prepared CeNPs with phosphatase and CAT-mimetic activities via the wet chemical method [147]. The kinetic studies using pNPP as the substrate indicated that their phosphatase-type catalytic mechanism followed the saturation-based kinetics with V_{max} and K_m values of 0.44 nmol min^{-1} and 0.74 mM, respectively. In their study, the tungstate and molybdate tend to inhibit the phosphatase mimetic activity of CeNPs owing to the interaction of anions with the CeNPs surface.

3.2 Regulation of Catalytic Activity

3.2.1 Morphology

Previous studies have demonstrated that the morphology control would affect the catalytic activity of nanozymes to a large extent [146]. Exploration on the relevance between morphology and catalytic activity mainly involved surface area, pore size and volume. Tian et al. prepared VO_2 NPs in three kinds of morphologies (fibers, sheets and rods) as POD mimics [221]. The VO_2 nanofibers performed best in the H_2O_2 and glucose colorimetric assay due to their largest specific surface area. Singh et al. [222] compared Mn_3O_4 NPs in cube-, polyhedron-, hexagonal plates-, lakes- and flower-like morphology (Mnf). The larger size and higher surface area seemed to create higher catalytic activity of Mnf. Moreover, the multi-enzyme property of Mnf could be ascribed to the larger pore size, which would hold the substrates and cofactor for the catalytic reactions.

The effect of surface facets has gradually become a focus in morphology control as it determines surface energy or surface reactivity [223]. Huang et al. [55] found the OXD-type activity of CeO_2 nanorods with unique {110} planes was more ingenious than that of nanopolyhedra and nanocubes. In the research of Mu et al. [224], the catalytic activities of Co_3O_4 materials were in the order of nanoplates > nanorods > nanocubes. The difference in lowering energy barrier and electron transfer ability might be related to distinct POD-like properties of three kinds of Co_3O_4 nanozymes. Ge et al. [67] reported that the Pd octahedrons enclosed by {111} facet structure showed lower surface energy, which were more sensitive to CAT-type property and ROS-eliminating capacity than the Pd nanocubes enclosed by {100} facet structure. As shown in Fig. 6a, the reaction energy on Pd {111} and Pd {100} was 2.81 and 2.64 eV respectively, indicating the more possible homolytic dissociation of H_2O_2 molecule on the surface of Pd {111} facet. In contrast, Fang et al. found that OXD- and POD-type activities of Pd nanocubes {100} were higher than that of Pd octahedrons {111} [225]. The binding between O_2 and Pd {100} facet (an adsorption energy of − 1.40 eV) was much stronger than that between O_2 and Pd {111} facet due to the higher adsorption energy at Pd {100} facet (Fig. 6b). Also, the activation energy of surficial O_2 dissociation for {100} facets (0.31 eV) was lower than that for the {111} facets (0.67 eV). Thus, the energetically more favorable dissociative adsorption of the O_2 molecule on the Pd {100} facet explained its higher OXD-like activity. In terms of POD capacity, the homolytic dissociation reaction on the Pd {100} facet was more feasible than on the Pd {111} facet considering the reaction energy (Fig. 6c).

3.2.2 Size

Generally speaking, size sheds significant influence on the properties of diverse nanomaterials [226]. In most cases, the nanozymes with smaller size tend to be more active in catalytic reactions ascribed to the larger specific surface area. For example, Xi et al. [32] reported the size-dependent POD-type properties of Pd–Ir NPs within the size range from 3.3 to 13.0 nm. With an enzyme-linked immunosorbent assay (ELISA) as a model platform, they attributed the higher catalytic properties of the smaller nanoparticles to their diffusivities and reduced steric effect. Luo et al. considered that the amount of surficial Au atoms was the key point to control the catalytic reaction rate, thus explaining the

 https://doi.org/10.1007/s40820-021-00674-8

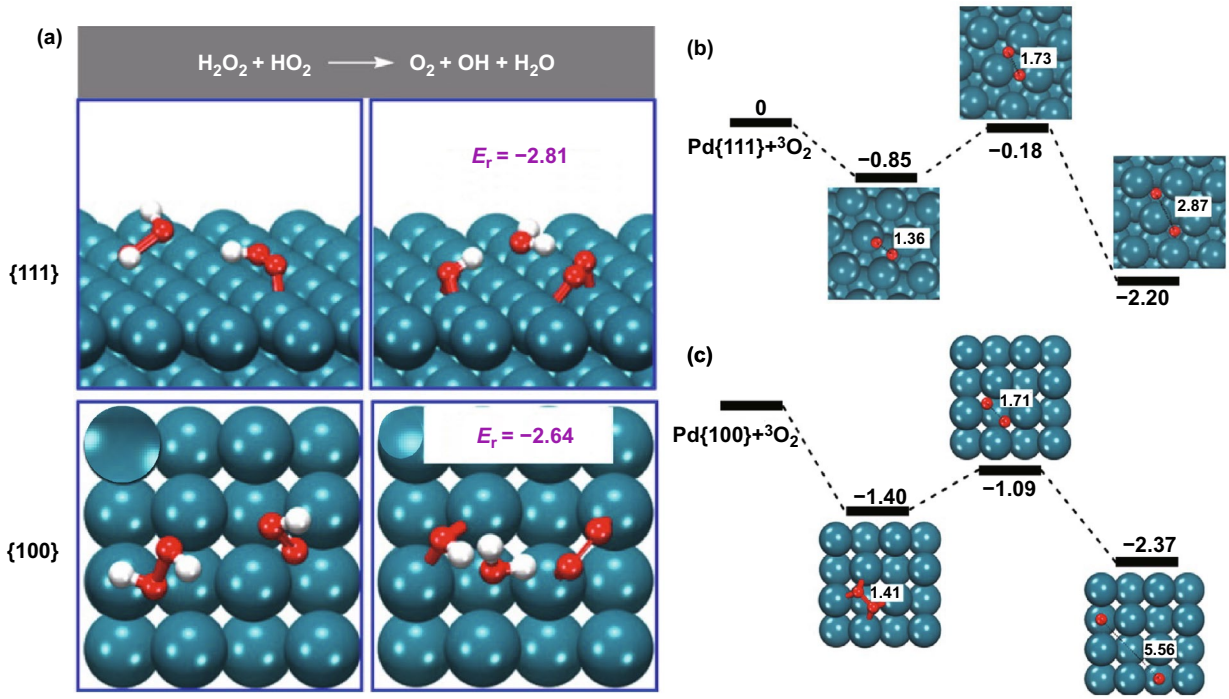

Fig. 6 **a** Lowest-energy adsorption structures and reaction energies (in eV) for the reactions on the Pd {111} and {100} facets. **b**, **c** Relative energies (eV) of O_2 dissociative adsorption and O–O atomic distances (Å) on the Pd {111} and {100} facets. Adapted from **a** Ref. [67], **b**, **c** Ref. [225] with permission

size-related GOx mimics activities of AuNPs [133]. They prepared CeO_2 NPs with SOD- and CAT-mimetic capacities in four kinds of sizes (4.5, 7.8, 23, and 28 nm) [227]. The decreased particle sizes could increase the Ce^{3+} fraction along with enhancing catalytic efficiency. Interestingly, Liu et al. [228] discovered that the catalytic activity of β-Casein–AuNPs (β-casein functionalized AuNPs) was increased in the order of 4.2, 2.8, and 8.7 nm. Obviously, the smallest β-Casein–AuNPs did not possess the best POD-like activity. They deduced that the coated protein might affect the proximity between substrates and the nanozyme core, which also determined the enzyme-like property.

3.2.3 Surface Valence State

The controls of the surface valence state and oxygen vacancies are considered as essential factors to modulate catalytic properties. Researches have demonstrated that the surface oxidation state of nanoceria played a considerable role in tuning the enzyme-like properties of CeO_2 due to the association between Ce^{3+} and oxygen vacancies. Pirmohamed et al. verified that the H_2O_2 decomposition rate of nanoceria increased with the decreasing of Ce^{3+}/Ce^{4+} redox state ratios [229]. In contrast, the reduced Ce^{3+}/Ce^{4+} ratio was responsible for the decay of SOD mimetic capacity [230]. Besides CeO_2 nanozymes, Wang et al. reported that the POD mimicking activity in Ni-based nanozymes was associated with the oxidation state of Ni [231]. In their study, the catalytic performance of porous $LaNiO_3$ perovskite was about 58- and 22-fold higher than that of NiO and Ni NPs, indicating the Ni oxidation state-dependent POD-like properties of Ni-based nanomaterials. Moreover, they proved the significance of Ni^{3+} in regulating catalytic activities via the comparison between $LaNiO_3$-H_2 and $LaNiO_3$ nanocubes, in which the ratios of Ni^{3+} were different. With tuning copper states from Cu^0 to Cu^{2+}, Xi et al. found that the multi-enzyme-like activities (POD, CAT and SOD) of copper/carbon nanozymes were closely related to the Cu state [232]. Fan et al. realized surface valence state control on Au-based nanozymes for the first time [233]. In their system, the catalytic efficiency for substrate oxidation (TMB and H_2O_2) decreased with the reduced ratio of Au(I) complex in Au Aerogels.

3.2.4 Composition

The composition control of nanozymes provides possibility to tune their catalytic activity [33]. Some studies demonstrated that the catalytic performance and Raman scattering (SERS) activities of AgAu, AgPd, and AgPt NPs are more obvious than that of Ag NPs [234–236]. Similarly, alloying with other metals (e.g., Pd, Au, Cu, and Co) has also been regarded as feasible solutions to catalytic ability regulation of Pt NPs [237]. In fact, adjusting the proportion of components and designing metallic core/shell structure-based nanomaterials are both feasible solutions modulate the enzyme-like properties [154, 238]. Liu et al. speculated that the Pt/Ru molar ratio would affect electronic variation and electronic charge transfer effects of PtRu nanoalloy, thereby tuning their POD- and OXD-like activity [239]. In their work, the enzyme-type property was enhanced in the order of $Pt_{40}Ru_{60}$, Pt, $Pt_{75}Ru_{25}$, and $Pt_{90}Ru_{10}$. He et al. reported that the change of Au/Pt molar ratio not only influenced structure of AuPt alloy NPs, but also improved the catalytic reaction rates when increasing Pt/Au ratio [85]. To investigate the metallic core/shell structure-based nanomaterials, Xia et al. adjusted the amount of Ir precursor to obtain Pd–Ir cubes with different Ir shells [240]. In this work, the Ir shells at certain thicknesses would effectively increase the surface reactivity of Pd and reduce the dissociation difficulty of H_2O_2 molecules. Moreover, the thickness of Ir shells could enhance or weaken the ligand effect stemming from the interaction of Ir monolayer with Pd substrate, in which the Pd(100) surface with single Ir layer was more active than that with three Ir layers during the oxidation process of TMB.

Owing to the synergetic effects between ceria and heteroatoms, doping CeO_2 with suitable foreign atoms is favorable to boost the catalytic activity [241]. By replacing Ce^{4+} ion in the CeO_2 lattice, the incorporation of heteroatoms tends to strengthen surface defects in the CeO_2 lattice via generating more oxygen vacancies for oxygen migration and diffusion [242, 243]. Among diverse heteroatoms, the introduction of one-dimensional nanowires achieved the best catalytic activity enhancement effect [244]. Zhang et al. synthetized CeO_2 nanozymes doped with different metal elements (such as Ag, Cr, Co, Rh, Pd, Mn, and Ni) and possessed multi-enzyme-like activities, herein the Cr/CeO_2 nanozymes owned best catalytic performance. The Cr^{3+} incorporation could improve surficial Ce^{3+}/Ce^{4+} ratio, thus reinforcing the catalytic capacity of CeO_2 NPs [245]. In addition to the types of doped atoms, the amounts are critical to regulate activity of nanozymes as well. Jampaiah et al. revealed that the catalytic efficiency toward TMB oxidation of 6% Fe^{3+}-doped CeO_2 NRs was the best among the CeO_2 NRs incorporated with 3, 6, 9, and 12% Fe respectively [246]. The Raman and X-ray photoelectron spectroscopy (XPS) results indicated the higher amount of surface defects including Ce^{3+} ions and oxygen vacancies in the 6% Fe^{3+}-doped CeO_2 nanozymes.

3.2.5 Surface Modification

Surface modification ranging from functional group, inorganic ions and small molecules to macromolecules has been revealed as a promising strategy to regulate the mimetic enzyme properties of metal- and metal oxide-based nanozymes by affecting their surface chemistry [247–249]. For instance, ligands such as glutathione (GSH), dendrimer, DNA, and protein tend to protect metal nanoclusters from aggregation, thence reinforcing the stability, biocompatibility and catalytic activity of nanozymes [250, 251]. Liu et al. reported that the catalytic efficiency of the DNA-capped iron oxide NPs as POD mimics was about tenfold higher than that of naked NPs [252]. The DNA coatings not only strengthened combining capacity with the amino groups of TMB via hydrogen bonding, but also provided the π–π stacking for nucleobase interacting with the benzene rings of TMB, which effectively enhanced the affinity of Fe_3O_4 NPs toward TMB. Huo et al. modified Co_3O_4 nanoplates with the amino group (NH_2-Co_3O_4), carboxyl group (COOH-Co_3O_4), hydroxyl group (OH-Co_3O_4), and sulfhydryl group (SH-Co_3O_4) in respective, and then systematically studied their catalytic activities [253]. Except hydroxyl group, the other functional groups all possessed positive effect to enhance POD-like activities, and among which the NH_2-Co_3O_4 nanoplates ranked the first. Huo et al. considered the functional groups' influence on the electron transfer ability of nanozymes was critical to modulating their catalytic properties. Yue et al. [254] prepared functionalized ceria nanorods catalysts M/CeO_2 (M = Fe^{3+}, Co^{2+}, Mn^{2+}, Ni^{2+}, Cu^{2+}, Zn^{2+}) via chelating metal ions onto ceria nanorods CeO_2 surface. These metal-chelated nanocerias have all possessed enhanced POD-mimicking property and Mn(II)/CeO_2 showed best catalytic performance. The researchers found that the synergistic effect of metal ions

 https://doi.org/10.1007/s40820-021-00674-8

and CeO_2, along with the carboxyl groups served as substrate binding sites, was critical to the promotional effect on the enzymatic activity. The addition of F^- into nanoceria obviously caused the generation of more oxygen vacancies, facilitating electron transfer between the Ce^{4+}/Ce^{3+} redox couple as well as the stimulating product desorption, thereby enhancing OXD-mimetic capacity of nanoceria by fluoride capping [255].

3.2.6 External Triggers

(1) pH and temperature

Up to date, the enzyme-like activities of numerous metal- and metal oxide-based nanozymes have been verified to be sensitive to pH and temperature [17, 256–258]. The POD-type property of Fe@PCN-224 NPs was optimal in pH 3.5 with the temperature of 45 °C [259]. And the activity could remain 80% and 90% of the highest activity at 25 and 37 °C, respectively. Although an increasing number of novel nanomaterials have shown high enzyme-like property within a wide temperature range, the catalytic activity of nanozymes would slightly decrease when the temperature was not at optimal [260]. Liu et al. [261] found that the ROS eliminating activity of Pt NPs was strengthened with the increment of environment pH by the assistance of electron spin resonance (ESR) spectroscopy and spin traps. It has been reported that Pt NPs [261], Ag NPs [262] functioned as POD mimics in acidic conditions while exhibited CAT-like activities in neutral and alkaline environment. What is more, Pt and Au NPs were demonstrated to show SOD mimetic capacity under neutral conditions [63, 261]. Li et al. [167] dug into the pH-switchable enzyme-like properties of Au, Ag, Pt, and Pd nanozymes. The adsorption of H^+ and OH^- ions on the metal surface was feasible under acidic and basic conditions, respectively. The base-like decompositions of H_2O_2 in low-pH conditions was fundamental to the POD-like activities of Au, Ag, Pt and Pd nanozymes while their CAT-type activity was related to the acid-like decompositions of H_2O_2 in high-pH conditions.

(2) Hydronium

The catalytic activity of nanozymes could also be affected by metal ions (e.g., Fe^{3+}, Hg^{2+}, Ni^{2+}, Cd^{2+}, and Al^{3+}) and anions (e.g., S^{2-}, F^-, Cl^-, Br^-, and I^-) [136, 263, 264]. For example, heavy metal ions might inhibit catalytic activities of metal- and metal oxide-based nanozymes, which could be ascribed to the metallophilic interaction between nanozymes and heavy metal ions, including the deposition of metal ions [265], the formation of alloy on the surface of nanomaterials [266], and the leaching of surface atoms [267]. The integration between heavy metal ions and the surface ligands also affected the catalytic performance of nanocomposites by deposing of ligands or decreasing affinity toward substrate [268, 269]. Han et al. conjectured that the promotional or block effects of Ca^{2+}, Fe^{3+}, Hg^{2+}, and Mn^{2+} toward the CAT-type property of Co_3O_4 NPs were related to their influence on the electron transfer rate in Co_3O_4 [270]. In the report of Liu et al., the S^{2-} at low ion concentration tended to inhibit the POD-mimetic catalytic reactions of β-casein stabilized Pt NPs (CM–PtNPs) toward TMB while switch on their enzyme-like activity toward ABTS [264]. Besides, the sulfide-mediated activity switching efficiency decreased with the increment of S^{2-} concentration. Fluorescence spectra and X-ray photoelectron spectroscopy (XPS) data revealed that the key of S^{2-}-mediated activity switching mechanism lied in the structure change of protein molecule and ratio change of Pt^{2+}/Pt^0 with the introduction of sulfide ions.

(2) Light

The photothermal effect and light-induced electron transfer have been demonstrated to be involved with the photo-enhanced enzyme-like activity of nanozymes [271–273]. With AuNPs and α-FeOOH microcrystals grown on porous carbons, Zhang et al. obtained Au/α-FeOOH–FPC catalysts with visible-light-driven enzymatic property [274]. Herein, the system temperature was raised to accelerate the process of glucose oxidation when the Au NPs converted the absorbed light energy into heat. And the generated gluconic acid could lower surrounding pH to stimulate the enzymatic reaction. Furthermore, hot electrons from plasmon-excited AuNPs promoted charge separation at the interface of Au/α-FeOOH, resulting in efficient cycling of Fe^{3+}/Fe^{2+} to produce Fenton reaction. The introduction of visible light has increased the POD-type activity of Fe_2O_3 NPs by at least 1.2 times in the research of Zhu et al. [275]. They found that the light-related catalytic property of Fe_2O_3 nanozymes was concerned with the bandgap and light absorption range, which were responsible for the barrier density generation and the light energy absorption. In addition, the influence on the

enzyme mimetic properties changed according to the type of light excitation. Wang et al. discovered that the catalytic activity of Au/Si/Azo (AuNPs encapsulated and dispersed by the azobenzene- modified expanded mesoporous silica) was activated under UV illumination while inhibited under visible light [276]. The control of the host–guest interaction between Azo and cyclodextrin (CD) via the isomerization between *trans* and *cis* conformations of Azo was significant to the activity regulation by UV or visible light.

(4) Others

Nucleoside triphosphates (NTPs) including adenosine triphosphate (ATP), guanosine triphosphate (GTP), cytidine triphosphate (CTP) and uridine triphosphate (UTP) have been considered as promoters for nanozymes owing to the coupling of their hydrolysis with oxidative reaction [220]. Vallabani et al. discovered that the employment of ATP could reinforce the affinity between Fe_3O_4 NPs and their substrate, thus maintaining the POD mimetic capacity of Fe_3O_4 nanozymes within a wide range of pH and temperature [277]. Interestingly, Cheng et al. [197] found that the introduction of ATP might restrain the enzymetic reaction of nanoceria in prolonged reactions despite its initial enhancing effect. They attributed the inhibition to Ce–PO_4 complexes formation in the presence of ATP, which could interact with nanoceria and shield active centers. Furthermore, Jia et al. [278] reported that the antioxidants possessed inhibitory effect on the POD-type property of Co_3O_4 NPs. The addition of gallic acid (GA), tannic acid (TA) and ascorbic acid (AA) would slow the catalytic reaction toward the TMB or OPD, among which the influence of TA was the highest because of its numerous phenolic groups.

4 Applications of Metal- and Metal Oxide-Based Nanozymes

4.1 Applications in Analytical Field

As mentioned above, metal- and metal oxide-based nanozymes normally come along with unique physicochemical properties including high surface-to-volume ratio, enzymatic activity and good biocompatibility. These capabilities endow them with promising applications in target substances detection following the extensive exploration of biosensing schemes [279]. The integration of nanozymes and conventional determination technologies containing colorimetric, electrochemical, and fluorescence has gradually become optimal candidate for biological analysis. The past decade has witnessed the inclusive utilization of novel nanozyme-based sensors in detecting proteins, glucose, heavy metal ions, pathogen microorganisms and many other substances.

4.1.1 Heavy Metal Ions

Previous studies have illustrated that excessive heavy metal ions are one of the culprits of environmental pollution [280]. Furthermore, heavy metal ions could invade human body through water and food, resulting in permanent chronic poisoning [281]. Therefore, detecting heavy metal ions is of great significance to protect ecology and human health. Nevertheless, most analytical platforms (e.g., atomic absorption spectrometry, energy-dispersive X-ray, and inductively coupled plasma mass spectrometry) for heavy metal ion analysis relied on expensive instruments and professional technicians [282]. Nanozymes provided a potential to simultaneously improve the performance of metal ion detection with low cost. For instance, Han et al. designed a portable paper chip based on AuNPs (AuNZ-PAD) to investigate Hg^{2+} in distilled and tap water samples, in which Au–Hg^{2+} integration could influence enzyme-like catalytic activity of AuNPs and caused paper discoloration (Fig. 7a) [226]. This ultrasensitive AuNZ-PAD further cooperated with mobile phone camera, effectively reducing the cost of assay and simplifying the operation.

Among the classical analytical assays basing nanozymes, colorimetric stood out for the operation convenience. Some references concluded that heavy metal ions might enhance or inhibit the POD-like property of nanozymes [283–285]. Hence, histidine(His)-Pd [268], $MMoO_4$ (M = Co, Ni) [286], DNA-Ag/Pt [287], MnO_2 [288] have been synthesized for Ag^+ [268], Cu^{2+} [286], Hg^{2+} [287, 288] monitoring by colorimetric assay. In addition, Pb^{2+} ions would accelerate the AuNPs leaching in presence of $S_2O_3^{2-}$ and lead to less oxidation of TMB, expanding the Pb^{2+} determination with the assistance of nanozymes [289, 290]. Xie et al. [291] fabricated a colorimetric probe by using metallic nanozyme to determine Pb^{2+}. The Au@Pt NPs served as POD mimics were introduced, which could detect Pb^{2+} ions in the lake water samples within a linear range from 20 to 800 nM.

 https://doi.org/10.1007/s40820-021-00674-8

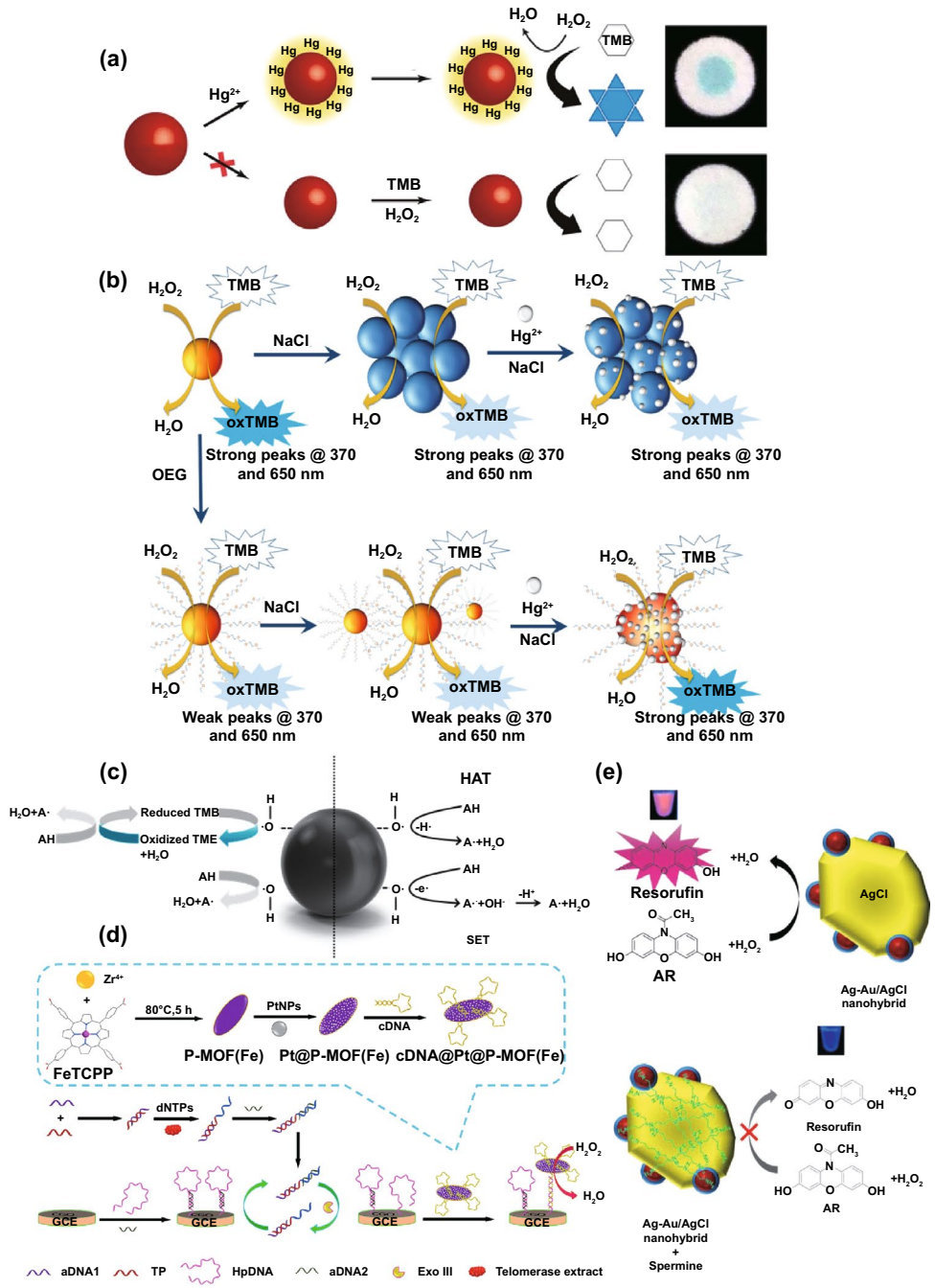

Fig. 7 **a** Detection progress of the Hg^{2+} in distilled and tap water samples with AuNZ-PAD based on the TMB–H_2O_2 catalytic reaction. **b** Principle of quantitative detection of Hg^{2+} ions in seawater (3.5% NaCl) using OEG-AuNPs compared with that using bare AuNPs. **c** Detection principle of TAC based on the reaction between antioxidants and H_2O_2 in the presence of Pt nanozymes as POD mimics. **d** Synthesis of cDNA@Pt@P-MOF(Fe) as the signal probe for the analysis of telomerase activity. **e** Preparation of Ag-Au/AgCl nanohybrid with OXD-like and POD-like activity and the working mechanism of Spm detection. *GCE* Glassy carbon electrode, *TP* telomerase primer. Adapted from **a** Ref. [226], **b** Ref. [293]. **c** Ref. [301], **d** Ref. [302], **e** Ref. [303] with permission

As high electrolyte has an adverse effect on the catalytic performance and stability of nanozymes, analyzing heavy metal ions in seawater is much more difficult than other liquid samples such as lake water and drinking water [292]. Logan et al. quantitatively determined mercury ions in complicated water matrices using OEG-Au complex by

functionalizing AuNPs with oligo-ethylene glycol (OEG) [293]. In this proposal, OEG-AuNPs exhibited enhanced stability and weakened catalytic properties in a wide pH range under high NaCl concentration, which effectively ameliorated the poor stability of bare-AuNPs (Fig. 7b). The Hg^{2+} detection limit of coastal seawater by this platform was 13 ppb in only 45 min.

4.1.2 Biomarkers

Biomarkers refer to biochemical indicators that mark the structure or functional changes of biosystems including organ, tissue and cell. The exploration of biomarkers is beneficial to clinical diagnosis, drug analysis and ecosystem protection. Enormous effort has been made in nanozyme-based biomarker detecting, including biological macromolecules (e.g., acid phosphatase (ACP) for prostate cancer [149]; human epidermal growth factor receptor-2 (HER2) for breast cancer [294, 295]; carcinoembryonic antigen (CEA) for rectal cancer [296, 297] and benzo[*a*] pyrene-7,8-diol 9,10-epoxide–DNA (BPDE–DNA) for woodsmoke exposure [298]) and small molecule biomarkers (e.g., sarcosine for prostate cancer [299] and uric acid [300]). Pedone et al. [301] developed a colorimetric approach to determine the total antioxidant capacity (TAC) in saliva on basis of the reaction between antioxidants and H_2O_2 in the presence of Pt nanozymes, which was acted as POD mimics. TAC acted as an important biological indicator closely associated with oxidative stress. It reflected the total effects of enzymes and non-enzymatic analytes in the body. The combination of Pt nanozymes and ·OH radical substrates allowed the detection scheme sensitive to both single electron transfer (SET) and hydrogen atom transfer (HAT) reactions (Fig. 7c).

The improvement in signal transduction rate is a breakthrough to raise the sensitivity of biomarker detection [298]. Thence, metal- and metal oxide-based nanozymes functioned as signal amplification has boosted biomarkers analysis in sundry assays involving electrochemical, fluorescent and so on [300]. Ling et al. obtained Pt@ P-MOF (Fe) nanozymes by growing ultra-small Pt nanoparticles on metalloporphyrin metal organic frameworks [302]. The novel artificial nanozymes were employed as signal probe, allosteric switch of DNA and Exo III recycling amplification in their electrochemical template for telomerase detection (Fig. 7d). The catalytic property of Pt NPs on P-MOF (Fe) could decompose H_2O_2, and hence strengthened the electrochemical signal. Kuo et al. [303] synthesized Ag-Au/AgCl nanohybrid with OXD- and POD-type capacities for spermine (Spm) analysis in urine, which could act as the diagnostic indicators for liver cancer and stroke. As is shown in Fig. 7e, Spm inhibited fluorescent molecules generation of H_2O_2-Amplex Red (AR) system when in the presence of Ag-Au/AgCl, thereby realizing highly selective and ingenious determination of Spm.

4.1.3 Pathogen Microorganisms

The analysis of pathogenic microorganisms, ranging from viruses, bacteria, parasites to prions, is crucial to prevention and control of infectious diseases [304]. The nanozymes have become powerful competitors for natural enzymes in field of pathogen detection due to their low-cost (especially for foodborne bacteria), timesaving operation and sensitivity [305–307]. For instance, Cheng et al. employed Pd@Pt NPs as a signal amplifier in the lateral flow immunoassay (LFIA) assays for *Salmonella Enteritidis* (*S. enteritidis*) and *Escherichia coli* (*E. coli*) *O157:H7* [57]. The integration of Pd@Pt NPs and smartphone-based device offered a portable platform for fast detection of foodborne pathogens. The studies involving nanozyme-based pathogen analysis in the past 5 years are listed in Table 2. All the metal- and metal oxide nanozymes mentioned in this table were functioned as POD mimics.

In contrast to POD mimics, other enzyme-like activities of nanozymes are waiting for further development in biological sensing. Yao et al. [308] designed a colorimetric immunoassay scheme to investigate *Staphylococcus aureus* (*S. aureus*) with the assistance of magnetic carbon dots (Mag-CDs) and AgNCs. AgNCs with OXD-mimicking properties could accelerate oxidatiing *o*-phenylenediamine (OPD) to produce yellow products. And the Mag-CDs were introduced to capture bacteria in their system. Bu et al. [309] built a point-of-care (POC) platform to analyze *Salmonella sp.* and *E. coli O157:H7* by using MnO_2 nanoflowers with CAT-type activity. Besides, MnO_2 possessed bacteria recognition ability via the binding between Con A and O-antigen on the bacterial surface.

 https://doi.org/10.1007/s40820-021-00674-8

Table 2 Nanozyme and analysis method for pathogen microorganism detection reported in recent years

Pathogenic microorganisms		Nanozyme	Method	References
RNA virus	Avian influenza A (H5N1)	Au	Colorimetric immunoassay	[310]
	Influenza virus A (H1N1)	Au	Magnetic nanozyme-linked immunosorbent assay (MagLISA)	[311]
	Murine Norovirus (MNV)	Au	Colorimetric immunoassay	[62]
	Mumps virus	Au@Pt@mesoporous SiO_2	Enzyme-linked immunosorbent assay (ELISA)	[64]
	Measles virus	Au@Pt	ELSA	[312]
DNA virus	Rubella virus	Au@ Pt	ELISA	[313]
Gram-positive bacteria	*Enterobacter sakazakii* (*ES*)	Fe_3O_4	Nanozyme strip	[314]
	Listeria monocytogenes (L. monocytogenes)	Fe_3O_4	Colorimetric	[315]
	Bacillus subtilis (DH ∞*)*	Dop- Fe_3O_4	Colorimetric	[316]
	Streptococcus mutans	Fe_3O_4/Sm_n(n = 1,2,3)	Colorimetric	[317]
	S. aureus	Fe_3O_4@SiO_2-Pt	ELISA	[318]
		Co_3O_4	Magnetophoretic chromatography	[319]
		Cu-MOF	Colorimetric immunoassay	[320]
Gram-negative bacteria	*Pseudomonas aeruginosa (P. aeruginosa)*	Au	Colorimetric and electrochemical detection	[69]
	E. coli O157:H7	Au	Immunochromatographic Assay(ICA)	[321]
		Pd–Pt	Lateral flow assay (LFA)	[322]
		Pt-Au	ICA	[323]
		Pd@Pt	LFIA	[57]
	S. enteritidis	Pd@Pt	LFIA	[57]
		Fe-MOF	Colorimetric immunoassay	[324]
	Escherichia coli (XL1)	Dop- Fe_3O_4	Colorimetric	[316]

4.1.4 Antibiotic

The dose control of antibiotics, which sheds significant influence on antibacterial and anti-cancer treatment, has been a hot topic in the medical field. It has been demonstrated that overdose causes serious side effects, while insufficient antibiotics are unconducive for clinical therapy [61, 325]. While, the pioneering works of antibiotic determination, including liquid chromatography-mass spectrometry (LC–MS) [326], electrochemical [327], high performance liquid chromatography (HPLC) [328], etc. suffer from time consuming, high cost, complicated operations and poor sensitivity. The prosper of Au nanozymes with intrinsic POD-like activity provided possibility to tune the functionalization of existing methods in analyzing multiple antibiotics (e.g., doxycycline [325], kanamycin [61], tetracycline [329]). Kong et al. [330] designed a novel photoelectrochemistry (PEC) biosensor for bleomycin (BLM) detection, which was natural antibiotics for Hodgkin's disease, cervical cancer therapy. The biosensor reached a detection limit to 0.18 nM in which Ag/ZnMOF nanozymes acted as a signal amplifier and Au NPs/tungsten sulfide nanorod array (Au/WS_2) photoelectrode used as a PEC matrix (Fig. 8a). When the Au/WS_2 photoelectrode generated PEC signals under light, the Ag/ZnMOF nanozymes with mimetic POD properties reduced the background signal via the catalyzing reaction between H_2O_2 and 3,3-diaminobenzidine (DAB), thus greatly improving the sensitivity and specificity of BLM analysis.

4.1.5 Antioxidant

Antioxidants, substance to scavenge ROS or free radicals, could prevent human body from cell apoptosis and nerve damage induced by oxidative stress [331]. Nevertheless, inappropriate supplementation of antioxidants may result in diseases and increase risk of death. Therefore, quantitatively analyzing antioxidants is of great significance. The nanozyme-related antioxidant detection is based on the inhibition of antioxidants on the

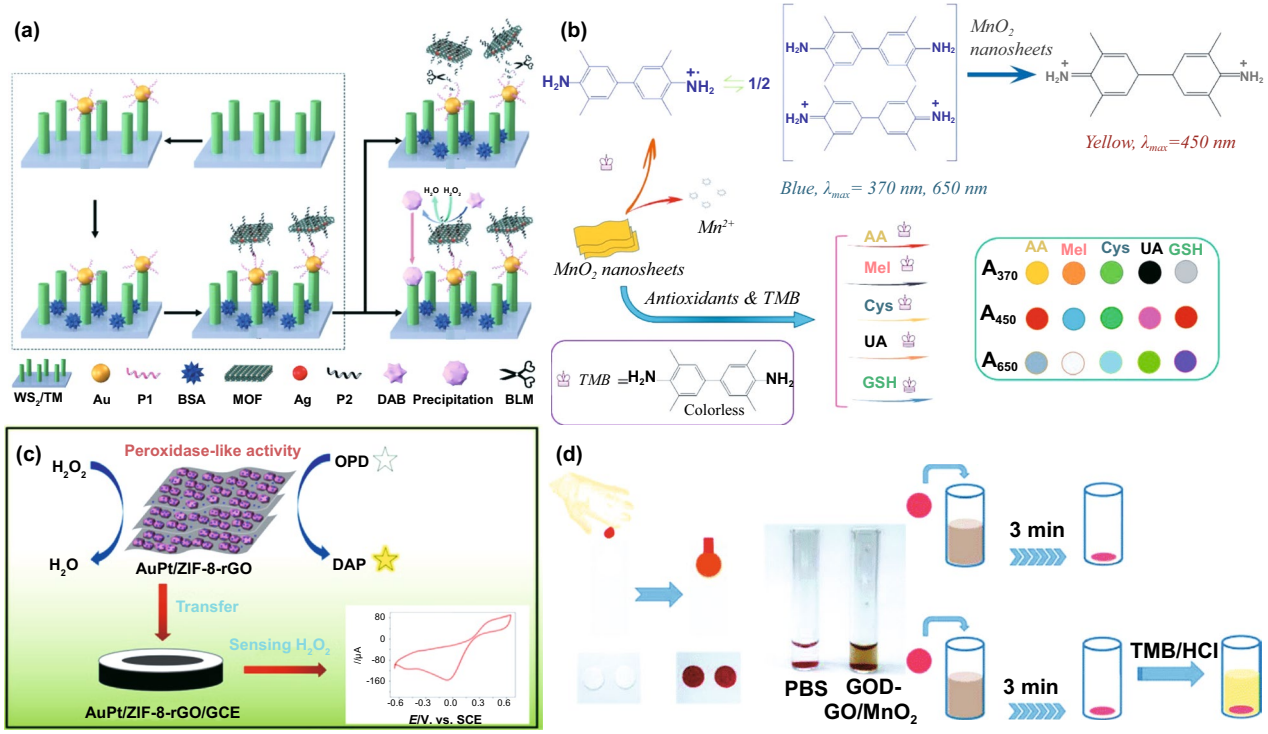

Fig. 8 **a** Fabrication of Ag/ZnMOF-based PEC biosensor with Au/WS_2 photoelectrode as a PEC matrix for detection of BLM. **b** Colorimetric sensor assay based on MnO_2 nanosheets with TMB as substrates for simultaneous detection of multiple antioxidants. **c** Detection of H_2O_2 based on AuPt/ZIF-8–rGO as POD mimics. **d** Application of the sensor platform based on GOD-GO/MnO_2 in blood glucose quantitative analysis. Adapted from **a** Ref. [330], **b** Ref. [340], **c** Ref. [349], **d** Ref. [362] with permission

nanozymes' catalytic activities [260, 278]. Following the evolvement of nanozymes and biosensing technology, the sensitive colorimetric determination for antioxidants has been extensively discussed, including ascorbic acid (AA, based on CoMn/NF@C [332], Pt/CeO_2 [333], Fe_3O_4/CoFe-LDH [158], Mn-CDs [334], etc.,), GSH (based on SPB-MnO_2 [335], Mn_3O_4 [336], Ir [337], V_2O_5 [338], etc.,) and L-Cysteine (L-Cys, based on Fe_3O_4 [339], etc.,). Most existing biosensors were designed for specific antioxidant analysis, while approaches for multiple antioxidants detection are scarce. Huang et al. [340] designed a MnO_2 nanosheets triggered colorimetric sensor array for simultaneous discrimination of UA, GSH, AA, L-Cys, and melatonin (Mel) in serum (Fig. 8b) [340]. The inhibitory effects on the catalytic performance of MnO_2 nanosheets vary according to the kind of antioxidants, resulting in different degrees of TMB oxidation and generating multicolors. Since the absorbance values at 370, 650, and 450 nm would change, the corresponding absorbance values A_{370}, A_{450}, and A_{650} were employed as three cross-reactive sensing elements in the visual colorimetric sensor array. The detection results revealed that the sensor could precisely and rapidly identify the five antioxidants and their mixture at a low concentration.

4.1.6 Other Substances

(1) H_2O_2

As a byproduct of respiratory metabolism, H_2O_2 is one of most common molecule in biological tissues [341]. When the concentration is at an abnormal status, H_2O_2 would cause damage to health and might induce oxidative stress related diseases [342]. Besides, hydrogen peroxide was widely used in biopharmaceuticals, environmental management, food manufacturing and some other fields due to its strong oxidant properties [343]. A bunch of methods have been designed to monitor H_2O_2 in various matrices considering its significant roles in biological metabolisms and broad utilization in industrial production [341, 344]. Among these assays, colorimetry and electrochemistry have gradually became main technologies for H_2O_2 determination owing to low cost, high

 https://doi.org/10.1007/s40820-021-00674-8

sensitivity and selectivity [345]. Up to now, a variety of metal- and metal oxide-based nanozymes (e.g., CuO-g-C_3N_4 [346], MnO_2 [347], V_2O_5-CeO_2 [348]) have been exploited for electrochemical analysis. Zhang et al. fixed ZIF-8 on graphene oxide (ZIF-8–rGO) and further synthesized AuPt/ZIF-8–rGO with POD-like activity to practically track H_2O_2 in human serum samples (Fig. 8c) [349]. The AuPt/ZIF-8–rGO-based electrochemical scheme showed remarkable electroanalysis performance along with excellent sensitivity and selectivity. This work reached the detection limit of 19 nM ($S/N = 3$), which obtained the lowest detection limit compared with previously reported electrochemical sensors.

The color change of peroxidase substrate (e.g., TMB) triggered by hydrogen peroxide is the foundation in colorimetric detection of H_2O_2. Diverse POD mimics (e.g., Cu_2O–Au [350], Fe–N–C [351], Cu(II)-coated Fe_3O_4 [352], PtCu [353], V_2O_5 [341], C-dots/Fe_3O_4 [130], and Rh [354, 355]) have been developed to manufacture colorimetric sensors. To our knowledge, the currently lowest detection limit of H_2O_2 based on colorimetry is 0.0625 μM reported by Tripathi et al. [356], and the palladium nanoclusters (Pd NCs) were designed by biological methods firstly in their study, in which Pd NCs were served as POD mimics.

(2) **Glucose**

Glucose is an indispensable nutrient for metabolism in organisms. The heat released during its oxidation reaction is a considerable energy source required by life events [357]. However, a surfeit of glucose might cause various diseases, including hyperlipidemia, arteriosclerosis, hypertension, diabetes and so on [358]. The concentration of glucose in blood or urine is a crucial indicator of physical condition [357, 359]. By combining the catalytic performance of glucose oxidase (GOD) and nanozymes with POD-type activity (e.g., Zn–CuO [331], Au@Ag [360], MoO_3/C [331], Ag [361], and Pt [135]), numerous optical technologies have described for glucose analysis in serum[135], beverage[279], and urine [331, 361] samples. Blood pretreatment and serum extraction were often demanded in conventional blood glucose detecting programs. To simplify determination steps, Lee et al. [362] designed a protocol that could directly monitor glucose in whole blood and avert pretreatment. They prepared a GOD-conjugated graphene oxide/MnO_2 (GOD-GO/MnO_2) sensor platform for quantitatively analyzing blood glucose with a detection limit of 3.1 mg dL^{-1} (Fig. 8d). The results indicated that this colorimetric sensor possessed clinical potential for blood glucose monitoring of diabetic patients.

4.2 Application in Antibacterial

The lack of non-antibiotic therapies and multiple drug resistance caused by bacteria diseases become one of the most serious problem, which threatens human health [363–365]. In the process of developing optimal antibacterial strategies, nanometallic materials have been discovered to exert antimicrobial nature [366, 367]. In addition, POD and OXD mimics were verified to catalyze producing harmful ROS, ranging from H_2O_2, superoxide, hydroxyl radicals to other small reactive molecules [27]. Hence, metal- and metal oxide-based nanozymes (e.g., V_2O_5 [368], CuO [369], CeO_2 [370], Au/MOF[371], and Tb_4O_7 [372]) have been gradually regarded as promising bactericides. For example, Fe_3O_4 NPs with POD-like properties could decompose H_2O_2 to generate toxic $^{\cdot}OH$ for bacterial infections treatment [373]. Evidence has emerged that enzyme mimic abilities of nanomaterials are closely associated with their composition and structure, which would affect antibacterial capacity [374]. Xi et al. [232] designed two types of copper/carbon nanozymes including two Cu states (Cu^0 and Cu^{2+}). The copper/carbon nanozymes displayed multi-enzyme activities and antibacterial mechanism dependent on Cu states. In the study, Xi et al. concluded that hollow carbon spheres (HCSs) modified with CuO (CuO-HCSs) nanozymes could induce Gram-negative bacteria death (*E. coli* and *P. aeruginosa*) when releasing Cu^{2+}. While the key of Cu-HCSs nanozymes to resist Gram-positive (*Salmonella typhimurium*, *S. typhimurium*) and Gram-negative bacteria (*E. coli* and *P. aeruginosa*) was based on POD-type activity, which was responsible for ROS generation (Fig. 9a).

The pH-dependent catalytic activity of nanozymes has been demonstrated that would limit their antimicrobial application under neutral pH, and was beneficial to grow bacteria like Escherichia coli, Staphylococcus aureus and so on [375, 376]. Fortunately, ATP served as modulators has been reported to improve the POD-like property of nanozymes, and it could interact with iron ions to produce $^{\cdot}OH$ under neutral pH [128, 377]. Therefore, Vallabani et al. [378] employed ATP as a synergist to enhance the catalysis ability of citrate modified Fe_3O_4 NPs. The results

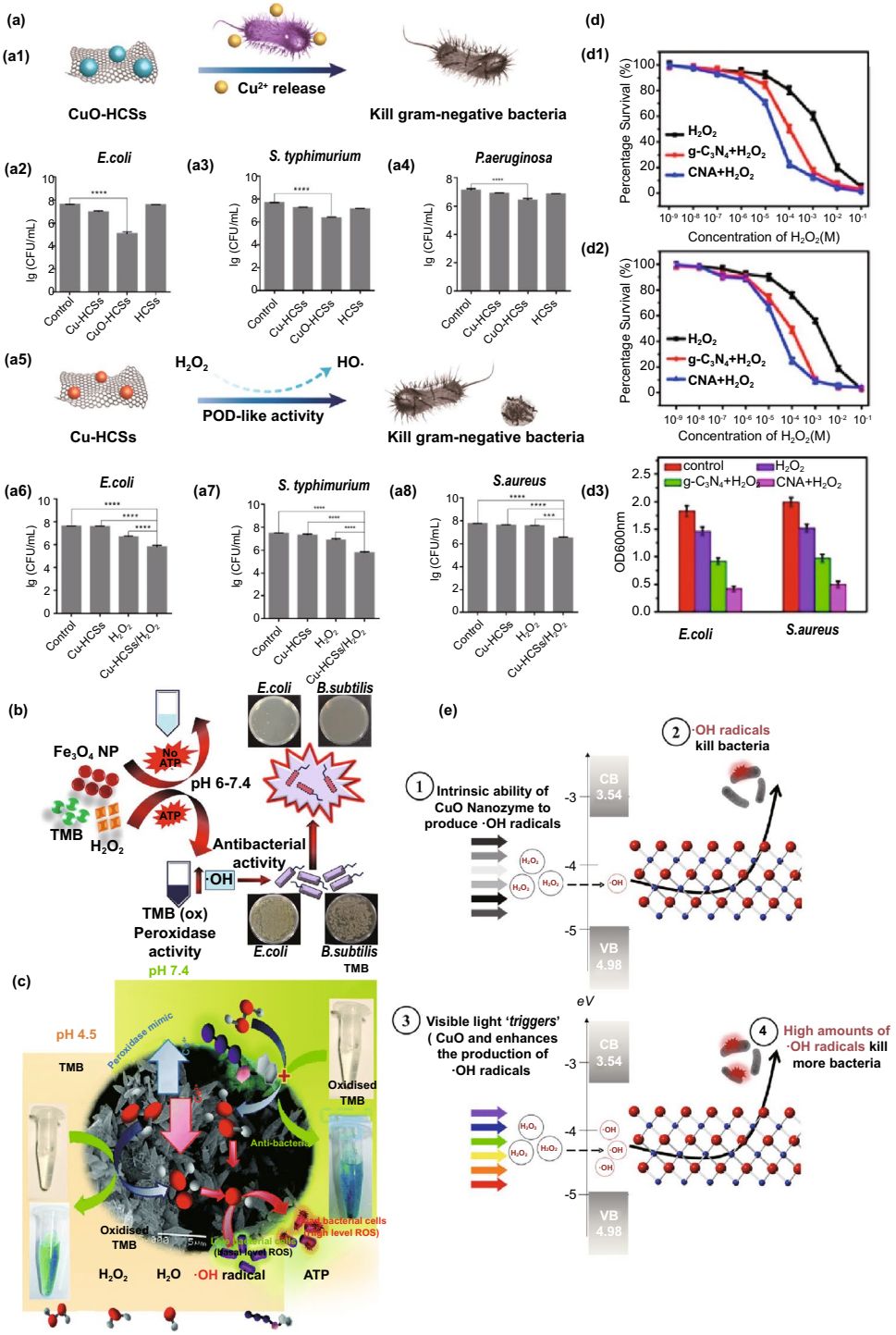

Fig. 9 **a1**, **a5** Antibacterial mechanism of Cu/C nanozymes with two Cu states (Cu^0 and Cu^{2+}). The actual antibacterial ability of CuO-HCSs, Cu-HCSs and HCSs against **a2** *E. coli*, **a3** *S. typhimurium*, and **a4** *P. aeruginosa*. The actual antibacterial ability of Cu-HCSs, H_2O_2 and Cu-HCSs/H_2O_2 against **a6** *E. coli*, **a7** *S. typhimurium* and **a8** *S. aureus*. **b** Antibacterial activity against *E. coli* and *B. subtilis* of Fe_3O_4 NPs before and after ATP introduction at pH 6–7.4. **c** Catalytic activity of CeO_2 nanocrystals before and after ATP introduction at pH 4.5 and 7.4. The bacterial viability of **d1** *E. coli* and **d2** *S. aureusand* with different treatments (H_2O_2, g-C_3N_4 + H_2O_2, CNA + H_2O_2). **d3** Optical density at 600 nm of bacterial suspension in different solutions. **e** Schematic illustration of the antibacterial principle of CuO NRs with the light as external triggers. Adapted from **a** Ref. [232], **b** Ref. [378], **c** Ref. [379], **d** Ref. [382], **e** Ref. [369] with permission

https://doi.org/10.1007/s40820-021-00674-8

showed that Fe_3O_4 NPs exhibited superior antibacterial performance against *E. coli* and *Bacillus subtilis* (*B. subtilis*, gram positive) in presence of H_2O_2 under a neutral pH environment with the assistance of ATP (Fig. 9b). Chishti et al. discovered that fluorite-structured CeO_2 nanocrystals with ~ 23.04% Ce^{3+} had recyclable POD-like activity [379]. Mechanism investigation indicated that the reduction of substrate affinity caused by ATP is the key to improve the low enzyme-like activity of nanoyzymes in a neutral environment (pH 7.4), further strengthening the sterilization sequel against both gram-positive (*S. aureus*) and gram-negative (*E. coli*) bacteria (Fig. 9c).

Besides optimizing the catalytic capacity, applying external triggers to control their antibacterial activity is essential to develop nanozyme-based antibacterial agents. Otherwise, the sustained action of nanozymes might induce bacteria to yield drug resistance. Karim et al. firstly reported that light could act as an external spark to control nanomaterials' catalysis [369]. A highly basic tertiary amine could produce visible light to excite CuO NRs. The increment of light intensity enhanced the affinity of CuO NRs and H_2O_2, thereby improving the POD-like activity and antimicrobial properties (Fig. 9e). Results showed that CuO NRs catalyzed H_2O_2 under visible light irradiation to output $^{\cdot}OH$ with 20 times higher than that under no light.

The exaltation of H_2O_2 sterilization efficiency has become an issue of increasing concern as H_2O_2 is a crucial and easily available ROS. Although numerous studies were devoted to this issue, applications of these systems were still restricted by the health hazard from high concentration of H_2O_2 (greatly higher than biologically relevant concentration) [380, 381]. Wang et al. integrated Au NPS with graphitized carbon nitride (g-C_3N_4) to synthesize non-toxic ultra-thin g-C_3N_4@AuNPs (CNA) nanozymes with high POD catalytic activity [382]. CNA nanozymes were firstly reported to possess excellent bactericidal properties under biosafety level of H_2O_2, and could efficiently decompose DR-biofilms to inhibit bacteria growth (Fig. 9d). In vitro experiments proved that CNA system provided significant advantages in preventing bacterial infections and accelerating wound healing.

4.3 Application in Relieving Inflammation

Inflammation, including acute and chronic inflammation, is regarded as a precursor to certain diseases [383]. An obvious feature of inflammatory tissue is the increasing of reactive oxygen or nitrogen species (RONS) content [384, 385]. Owing to the ROS scavenging ability, favorable stability in extreme environments and excellent biocompatibility, nanozymes have been indicated to be potential substitutes for broad-spectrum antioxidants in terms of inflammation treatment [386–388]. So far, a variety of metal-based and metal oxide-based nanozymes (such as Mn_3O_4 [56], CeO_2 [389], Pt/CeO_2 [390], and Cu-TCPP MOF [391]) have been reported for anti-inflammatory therapy. The main challenge to realize clinical transformation of nanozymes is to enhance the ROS eliminating performance and simplify nanomaterials' structure. Liu et al. synthesized ultra-small $Cu_{5.4}O$ nanoparticles ($Cu_{5.4}O$ USNPs) with mimic enzyme properties of CAT, SOD and GPx (Fig. 10a1) [392]. The ultra-micro size of $Cu_{5.4}O$ USNPs ensured their biocompatibility via the rapid removal of nanomaterials in the kidney (Fig. 10a2). $Cu_{5.4}O$ USNPs were confirmed to protect healthy cells from ROS at extremely low dosage. They also showed the promoting effect on the treatment of acute kidney injury, acute liver injury and wound healing in animal experiments. Wu et al. introduced RuO_2-PVP NPs to set up a therapeutic nanoplatform for inflammation alleviation and neuroprotection [393]. In this work, RuO_2-PVP NPs with multi-enzymatic properties effectively protected lipid, DNA and protein from oxidative stress in parallel with the broad-spectrum ROS elimination performance against inflammation and Parkinson's disease in vivo. Yao et al. [56] expanded the use of Mn SOD in anti-inflammatory. Their team demonstrated the multiple enzyme mimics activities of Mn_3O_4 NPs, which could scavenge superoxide free radicals, H_2O_2 and hydroxyl free radicals. In in-vitro experiments, the ROS-eliminating level of Mn_3O_4 NPs was much higher than traditional CeO_2 nanozymes. The experimental results indicated the obvious prospects of Mn-based nanozymes in treating and preventing ROS-mediated neuroinflammation.

The combination of nanozymes and other kinds of anti-inflammatory agents could bring a turning point for refractory inflammatory diseases. For example, the lack of targeting strategies and the risk of side effects with increasing dosage increased the difficulty in treating inflammatory bowel disease (IBD) [397]. By growing CeO_2 NPs in situ on montmorillonite (MMT) sheets, Zhao et al. designed CeO_2@MMT nanozymes with SOD-type, CAT-type and $^{\cdot}OH$ scavenging properties to directly target the inflammatory colon for IBD therapy [394]. In this system, MMT alleviated the potential nanotoxicity of CeO_2 NPs via reducing their

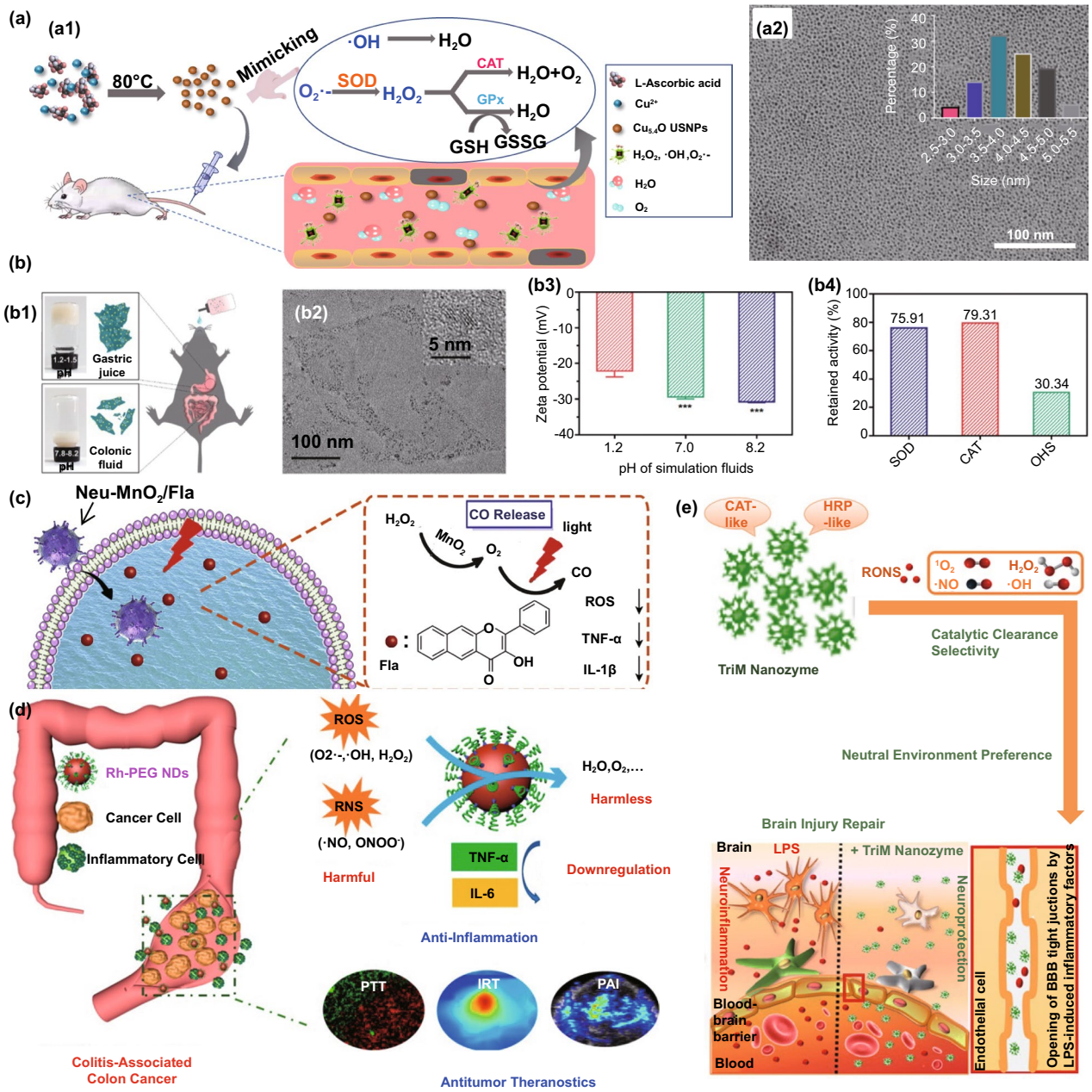

Fig. 10 **a1** Schematic illustration of the ROS scavenging and anti-inflammation function of $Cu_{5.4}O$ USNPs with the mimic enzyme properties of CAT, SOD, GPx ability. **a2** TEM image and particle size distribution of $Cu_{5.4}O$ USNPs; **b** Stability and enzymatic activity of CeO_2@MMT(1:9). **b1** Delivery process of CeO_2@MMT through the simulated stomach (pH 1.2–1.5) and colon (pH 7.8–8.2) fluids via oral absorption. **b2** TEM image of CeO_2@MMT(1:9) after treating with HCl solution (pH≈1.2) for 4 h at 37 °C. **b3** Zeta potentials of CeO_2@MMT in simulated stomach and colon fluids. **b4** CAT- and SOD-mimicking property and ·OH scavenging activities (OHS) of CeO_2@MMT treated with simulated gastric fluid. **c** The facilitated in situ CO release for synergistic anti-inflammatory effects induced by MnO_2 nanozymes modified with neutrophil membrane. **d** Rh-PEG NDs with excellent RONS scavenging ability, multi-enzyme-like activity and high photothermal conversion efficiency for relieving colon inflammation and anti-tumor treatment. **e** Application of PtPdMo nanozymes with multi-enzyme-like activity and high catalytic selectivity in improving neuroinflammation. *PTT* Photothermal therapy, *PAI* Photoacoustic imaging, *IRT* interventional radiotherapy. Adapted from **a** Ref. [392], **b** Ref. [394], **c** [395] **d** Ref. [396], **e** Ref [52] with permission

 https://doi.org/10.1007/s40820-021-00674-8

systemic absorption, which in turn endowed MMT sheets with ROS eliminating activity. Animal experiments have also proved that the nanozyme-based drugs were suitable for oral delivery and stable in gastrointestinal environment (Fig. 10b). CeO_2@MMT exhibited good targeting for colon disease sites, effectively treating IBD induced by dextran sulfate sodium in mice model. Although carbon monoxide (CO) gas therapy was recently revealed as a novel anti-inflammatory strategy, it still suffered from the low tissue specificity and troublesome amount control [398–400]. By integrating 3-hydroxybenzo [g]flavone (Fla), MnO_2, and neutrophil membrane (Neu), Liu et al. [395] fabricated Neu-MnO_2/Fla platform for the CO controllable releasing and specific anti-inflammation. As illustrated in Fig. 10c, the MnO_2 NPs modified with neutrophil membrane endowed Neu-MnO_2/Fla platform favorable targeted ability. Herein, hollow mesoporous MnO_2 NPs not only acted as ideal carrier for their superior drug-loading capacity and brilliant biodegradability, but also could decompose endogenous H_2O_2 and facilitated in situ CO release under light owing to the CAT-like ability, thereby achieving synergistic anti-inflammatory. The decrease of local ROS level and pro-inflammatory cytokines (tumor necrosis factor-α, TNF-α and Interleukin-1β, IL-1β) in a lipopolysaccharide (LPS)-induced inflammation model has indicated the effectiveness and controllability of Neu-MnO_2/Fla platform.

Despite the tremendous attention that paid to nanozyme-related anti-inflammatory therapies, there are still few reports about metal- and metal oxide-based nanozymes with reactive nitrogen species (RNS) scavenging ability. RNS including nitric oxide ($^{\cdot}NO$), nitrogen dioxide ($^{\cdot}NO_2$) and peroxynitrite ($^{\cdot}ONOO^-$) etc. are a major culprit in aggravating neuroinflammation induced by traumatic brain injury (TBI) [401]. Miao et al. prepared polyethylene glycol (PEG) coated (PEGylated) ultra-small rhodium nanodots (Rh-PEG NDs) showing excellent multi-enzyme-like activity and high photothermal conversion efficiency [396]. On the one hand, Rh-PEG NDs possessed similar RONS removal capacity as natural CAT, thereby alleviating the inflammation of colon disease. On the other hand, they could be used for photoacoustic imaging and photothermal therapy (Fig. 10d). Mu et al. [52] prepared PtPdMo trimetallic (triM) nanozymes for neuroinflammation treatment through multi-enzyme mimetics reaction-based RONS elimination. In addition, triM nanozymes displayed highly catalytic selectivity in neutral environments, which provided possible application of nanozymes in brain science (Fig. 10e). Zhang et al. doped Cr^{3+} ions into CeO_2 to prepare Cr/CeO_2 nanozymes by increasing Ce^{3+} states [402]. The higher Ce^{3+}/Ce^{4+} ratio contributed to strengthening enzyme-like activity of nanozymes with 3–5 times higher than undoped CeO_2. The Cr/CeO_2-based catalytic patch has been demonstrated as a promising choice for non-invasive TBI treatment and neuroinflammation relief owing to the satisfactory RONS (including $^{\cdot}OH$, $ONOO^-$ and H_2O_2) scavenging ability.

4.4 Application in Cancer Treatment

According to the latest global cancer statistics from the World Health Organization/International Cancer Center team, cancer is expected to become the main cause of death in countries around the world in twenty-first century [403]. Compared with traditional tumor treatment methods (surgery, chemotherapy, radiotherapy, etc.), external minimally invasive or non-invasive strategies containing photodynamic therapy (PDT), chemodynamic therapy (CDT), sonodynamic therapy (SDT), immunotherapy etc. show a favorable development prospect due to their accurate tumor specificity, space/time controllability and biosafety [404, 405]. However, the complex tumor microenvironment (TME) limited the therapeutic effects of many methods. TME not only refers to structure, function and metabolism of tumor tissue, but is also related to the internal environment of tumor cell (nuclear and cytoplasm) possessing the characteristics of hypoxia, acidity, glutathione and overexpression of H_2O_2 [406, 407]. The intrinsic catalytic activity enables nanozymes to regulate TME via changing RONS content or eliminating hypoxia [43, 408–410]. The biological safety, photothermal performance and some other physicochemical properties of nanozymes also indicated their potential in cancer therapy [411]. Given these reasons, nanozymes have been regarded as the prospective standalone agents or synergist for the progress of tumor treatment [43].

4.4.1 Photodynamic Therapy

PDT relied on ROS generated by photosensitizers (PSs) under light irradiation to induce cancer cell apoptosis [412]. Nevertheless, most PSs still face disadvantages of low selectivity, poor water solubility and high self-destruction [413]. In order to reinforce the stability of

loading PSs, various nanozymes such as MnO_2 [414], Pt[51] and so on were utilized. In the research of Xu et al. [415], Pt/C nanozymes not only served as chlorin e6 (Ce6) nanocarriers, but also promoted the conversion of H_2O_2 and O_2 into ROS with anti-tumor property (Fig. 11a). They compared the nanozymes with various structures and found that HCS@Pt NPs (Pt NPs decorated with hollow carbon spheres) showed favorable POD- and OXD-like activity, thereby further firming the therapeutic efficacy of PDT for cancer.

In addition to PSs transportation, studies have also confirmed that tumor hypoxia would weaken PDT efficiency [417]. Hence, nanozymes (e.g., Pt [418], Mn_3O_4[419]) as CAT mimics were employed to consume intratumoral H_2O_2 and generate oxygen in parallel with photosensitizer carriage. However, tumor hypoxia was difficult to be

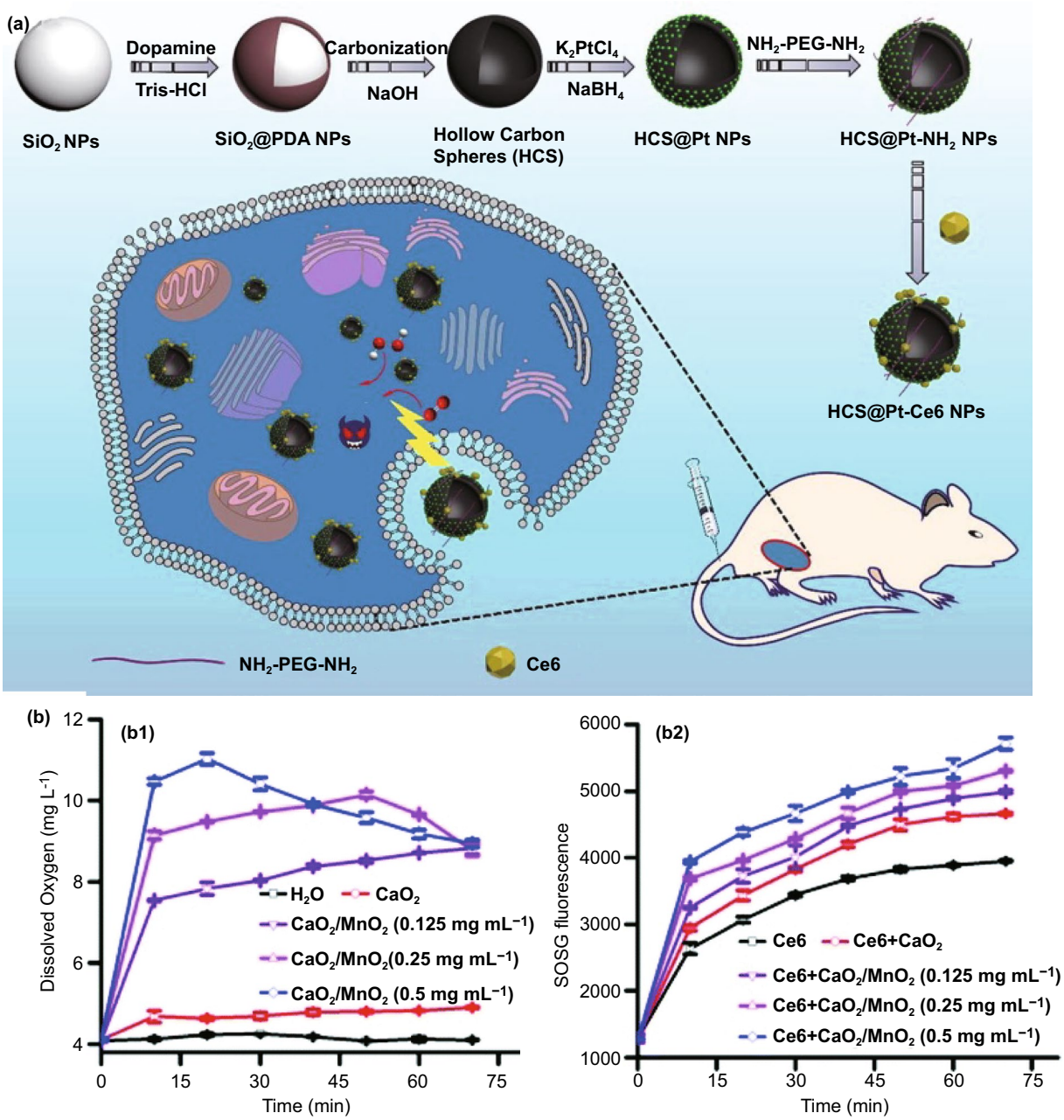

Fig. 11 **a** Synthesis progress of HCS@Pt-Ce6 NPs with multi-enzyme-like activity for PDT enhancement. The content of produced b**1** O_2 and **b2** $^1O_2$ (via Ce6) with CaO_2 NPs at 0.5 mg mL^{-1} and MnO_2 NPs at different concentrations. Adapted from **a** Ref. [415], **b** Ref. [416] with permission

https://doi.org/10.1007/s40820-021-00674-8

continuously suppressed due to the respiration of intratumoral mitochondria [420]. Yang et al. integrated IR780 PSs into mesoporous silica NPs (MSNs) and then covered with Mn_3O_4 NPs to produce Mn_3O_4@MSNs@IR780 nanocomposites [419]. Mn_3O_4 nanozymes that accumulated in the tumor sites could decompose H_2O_2 and trigger switch to release IR780, which specifically targeted to mitochondria and produced ROS to inhibit cancer cells respiration after destroying mitochondria. In vitro experiments proved that oxygen supplementation and mitochondrial destruction were vital to PDT enhancement. Hu et al. [416] employed exogenous oxygen-generating materials (CaO_2 NPs) to alleviate tumor hypoxia. In this report, MnO_2 nanozymes with CAT-mimicking activity not only catalyzed CaO_2 NPs to generate O_2, but also allowed image-guided PDT as a promising MR T1 nanoprobe (Fig. 11b).

4.4.2 Chemodynamic Therapy

Chemodynamic therapy generates ˙OH by catalyzing intratumoral H_2O_2 via Fenton or Fenton-like reactions, thereby killing tumor cells [421]. Nanozymes with POD-like activity (e.g., Fe_3O_4 NPs [422], AFeNPs [423]) have been recognized as Fenton reaction catalysts for CDT in acidic environments. Since existing reports revealed the pH-dependence of CDT, the pH-independent nanozymes (e.g., Fe/Al-GNE [424], Au_2Pt [142]) were designed to provide efficient Fenton reactions in neutral TME. What's worse, high concentration of GSH and low H_2O_2 in TME have also been demonstrated to restricted CDT effect [425]. Therefore, conquering the above-mentioned TME is a challenge to optimize CDT reaction efficiency.

Fu et al. synthesized CoO@AuPt nanocatalyst with high biocompatibility and stability under physiological environment, which regulated responsive CDT by lowering pH, increasing H_2O_2 level and consuming GSH content [426]. In the work, CoO template could degrade and generate Co^{2+} in acidic and high-level H_2O_2 environment, which was further acted as a useful Fenton-like reagent. The released Au/Pt nanozymes as multi-enzyme (GPx, CAT, POD, and GOx) mimics were responsible for decreasing GSH concentration and catalyzing H_2O_2 into O_2 and ˙OH (Fig. 12a). Moreover, the nanosatellites consumed intratumoral glucose to generate numerous H_2O_2 and induced starvation therapy, thereby enhancing the effect of CDT.

Another challenge to achieve augmented CDT is to increase the generation rate of ˙OH. Ma et al. [131] introduced microwave (MW) as an external stimulus to regulate CDT and realize controllable tumor therapy, named as microwave enhancing dynamic-therapy (MEDT). By coupling gold nanoclusters (BSA-Au NCs) with Fe-metal organic frameworks (MIL-101(Fe)), IL@MIL-101@BSA-AuNCs NPs were prepared after loading methylimidazolium hexafluorophosphate (IL) on MIL-101(Fe) NPs. Under microwave irradiation, MIL-101(Fe) enzymes owned MEDT by catalyzing H_2O_2 to produce toxic ˙OH in tumor. The dynamic distribution of MIL-101 (Fe) NPs in vivo and tumor site could be real-time monitored by magnetic resonance imaging (MRI) and fluorescence imaging (FI) (Fig. 12b).

4.4.3 Sonodynamic Therapy

PDT is commonly suitable for relatively small superficial tumors due to the limited depth of light penetration through tissues [427]. In contrast, ultrasound (US) owns a higher tissue penetration depth than light waves. Thus, US-triggered sonodynamic therapy is promising to treat deep or large tumors by activating sonosensitizers to generate ROS [428, 429]. Resemble to PSs in PDT, the performance of sonosensitizers plays a fundamental role in SDT [430]. The past 5 years witnessed the development of novel marvelous sonosensitizers [429, 431]. The stability and catalytic activity allowed some metal- and metal oxide-based nanozymes to function as sonosensitizers and Fenton reagents simultaneously to achieve CDT-enhanced SDT. For instance, Wang et al. designed polyethylene glycol (PEG)-modified nanozymes with ultrafine rod-like structure, named PEG-TiO_{1+x} NRs for tumor ablation [432]. Compared with traditional inorganic sonosensitizers, the sensitivity of PEG-TiO_{1+x} NRs was more prominent due to hypoxic structure. Furthermore, PEG-TiO_{1+x} NRs with HRP-type activity showed Fenton-like catalytic property. As SDT reagent possessing CDT function, the intravenously injected PEG-TiO_{1+x} NRs were significantly more effective in inhibiting tumors than traditional TiO_2 NPs under US irradiation (Fig. 13a). Zhong et al. prepared uniform $PtCu_3$ nanocages as sensitizers, HRP mimics and GPx mimics by one-step solvothermal method after pegylation [433]. Their research confirmed that $PtCu_3$ for cancer therapy improved sound

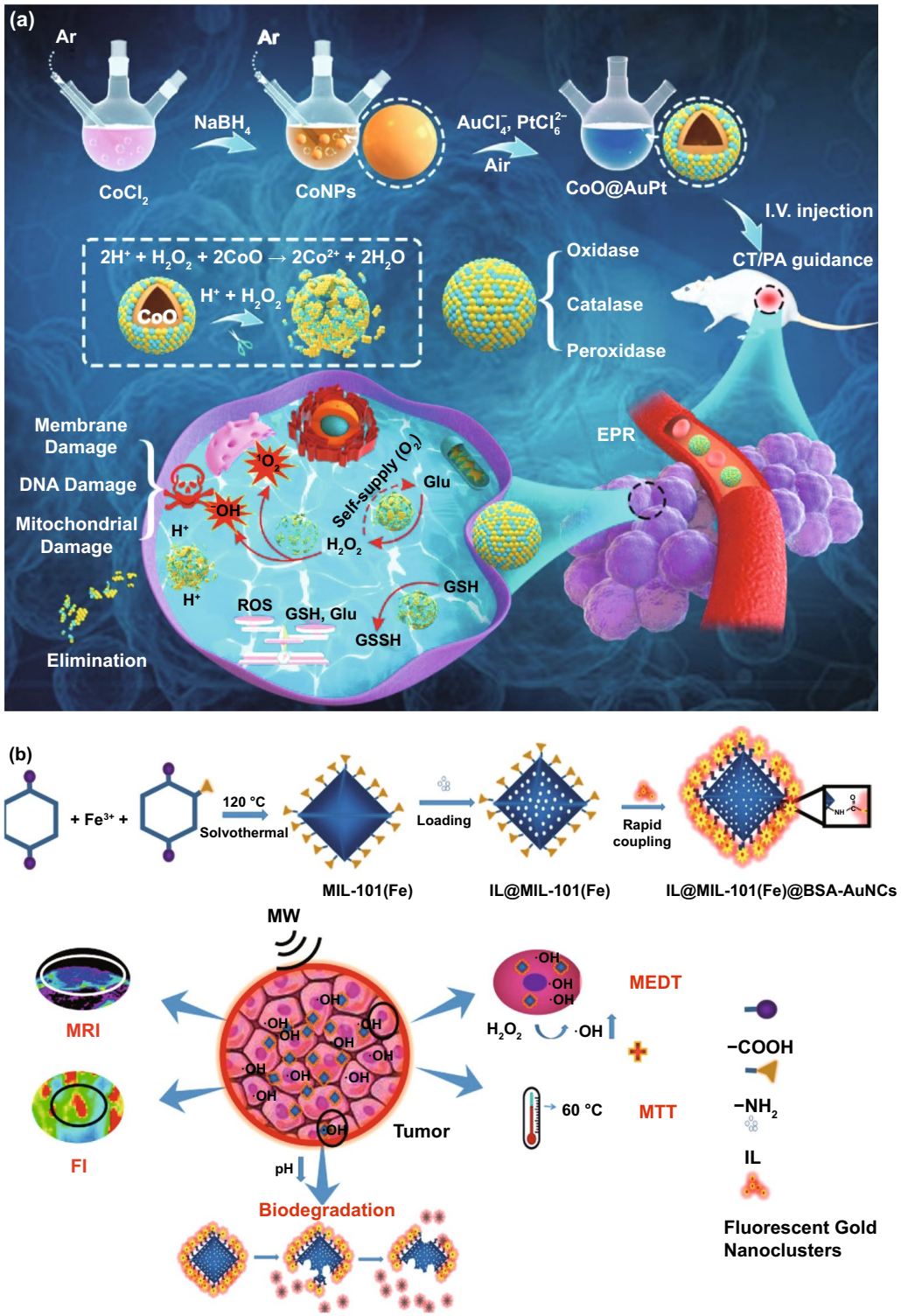

Fig. 12 **a** Preparation and the catalytic mechanism for CDT enhancement of CoO@AuPt NPs via Fenton reactions and regulating the response environment. **b** Preparation, the degradation process and the therapy principle of IL@MIL-101(Fe)@BSA-AuNCs NPs for MEDT. *GSSH* Glutathione disulfide, *EPR* enhanced permeation and retention, *MW* microwave, *MRI* magnetic resonance imaging, *MTT* microwave thermal therapy, *FI* fluorescence imaging. Adapted from **a** Ref. [426], **b** Ref. [131] with permission

 https://doi.org/10.1007/s40820-021-00674-8

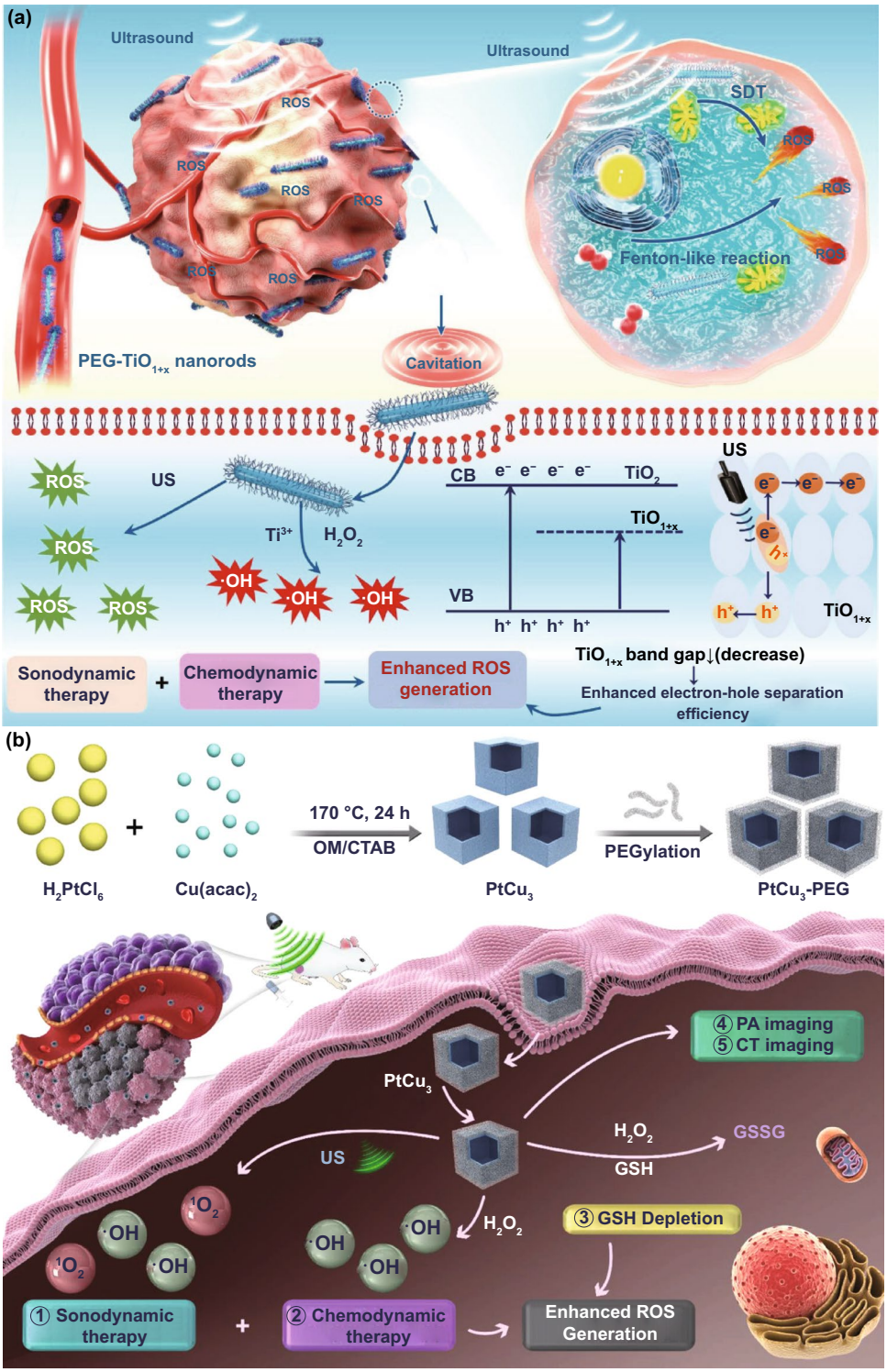

Fig. 13 **a** Schematic illustration of the working mechanism of TiO_{1+x} NRs with HRP-like activity for SDT/CDT-combined tumor therapy. **b** Preparation procedure and working mechanism of $PtCu_3$-PEG nanocages with HRP- and GPx-type property for PA/CT dual-modal imaging-guided CDT-enhanced SDT. Adapted from **a** Ref. [432], **b** Ref. [433] with permission

toxicity and inhibited tumor growth by generating ROS by decomposing H_2O_2 into $^{\cdot}OH$ and depleting GSH under US, in which $PtCu_3$ could obviously optimize the reaction environment of CDT. Meanwhile, owing to high light absorption and strong X-ray attenuation in near-infrared region, $PtCu_3$ could be employed for photoacoustic (PA)/computed tomography (CT) imaging-guided CDT-enhanced SDT (Fig. 13b).

4.4.4 Photothermal Therapy

Materials with high photothermal conversion efficiency are exploited in photothermal therapy (PTT), which could convert light energy into heat energy for the death of cancer cells under external light irradiating [434]. Numerous metal-based and metal oxide-based nanozymes (e.g., MnO_2 [435], Ru-Te [436], $Ru@CeO_2$ [437]) have been reported as photothermal agents (PTAs). In these studies, nanozymes ameliorated PTT efficacy due to their enzyme-like abilities and other superior properties at the same time. Wang et al. [435] synthesized 2D MnO_2 nanosheets (M-NSs) with controllable protein orientation through a wet chemical method, and then functionalized M-NSs via a sonochemical proposal. As is shown in Fig. 14a, the M-NS served as GOx mimics with highly dispersion and stability, which finally realized starvation therapy by consuming glucose of tumor cells. The nanozymes also presented remarkable photothermal conversion efficiency and PA imaging performance under near-infrared (NIR) irradiation, thereby achieving PA imaging-guided synergistic cancer treatment of starvation therapy and PTT.

However, the effect of PTT is stinted by light penetration depth and thermal damage to healthy tissue induced by overexposure [438]. Therefore, a series of studies tried to combine PTT with other treatment methods to achieve synergistic therapy [439]. For example, Au_2Pt nanozymes as POD and CAT mimics with potent photothermal performance were reported for PDT/CDT/PTT synergistic cancer therapeutics [142]. AgPd NPs with POD-like activity could improve photothermal conversion efficiency, and have been proved to be acted as carriers for chemotherapeutic drugs transmission during a weakly acidic environment (pH 5.5), thus achieving ROS/PTT/chemotherapy guided by NIR laser [440]. Pt-CuS Janus nanozymes were adopted in synergistically enhanced SDT and PTT [441]. In this system, Pt-CuS Janus hollow structure was used as sonosensitizers carrier, showing photothermal conversion capacity under laser irradiation, and could decompose endogenous H_2O_2 expeditiously. The Pt NPs [442] with CAT-mimicking capacity and Ru–Te hollow nanorods [436] with OXD, POD-, CAT- and SOD-type activity both acted as carriers and relieved TME hypoxia to enhance cancer PDT/PTT effect. Different from most nanozyme-based synergistic therapy, Yang et al. [443] covered Pt-carbon integrated nanozymes as PSs via one-step reduction. Under NIR light lasering, the nanozymes provided brilliant photosensitivity and photothermal effect. And the PDT reinforcement was relied on the CAT-like catalysis activity. In vivo experiments revealed that Pt-carbon nanozymes inhibited mice colon cancer reaching an 90% efficiency (Fig. 14b). Li et al. [411] prepared the H_2O_2-responsive $PtFe@Fe_3O_4$, which possessed POD-like activity, CAT-type property and exceptional photothermal performance under acidic TME environment. Experimental results indicated that tumor catalytic therapy based on $PtFe@Fe_3O_4$ nanozymes obtained a 99.8% anti-tumor rate for deep pancreatic cancer when cooperating with photothermal therapy What is more, the electron transfer process between PtFe nanorods, Fe_3O_4 NPs and H_2O_2 molecules was also firstly described in their study (Fig. 14c).

4.4.5 Immunotherapy

Cancer immunotherapies, regarded as promising strategies for tumor therapy, utilize the immune system of patients to treat cancer [444], and might include cytokine therapy, tumor vaccines, immune checkpoint blockade (ICB) therapy, adoptive cell therapy and so on [445]. Studies have demonstrated that the modulation of TME is conducive to tumor immunotherapy [43]. Yang et al. [446] designed a polyethylene glycol (PEG)-modified hollow manganese dioxide (H-MnO_2) nanoshells to load photodynamic agent Ce6 and chemotherapy drug doxorubicin (DOX), forming H-MnO_2-PEG/C&D complex for cancer combination immunotherapy. The H-MnO_2 could alleviate tumor hypoxia via catalytically decomposing hydrogen peroxide to generate O_2. A series of immunological responses were discovered with synergistic treatment of H-MnO_2-PEG/C&D and Chemo-PDT, resulting remarkable decreasing in the secretion of IL-10 (predominant cytokine secreted by M2 macrophages) and the increment in the secretion of IL-12 (predominant cytokine secreted by M1 macrophages). Moreover, the introduction of

https://doi.org/10.1007/s40820-021-00674-8

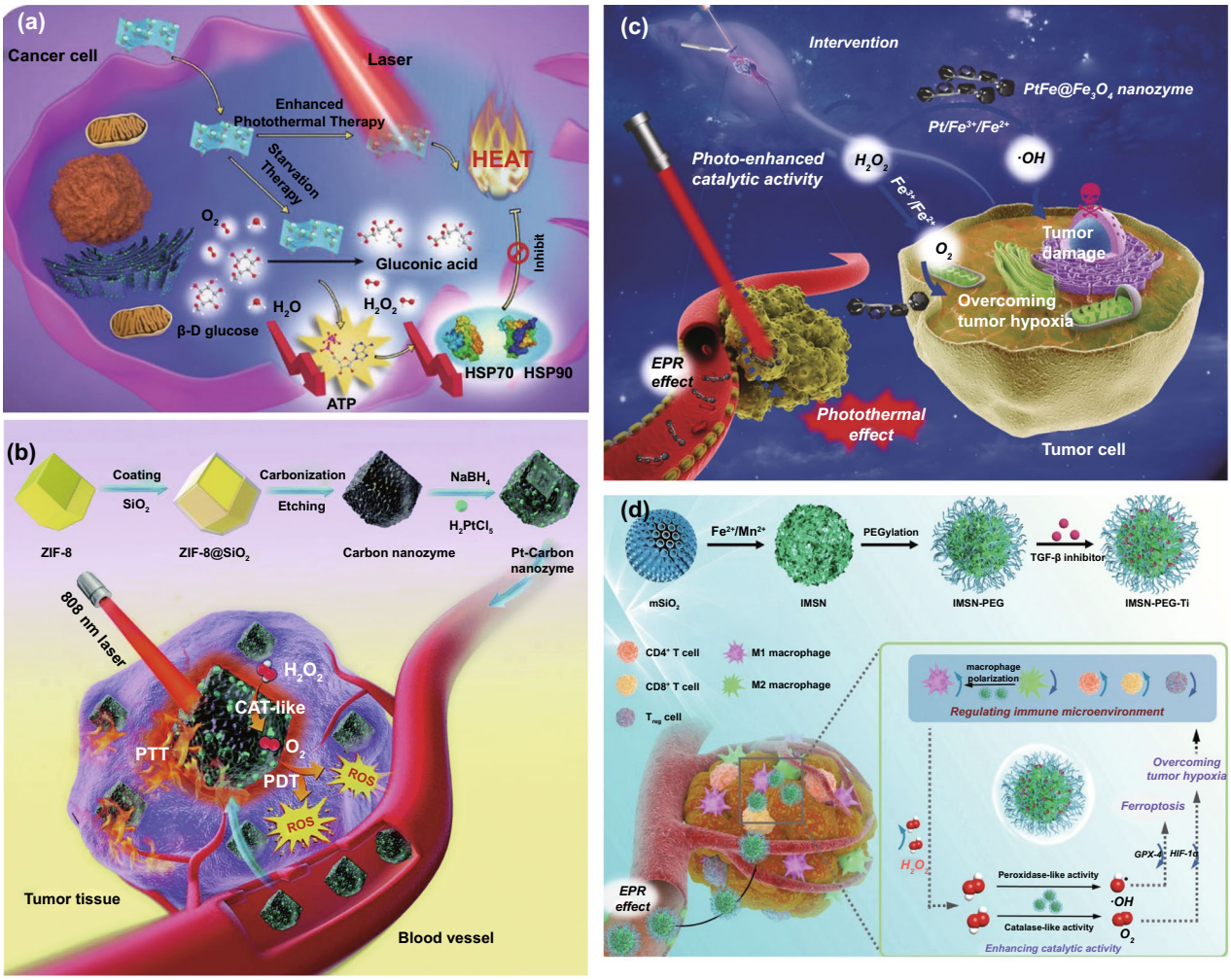

Fig. 14 **a** Working principle of M-NSs as GOx mimics and PTAs with effective PA imaging performance for the synergistic starvation-enhanced PTT guided by PA imaging. **b** Synthesis procedure and the working mechanism of Pt-carbon-integrated nanozymes for synergistic PDT/PTT cancer therapy. **c** Working mechanism of PtFe@Fe_3O_4 with POD-, CAT-like activity and excellent photothermal effect under acidic TME environment for tumor catalytic therapy combined with PTT. **d** Illustration of the cancer immunotherapy using the IMSN-PEG-TI nanoplatform. Adapted from **a** Ref. [435], **b** Ref. [443], **c** Ref. [411] with permission

anti-PD-L1 checkpoint blockade showed further enhanced therapeutic efficacy for tumor with by improving TNF-α.

Moreover, it has been reported that tumor-associated macrophages (TAMs) are critical to tumor growth and metastasis, thereby playing an important role in the cancer immunotherapy [447]. Regulating TME could facilitate macrophage polarization from M2 to M1 since the tumor hypoxia is associated with macrophage recruitment and polarization [448]. Xu et al. [449] loaded TGF-β inhibitor (TI) to the PEGylated iron manganese silicate nanoparticles to prepare IMSN-PEG-TI nanoplatform for tumor immunotherapy (Fig. 14d). In this system, IMSN nanozymes with POD- and CAT-like property could decompose H_2O_2 into ·OH and O_2 to kill tumor cells and overcome tumor hypoxia in respective. The interaction of IMSN and TI effectively regulated the tumor immune microenvironment, leading to elevated ratio of M1 to M2 macrophages, $CD4^+$ T to T_{reg} cells, and $CD8^+$ T to T_{reg} cells. Furthermore, the enhanced macrophages polarization would in turn induce the reproduction of H_2O_2, thus promoting enzymatic properties of IMSN nanozymes.

5 Conclusion

The prosperity of nanotechnology and biology created a series of novel artificial enzymes. As promising natural enzymes mimics, nanozymes have demonstrated remarkable performance in clinical medicine, biopharmaceuticals, environmental monitoring and many other fields. In this review, we meticulously elaborated the intrinsic activity and catalytic mechanism of the classical metal- and metal oxide-based nanozymes, including monometal-, metal alloy-, metal oxide-, metallic core/shell nanostructure-based and hybrid nanomaterials. The recent research progress of metal- and metal oxide-based nanozymes in analysis, antibacterial, relieving inflammation, and cancer therapy was also involved. Although nanozymes have been revealed to overcome many limitations of natural enzymes such as low stability, complicated preparation and expensive storage, there are still severe challenges for future researches. (1) Compared with most natural enzymes, metal- and metal oxide-based nanozymes seem to lack the substrate specificity. Even though researchers have discovered amounts of inner and external factors that influencing enzymatic properties, the precise control of catalytic performance, especially for the nanozymes with multi-enzyme-like activities, still has a long way to go. (2) The exploration of the internal catalytic mechanism is fundamental for understanding and mastering the catalytic reaction of nanozymes. In contrast to the synthesis and employment of novel nanomaterials, studies that involved the deep comprehension of working mechanism are relatively rare. What's worse, the advanced strategies dedicated to mechanism clarification are also limited. (3) The POD mimics have become an issue of extensive concern in most nanozyme-related applications, especially in the field of analysis and detection. While other component of oxidoreductase family have also been proved to possess unsubstituted function in many circumstances. Therefore, the spread utilization of SOD, CAT, OXD mimics are yet to be developed. (4) Most previous biosensors based on nanozymes could only detect one or two substances. The schemes for simultaneous discrimination and quantification of multiple (≥ 3) substances with high sensitivity are required to be further investigated and simplified. (5) Considering the cost control in large-scale preparation, seeking alternatives for noble metal nanozymes has gradually received increasing attention. Besides, the reduction of their content in nanoalloys and nanocomposites while guaranteeing the performance is also worth more efforts. (6) The long-term in vivo toxicity of nanozymes still remains a challenge for their clinical employment. Although a large amount of studies have involved the discussion about the biocompatibility, the systematic mechanisms of toxicity and corresponding solutions are in urgent need.

Acknowledgements We thank the supports of the National Foundational Basic Research Project of China (2017YFA0205301), National Nature Scientific Foundation Innovation Team of China(81921002), National Nature Scientific foundation of China (8202010801, 81903169, 81803094, 81602184, 81822024 and 81571729), Shanghai Municipal Commission of Economy and Information Technology Fund (No. XC-ZXSJ-02-2016-05), the medical engineering cross project of Shanghai Jiao Tong University (YG2017Z D05), the Project of Thousand Youth Talents from China, and the National Key Research and Development Program of China (2017YFC1200904). We also thanks the financial support of China Postdoctoral Science Foundation (2020TQ0191) and Shanghai Engineering Research Center for Intelligent Diagnosis and Treatment Instrument (No. 15DZ2252000).

References

1. Z. Qu, H. Xu, P. Xu, K. Chen, R. Mu et al., Ultrasensitive ELISA using enzyme-loaded nanospherical brushes as labels. Anal. Chem. **86**(19), 9367–9371 (2014). https://doi.org/10.1021/ac502522b
2. L. Chen, N. Wang, X. Wang, S. Ai, Protein-directed in situ synthesis of platinum nanoparticles with superior peroxidase-like activity, and their use for photometric determination of hydrogen peroxide. Microchim. Acta **180**(15), 1517–1522 (2013). https://doi.org/10.1007/s00604-013-1068-6
3. Y.H. Lin, J.S. Ren, X.G. Qu, Catalytically active nanomaterials: a promising candidate for artificial enzymes. Acc. Chem. Res. **47**(4), 1097–1105 (2014). https://doi.org/10.1021/ar400250z

4. Z. Gao, M. Xu, M. Lu, G. Chen, D. Tang, Urchin-like (gold core)@(platinum shell) nanohybrids: a highly efficient peroxidase-mimetic system for in situ amplified colorimetric immunoassay. Biosens. Bioelectron. **70**, 194–201 (2015). https://doi.org/10.1016/j.bios.2015.03.039
5. W. Song, B. Zhao, C. Wang, Y. Ozaki, X. Lu, Functional nanomaterials with unique enzyme-like characteristics for sensing applications. J. Mater. Chem. B **7**(6), 850–875 (2019). https://doi.org/10.1039/C8TB02878H
6. L. Gao, J. Zhuang, L. Nie, J. Zhang, Y. Zhang et al., Intrinsic peroxidase-like activity of ferromagnetic nanoparticles. Nat. Nanotechnol. **2**(9), 577–583 (2007). https://doi.org/10.1038/nnano.2007.260
7. M. Mirhosseini, A. Shekari-Far, F. Hakimian, B.F. Haghiralsadat, S.K. Fatemi et al., Core–shell Au@Co-Fe hybrid nanoparticles as peroxidase mimetic nanozyme for antibacterial application. Process Biochem. **95**, 131–138 (2020). https://doi.org/10.1016/j.procbio.2020.05.003
8. D. Li, Q. Guo, L. Ding, W. Zhang, L. Cheng et al., Bimetallic $CuCo_2S_4$ nanozymes with enhanced peroxidase activity at neutral ph for combating burn infections. ChemBioChem **21**(18), 2620–2627 (2020). https://doi.org/10.1002/cbic.202000066
9. L. Han, J. Shi, A. Liu, Novel biotemplated MnO_2 1D nanozyme with controllable peroxidase-like activity and unique catalytic mechanism and its application for glucose sensing. Sens. Actuators B-Chem. **252**, 919–926 (2017). https://doi.org/10.1016/j.snb.2017.06.096
10. H. Gu, Q. Huang, J. Zhang, W. Li, Y. Fu, Heparin as a bifunctional biotemplate for Pt nanocluster with exclusively peroxidase mimicking activity at near-neutral pH. Colloids Surf. A **606**, 125455 (2020). https://doi.org/10.1016/j.colsurfa.2020.125455
11. T. Zhang, F. Tian, L. Long, J. Liu, X. Wu, Diagnosis of rubella virus using antigen-conjugated Au@ Pt nanorods as nanozyme probe. Int. J. Nanomed. **13**, 4795 (2018). https://doi.org/10.2147/IJN.S202056
12. Y. Song, K. Qu, C. Zhao, J. Ren, X. Qu, Graphene oxide: Intrinsic peroxidase catalytic activity and its application to glucose detection. Adv. Mater. **22**(19), 2206–2210 (2010). https://doi.org/10.1002/adma.200903783
13. N. Alizadeh, A. Salimi, T.-K. Sham, P. Bazylewski, G. Fanchini, Hierarchical $Co(OH)_2$/FeOOH/WO_3 ternary nanoflowers as a dual-function enzyme with pH-switchable peroxidase and catalase mimic activities for cancer cell detection and enhanced photodynamic therapy. Chem. Eng. J. **417**, 129134 (2021). https://doi.org/10.1016/j.cej.2021.129134
14. J. Shah, R. Purohit, R. Singh, A.S. Karakoti, S. Singh, ATP-enhanced peroxidase-like activity of gold nanoparticles. J. Colloids Interface Sci. **456**, 100–107 (2015). https://doi.org/10.1016/j.jcis.2015.06.015
15. M. Sharifi, S.H. Hosseinali, P. Yousefvand, A. Salihi, M.S. Shekha et al., Gold nanozyme: biosensing and therapeutic activities. Mater. Sci. Eng. C **108**, 110422 (2020). https://doi.org/10.1016/j.msec.2019.110422
16. S. Guo, Y. Han, L. Guo, Mechanistic study of catalase-and superoxide dismutation-mimic activities of cobalt oxide nanozyme from first-principles microkinetic modeling. Catal. Surv. Asia **24**(1), 70–85 (2020). https://doi.org/10.1007/s10563-019-09290-4
17. M. Gharib, A. Kornowski, H. Noei, W.J. Parak, I. Chakraborty, Protein-protected porous bimetallic AgPt nanoparticles with pH-switchable peroxidase/catalase-mimicking activity. ACS Mater. Lett. **1**(3), 310–319 (2019). https://doi.org/10.1021/acsmaterialslett.9b00164
18. J. Xi, G. Wei, Q. Wu, Z. Xu, Y. Liu et al., Light-enhanced sponge-like carbon nanozyme used for synergetic antibacterial therapy. Biomater. Sci. **7**(10), 4131–4141 (2019). https://doi.org/10.1039/C9BM00705A
19. N. Singh, M.A. Savanur, S. Srivastava, P. D'Silva, G. Mugesh, A redox modulatory Mn_3O_4 nanozyme with multi-enzyme activity provides efficient cytoprotection to human cells in a Parkinson's disease model. Angew. Chem. Int. Ed. **56**(45), 14267–14271 (2017). https://doi.org/10.1002/anie.201708573
20. B. Jiang, L. Fang, K. Wu, X. Yan, K. Fan, Ferritins as natural and artificial nanozymes for Theranostics. Theranostics **10**(2), 687 (2020). https://doi.org/10.7150/thno.39827
21. B. Unnikrishnan, C.-W. Lien, H.-W. Chu, C.-C. Huang, A review on metal nanozyme-based sensing of heavy metal ions: challenges and future perspectives. J. Hazard. Mater. **401**, 123397 (2020). https://doi.org/10.1016/j.jhazmat.2020.123397
22. J. Wu, X. Wang, Q. Wang, Z. Lou, S. Li et al., Nanomaterials with enzyme-like characteristics (nanozymes): next-generation artificial enzymes (II). Chem. Soc. Rev. **48**(4), 1004–1076 (2019). https://doi.org/10.1039/C8CS00457A
23. N. Cheng, J.C. Li, D. Liu, Y.H. Lin, D. Du, Single-atom nanozyme based on nanoengineered Fe–N–C catalyst with superior peroxidase-like activity for ultrasensitive bioassays. Small **15**(48), 7 (2019). https://doi.org/10.1002/smll.201901485
24. B. Xu, H. Wang, W. Wang, L. Gao, S. Li et al., A single-atom nanozyme for wound disinfection applications. Angew. Chem. Int. Ed. **131**(15), 4965–4970 (2019). https://doi.org/10.1002/ange.201813994
25. M.S. Kim, J. Lee, H.S. Kim, A. Cho, K.H. Shim et al., Heme cofactor-resembling Fe–N single site embedded graphene as nanozymes to selectively detect H_2O_2 with high sensitivity. Adv. Funct. Mater. **30**(1), 1905410 (2020). https://doi.org/10.1002/adfm.201905410
26. X.H. Niu, Q.R. Shi, W.L. Zhu, D. Liu, H.Y. Tian et al., Unprecedented peroxidase-mimicking activity of single-atom nanozyme with atomically dispersed Fe–N-x moieties hosted by MOF derived porous carbon. Biosens. Bioelectron. **142**, 8 (2019). https://doi.org/10.1016/j.bios.2019.111495
27. H. Wang, K. Wan, X. Shi, Recent advances in nanozyme research. Adv. Mater. **31**(45), 1805368 (2019). https://doi.org/10.1002/adma.201805368
28. W. Chen, S. Li, J. Wang, K. Sun, Y. Si, Metal and metal-oxide nanozymes: bioenzymatic characteristics, catalytic

mechanism, and eco-environmental applications. Nanoscale **11**(34), 15783–15793 (2019). https://doi.org/10.1039/C9NR04771A

29. S. Cai, R. Yang, *Noble Metal-Based Nanozymes* (Springer, Singapore, 2020), pp. 331–365
30. A. Zhang, W. Guo, H. Ke, X. Zhang, H. Zhang et al., Sandwich-format ECL immunosensor based on Au star@BSA-Luminol nanocomposites for determination of human chorionic gonadotropin. Biosens. Bioelectron. **101**, 219–226 (2018). https://doi.org/10.1016/j.bios.2017.10.040
31. X. Niu, Q. Shi, W. Zhu, D. Liu, H. Tian et al., Unprecedented peroxidase-mimicking activity of single-atom nanozyme with atomically dispersed Fe–N_x moieties hosted by MOF derived porous carbon. Biosens. Bioelectron. **142**, 111495 (2019). https://doi.org/10.1016/j.bios.2019.111495
32. Z. Xi, W. Gao, X. Xia, Size effect in Pd−Ir core–shell nanoparticles as nanozymes. ChemBioChem **21**(17), 2440–2444 (2020). https://doi.org/10.1002/cbic.202000147
33. L. Jin, Y. Sun, L. Shi, C. Li, Y. Shen, PdPt bimetallic nanowires with efficient oxidase mimic activity for the colorimetric detection of acid phosphatase in acidic media. J. Mater. Chem. B **7**(29), 4561–4567 (2019). https://doi.org/10.1039/C9TB00730J
34. X. Wang, Q. Tu, B. Zhao, Y. An, J.-C. Wang et al., Effects of poly(l-lysine)-modified Fe_3O_4 nanoparticles on endogenous reactive oxygen species in cancer stem cells. Biomaterials **34**(4), 1155–1169 (2013). https://doi.org/10.1016/j.Biomaterials2012.10.063
35. S. Fan, M. Zhao, L. Ding, H. Li, S. Chen, Preparation of Co_3O_4/crumpled graphene microsphere as peroxidase mimetic for colorimetric assay of ascorbic acid. Biosens. Bioelectron. **89**, 846–852 (2017). https://doi.org/10.1016/j.bios.2016.09.108
36. W. Lu, J. Zhang, N. Li, Z. You, Z. Feng et al., Co_3O_4@β-cyclodextrin with synergistic peroxidase-mimicking performance as a signal magnification approach for colorimetric determination of ascorbic acid. Sens. Actuators B-Chem. **303**, 127106 (2020). https://doi.org/10.1016/j.snb.2019.127106
37. Q. Chen, S. Li, Y. Liu, X. Zhang, Y. Tang et al., Size-controllable Fe–N/C single-atom nanozyme with exceptional oxidase-like activity for sensitive detection of alkaline phosphatase. Sens. Actuators B-Chem. **305**, 127511 (2020). https://doi.org/10.1016/j.snb.2019.127511
38. K.L. Fan, J.Q. Xi, L. Fan, P.X. Wang, C.H. Zhu et al., In vivo guiding nitrogen-doped carbon nanozyme for tumor catalytic therapy. Nat. Commun. **9**, 11 (2018). https://doi.org/10.1038/s41467-018-03903-8
39. A. Zhang, S. Pan, Y. Zhang, J. Chang, J. Cheng et al., Carbon-gold hybrid nanoprobes for real-time imaging, photothermal/photodynamic and nanozyme oxidative therapy. Theranostics **9**(12), 3443–3458 (2019). https://doi.org/10.7150/thno.33266
40. A. Zhang, Q. Zhang, G. Alfranca, S. Pan, Z. Huang et al., GSH-triggered sequential catalysis for tumor imaging and eradication based on star-like Au/Pt enzyme carrier system. Nano Res. **13**(1), 160–172 (2020). https://doi.org/10.1007/s12274-019-2591-5
41. Z. Chen, J.-J. Yin, Y.-T. Zhou, Y. Zhang, L. Song et al., Dual enzyme-like activities of iron oxide nanoparticles and their implication for diminishing cytotoxicity. ACS Nano **6**(5), 4001–4012 (2012). https://doi.org/10.1021/nn300291r
42. J. Zhao, X. Cai, W. Gao, L. Zhang, D. Zou et al., Prussian blue nanozyme with multienzyme activity reduces colitis in mice. ACS Appl. Mater. Interfaces **10**(31), 26108–26117 (2018). https://doi.org/10.1021/acsami.8b10345
43. J. Ma, J. Qiu, S. Wang, Nanozymes for catalytic cancer immunotherapy. ACS Appl. Nano Mater. **3**(6), 4925–4943 (2020). https://doi.org/10.1021/acsanm.0c00396
44. H. Dong, Y. Fan, W. Zhang, N. Gu, Y. Zhang, Catalytic mechanisms of nanozymes and their applications in biomedicine. Bioconjug. Chem. **30**(5), 1273–1296 (2019). https://doi.org/10.1021/acs.bioconjchem.9b00171
45. Z. Wang, R. Zhang, X. Yan, K. Fan, Structure and activity of nanozymes: inspirations for de novo design of nanozymes. Mater. Today **41**, 81–119 (2020). https://doi.org/10.1016/j.mattod.2020.08.020
46. H. Sun, Y. Zhou, J. Ren, X. Qu, Carbon Nanozymes: enzymatic properties, catalytic mechanism, and applications. Angew. Chem. Int. Ed. **57**(30), 9224–9237 (2018). https://doi.org/10.1002/anie.201712469
47. M. Liang, X. Yan, Nanozymes: from new concepts, mechanisms, and standards to applications. Acc. Chem. Res. **52**(8), 2190–2200 (2019). https://doi.org/10.1021/acs.accounts.9b00140
48. J. Zhang, J. Liu, Light-activated nanozymes: catalytic mechanisms and applications. Nanoscale **12**(5), 2914–2923 (2020). https://doi.org/10.1039/C9NR10822J
49. L. Shen, D. Ye, H. Zhao, J. Zhang, Perspectives for single-atom nanozymes: advanced synthesis, functional mechanisms, and biomedical applications. Anal. Chem. **93**(3), 1221–1231 (2021). https://doi.org/10.1021/acs.analchem.0c04084
50. Y. Huang, J. Ren, X. Qu, Nanozymes: classification, catalytic mechanisms, activity regulation, and applications. Chem. Rev. **119**(6), 4357–4412 (2019). https://doi.org/10.1021/acs.chemrev.8b00672
51. Y. Zhang, F.M. Wang, C.Q. Liu, Z.Z. Wang, L.H. Kang et al., Nanozyme decorated metal-organic frameworks for enhanced photodynamic therapy. ACS Nano **12**(1), 651–661 (2018). https://doi.org/10.1021/acsnano.7b07746
52. X.Y. Mu, J.Y. Wang, Y.H. Li, F.J. Xu, W. Long et al., Redox trimetallic nanozyme with neutral environment preference for brain injury. ACS Nano **13**(2), 1870–1884 (2019). https://doi.org/10.1021/acsnano.8b08045
53. J. Han, L. Zhang, L. Hu, K. Xing, X. Lu et al., Nanozyme-based lateral flow assay for the sensitive detection of Escherichia coli O157: H7 in milk. J. Dairy Sci. **101**(7), 5770–5779 (2018). https://doi.org/10.3168/jds.2018-14429
54. X. Lin, Y. Liu, Z. Tao, J. Gao, J. Deng et al., Nanozyme-based bio-barcode assay for high sensitive and logic-controlled

specific detection of multiple DNAs. Biosens. Bioelectron. **94**, 471–477 (2017). https://doi.org/10.1016/j.bios.2017.01.008

55. L. Huang, W. Zhang, K. Chen, W. Zhu, X. Liu et al., Facet-selective response of trigger molecule to CeO2 1 1 0 for up-regulating oxidase-like activity. Chem. Eng. J. **330**, 746–752 (2017). https://doi.org/10.1016/j.cej.2017.08.026
56. J. Yao, Y. Cheng, M. Zhou, S. Zhao, S.C. Lin et al., ROS scavenging Mn_3O_4 nanozymes for in vivo anti-inflammation. Chem. Sci. **9**(11), 2927–2933 (2018). https://doi.org/10.1039/c7sc05476a
57. N. Cheng, Y. Song, M.M.A. Zeinhom, Y.C. Chang, L. Sheng et al., Nanozyme-mediated dual immunoassay integrated with smartphone for use in simultaneous detection of pathogens. ACS Appl. Mater. Interfaces **9**(46), 40671–40680 (2017). https://doi.org/10.1021/acsami.7b12734
58. J. Liu, L. Meng, Z. Fei, P.J. Dyson, L. Zhang, On the origin of the synergy between the Pt nanoparticles and MnO_2 nanosheets in Wonton-like 3D nanozyme oxidase mimics. Biosens. Bioelectron. **121**, 159–165 (2018). https://doi.org/10.1016/j.bios.2018.08.004
59. T. Zhang, F. Tian, L. Long, J. Liu, X. Wu, Diagnosis of rubella virus using antigen-conjugated Au@ Pt nanorods as nanozyme probe [Corrigendum]. Int. J. Nanomed. **14**, 1281–1282 (2019). https://doi.org/10.2147/IJN.S202056
60. H. Yang, R. Yang, P. Zhang, Y. Qin, T. Chen et al., A bimetallic (Co/2Fe) metal-organic framework with oxidase and peroxidase mimicking activity for colorimetric detection of hydrogen peroxide. Microchim. Acta **184**(12), 4629–4635 (2017). https://doi.org/10.1007/s00604-017-2509-4
61. C. Wang, C. Liu, J. Luo, Y. Tian, N. Zhou, Direct electrochemical detection of kanamycin based on peroxidase-like activity of gold nanoparticles. Anal. Chim. Acta **936**, 75–82 (2016). https://doi.org/10.1016/j.aca.2016.07.013
62. P. Weerathunge, R. Ramanathan, V.A. Torok, K. Hodgson, Y. Xu et al., Ultrasensitive colorimetric detection of murine norovirus using NanoZyme aptasensor. Anal. Chem. **91**(5), 3270–3276 (2019)
63. W. He, Y.-T. Zhou, W.G. Wamer, X. Hu, X. Wu et al., Intrinsic catalytic activity of Au nanoparticles with respect to hydrogen peroxide decomposition and superoxide scavenging. Biomaterials **34**(3), 765–773 (2013). https://doi.org/10.1016/j.Biomaterials2012.10.010
64. L. Long, R. Cai, J. Liu, X. Wu, A novel nanoprobe based on core–shell Au@Pt@Mesoporous SiO_2 nanozyme with enhanced activity and stability for mumps virus diagnosis. Front. Chem. **8**, 463 (2020). https://doi.org/10.3389/fchem.2020.00463
65. C. Wei, Y. Liu, X. Zhu, X. Chen, Y. Zhou et al., Iridium/ruthenium nanozyme reactors with cascade catalytic ability for synergistic oxidation therapy and starvation therapy in the treatment of breast cancer. Biomaterials **238**, 119848 (2020). https://doi.org/10.1016/j.Biomaterials2020.119848
66. B. Jiang, D. Duan, L. Gao, M. Zhou, K. Fan et al., Standardized assays for determining the catalytic activity and kinetics of peroxidase-like nanozymes. Nat. Protoc. **13**(7), 1506–1520 (2018). https://doi.org/10.1038/s41596-018-0001-1
67. C. Ge, G. Fang, X. Shen, Y. Chong, W.G. Wamer et al., Facet energy versus enzyme-like activities: the unexpected protection of palladium nanocrystals against oxidative damage. ACS Nano **10**(11), 10436–10445 (2016). https://doi.org/10.1021/acsnano.6b06297
68. F. Ratto, P. Matteini, F. Rossi, R. Pini, Size and shape control in the overgrowth of gold nanorods. J. Nanopart. Res. **12**(6), 2029–2036 (2010). https://doi.org/10.1007/s11051-009-9712-0
69. R. Das, A. Dhiman, A. Kapil, V. Bansal, T.K. Sharma, Aptamer-mediated colorimetric and electrochemical detection of Pseudomonas aeruginosa utilizing peroxidase-mimic activity of gold NanoZyme. Anal. Bioanal. Chem. **411**(6), 1229–1238 (2019). https://doi.org/10.1007/s00216-018-1555-z
70. Y. Li, X. Jian, S. Zhou, Y. Lu, C. Zhao et al., Protein shell-encapsulated pt clusters as continuous O_2-supplied biocoats for photodynamic therapy in hypoxic cancer cells. ACS Appl. Mater. Interfaces **11**(19), 17215–17225 (2019). https://doi.org/10.1021/acsami.9b02484
71. M. Cui, J. Zhou, Y. Zhao, Q. Song, Facile synthesis of iridium nanoparticles with superior peroxidase-like activity for colorimetric determination of H_2O_2 and xanthine. Sens. Actuators B-Chem. **243**, 203–210 (2017). https://doi.org/10.1016/j.snb.2016.11.145
72. A.J. Kora, Multifaceted activities of plant gum synthesised platinum nanoparticles: catalytic, peroxidase, PCR enhancing and antioxidant activities. IET Nanobiotechnol. **13**(6), 602–608 (2019)
73. J. Ali, N. Ali, L. Wang, H. Waseem, G. Pan, Revisiting the mechanistic pathways for bacterial mediated synthesis of noble metal nanoparticles. J. Microbiol. Methods **159**, 18–25 (2019). https://doi.org/10.1016/j.mimet.2019.02.010
74. K. Tapan, L. Sau Andrey, Nonspherical noble metal nanoparticles: colloid-chemical synthesis and morphology control. Adv. Mater. **22**(16), 1781–1804 (2010). https://doi.org/10.1002/adma.200901271
75. S. Biswas, P. Tripathi, N. Kumar, S. Nara, Gold nanorods as peroxidase mimetics and its application for colorimetric biosensing of malathion. Sens. Actuators B-Chem. **231**, 584–592 (2016). https://doi.org/10.1016/j.snb.2016.03.066
76. M. Sharifi, K. Faryabi, A.J. Talaei, M.S. Shekha, M. Ale-Ebrahim et al., Antioxidant properties of gold nanozyme: a review. J. Mol. Liq. **297**, 112004 (2020). https://doi.org/10.1016/j.molliq.2019.112004
77. L.T. Lanh, T.T. Hoa, N.D. Cuong, D.Q. Khieu, D.T. Quang et al., Shape and size controlled synthesis of Au nanorods: H_2S gas-sensing characterizations and antibacterial application. J. Alloys Compd. **635**, 265–271 (2015). https://doi.org/10.1016/j.jallcom.2015.02.146
78. G.-W. Wu, S.-B. He, H.-P. Peng, H.-H. Deng, A.-L. Liu et al., Citrate-capped platinum nanoparticle as a smart probe for ultrasensitive mercury sensing. Anal. Chem. **86**(21), 10955–10960 (2014). https://doi.org/10.1021/ac503544w

79. M.S. Hizir, M. Top, M. Balcioglu, M. Rana, N.M. Robertson et al., Multiplexed activity of perauxidase: DNA-capped AuNPs act as adjustable peroxidase. Anal. Chem. **88**(1), 600–605 (2016). https://doi.org/10.1021/acs.analchem.5b03926
80. C.P. Liu, T.H. Wu, C.Y. Liu, K.C. Chen, Y.X. Chen et al., Self-supplying O_2 through the catalase-like activity of gold nanoclusters for photodynamic therapy against hypoxic cancer cells. Small **13**(26), 9 (2017). https://doi.org/10.1002/smll.201700278
81. W. He, X. Han, H. Jia, J. Cai, Y. Zhou et al., AuPt alloy nanostructures with tunable composition and enzyme-like activities for colorimetric detection of bisulfide. Sci. Rep. **7**(1), 1–10 (2017). https://doi.org/10.1038/srep40103
82. S. Ge, W. Liu, H. Liu, F. Liu, J. Yu et al., Colorimetric detection of the flux of hydrogen peroxide released from living cells based on the high peroxidase-like catalytic performance of porous PtPd nanorods. Biosens. Bioelectron. **71**, 456–462 (2015). https://doi.org/10.1016/j.bios.2015.04.055
83. Q. Wang, L. Zhang, C. Shang, Z. Zhang, S. Dong, Triple-enzyme mimetic activity of nickel–palladium hollow nanoparticles and their application in colorimetric biosensing of glucose. Chem. Commun. **52**(31), 5410–5413 (2016). https://doi.org/10.1039/C6CC00194G
84. S. Cai, C. Qi, Y. Li, Q. Han, R. Yang et al., PtCo bimetallic nanoparticles with high oxidase-like catalytic activity and their applications for magnetic-enhanced colorimetric biosensing. J. Mater. Chem. B **4**(10), 1869–1877 (2016). https://doi.org/10.1039/C5TB02052B
85. W. He, X. Han, H. Jia, J. Cai, Y. Zhou et al., AuPt alloy nanostructures with tunable composition and enzyme-like activities for colorimetric detection of bisulfide. Sci. Rep. **7**(1), 40103 (2017). https://doi.org/10.1038/srep40103
86. V. Mariyappan, M. Keerthi, S.-M. Chen, G. Boopathy, Facile synthesis of α-Sm_2S_3/MoS_2 bimetallic sulfide as a high-performance electrochemical sensor for the detection of antineoplastic drug 5-fluorouracil in a biological samples. J. Electrochem. Soc. **167**(11), 117506 (2020). https://doi.org/10.1149/1945-7111/aba1a5
87. U. Jain, S. Gupta, N. Chauhan, Construction of an amperometric glycated hemoglobin biosensor based on Au–Pt bimetallic nanoparticles and poly (indole-5-carboxylic acid) modified Au electrode. Int. J. Biol. Macromol. **105**, 549–555 (2017). https://doi.org/10.1016/j.ijbiomac.2017.07.084
88. I. Taurino, G. Sanzò, R. Antiochia, C. Tortolini, F. Mazzei et al., Recent advances in third generation biosensors based on Au and Pt nanostructured electrodes. TrAC Trend. Anal. Chem. **79**, 151–159 (2016). https://doi.org/10.1016/j.trac.2016.01.020
89. T.L. Botha, E.E. Elemike, S. Horn, D.C. Onwudiwe, J.P. Giesy et al., Cytotoxicity of Ag, Au and Ag–Au bimetallic nanoparticles prepared using golden rod (*Solidago canadensis*) plant extract. Sci. Rep. **9**(1), 4169 (2019). https://doi.org/10.1038/s41598-019-40816-y
90. İ Aktitiz, R. Varol, N. Akkurt, M.F. Saraç, In-situ synthesis of 3D printable mono- and Bi-metallic (Cu/Ag) nanoparticles embedded polymeric structures with enhanced electromechanical properties. Polym. Test. **90**, 106724 (2020). https://doi.org/10.1016/j.polymertesting.2020.106724
91. S.A. Nadeem, S. Naz, J.S. Ali, A. Mannan et al., Synthesis, characterization and biological activities of monometallic and bimetallic nanoparticles using *Mirabilis jalapa* leaf extract. Biotechnol. Rep. **22**, e00338 (2019). https://doi.org/10.1016/j.btre.2019.e00338
92. S. Yallappa, J. Manjanna, B.L. Dhananjaya, Phytosynthesis of stable Au, Ag and Au–Ag alloy nanoparticles using *J. Sambac* leaves extract, and their enhanced antimicrobial activity in presence of organic antimicrobials. Spectrochim. Acta A **137**, 236–243 (2015). https://doi.org/10.1016/j.saa.2014.08.030
93. Y. Sun, J. Wang, W. Li, J. Zhang, Y. Zhang et al., DNA-stabilized bimetallic nanozyme and its application on colorimetric assay of biothiols. Biosens. Bioelectron. **74**, 1038–1046 (2015). https://doi.org/10.1016/j.bios.2015.08.001
94. Z. Zhu, Y. Zhai, C. Zhu, Z. Wang, S. Dong, Bimetallic alloy nanowires and nanosponges: a comparative study of peroxidase mimetics and as enhanced catalysts for oxygen reduction reaction. Electrochem. Commun. **36**, 22–25 (2013). https://doi.org/10.1016/j.elecom.2013.08.024
95. F.F. Tao, Synthesis, catalysis, surface chemistry and structure of bimetallic nanocatalysts. Chem. Soc. Rev. **41**(24), 7977–7979 (2012). https://doi.org/10.1039/C2CS90093A
96. R. Narayanan, M.A. El-Sayed, Catalysis with transition metal nanoparticles in colloidal solution: nanoparticle shape dependence and stability. J. Phys. Chem. B **109**(26), 12663–12676 (2005). https://doi.org/10.1021/jp051066p
97. J. Golchin, K. Golchin, N. Alidadian, S. Ghaderi, S. Eslamkhah et al., Nanozyme applications in biology and medicine: an overview. Artif. Cell. Nanomed. B **45**(6), 1069–1076 (2017). https://doi.org/10.1080/21691401.2017.1313268
98. B. Liu, J. Liu, Sensors and biosensors based on metal oxide nanomaterials. TrAC Trend. Anal. Chem. **121**, 115690 (2019). https://doi.org/10.1016/j.trac.2019.115690
99. L. Huang, Q. Zhu, J. Zhu, L. Luo, S. Pu et al., Portable colorimetric detection of mercury(II) Based on a non-noble metal nanozyme with tunable activity. Inorg. Chem. **58**(2), 1638–1646 (2019). https://doi.org/10.1021/acs.inorgchem.8b03193
100. Q. Wang, J. Jiang, L. Gao, Nanozyme-based medicine for enzymatic therapy: progress and challenges. Biomed. Mater. **16**(4), 042002 (2021). https://doi.org/10.1088/1748-605x/abe7b4
101. S.V. Salihov, Y.A. Ivanenkov, S.P. Krechetov, M.S. Veselov, N.V. Sviridenkova et al., Recent advances in the synthesis of Fe_3O_4@AU core/shell nanoparticles. J. Magn. Magn. Mater. **394**, 173–178 (2015). https://doi.org/10.1016/j.jmmm.2015.06.012
102. S. Likhitkar, A.K. Bajpai, Magnetically controlled release of cisplatin from superparamagnetic starch nanoparticles. Carbohydr. Polym. **87**(1), 300–308 (2012). https://doi.org/10.1016/j.carbpol.2011.07.053
103. J. Mu, L. Zhang, M. Zhao, Y. Wang, Co_3O_4 nanoparticles as an efficient catalase mimic: properties, mechanism and its

 https://doi.org/10.1007/s40820-021-00674-8

electrocatalytic sensing application for hydrogen peroxide. J. Mol. Catal. A-Chem. **378**, 30–37 (2013). https://doi.org/10.1016/j.molcata.2013.05.016

104. W. Qin, L. Su, C. Yang, Y. Ma, H. Zhang et al., Colorimetric detection of sulfite in foods by a TMB–O_2–Co_3O_4 nanoparticles detection system. J. Agric. Food Chem. **62**(25), 5827–5834 (2014). https://doi.org/10.1021/jf500950p
105. W. Li, G.-C. Fan, F. Gao, Y. Cui, W. Wang et al., High-activity Fe_3O_4 nanozyme as signal amplifier: a simple, low-cost but efficient strategy for ultrasensitive photoelectrochemical immunoassay. Biosens. Bioelectron. **127**, 64–71 (2019). https://doi.org/10.1016/j.bios.2018.11.043
106. J. Mu, X. Zhao, J. Li, E.-C. Yang, X.-J. Zhao, Novel hierarchical NiO nanoflowers exhibiting intrinsic superoxide dismutase-like activity. J. Mater. Chem. B **4**(31), 5217–5221 (2016). https://doi.org/10.1039/C6TB01390B
107. Q. Han, X. Wang, X. Liu, Y. Zhang, S. Cai et al., MoO_{3-x} nanodots with dual enzyme mimic activities as multifunctional modulators for amyloid assembly and neurotoxicity. J. Colloids Interface Sci. **539**, 575–584 (2019). https://doi.org/10.1016/j.jcis.2018.12.093
108. D.-X. Nie, G.-Y. Shi, Y.-Y. Yu, Fe_3O_4 magnetic nanoparticles as peroxidase mimetics used in colorimetric determination of 2,4-dinitrotoluene. Chin. J. Anal. Chem. **44**(2), 179–185 (2016). https://doi.org/10.1016/S1872-2040(16)60902-7
109. X. Ai, L. Wu, M. Zhang, X. Hou, L. Yang et al., Analytical method for the determination of trace toxic elements in milk based on combining Fe_3O_4 nanoparticles accelerated UV fenton-like digestion and solid phase extraction. J. Agric. Food Chem. **62**(34), 8586–8593 (2014). https://doi.org/10.1021/jf501638k
110. F.F. Peng, Y. Zhang, N. Gu, Size-dependent peroxidase-like catalytic activity of Fe_3O_4 nanoparticles. Chin. Chem. Lett. **19**(6), 730–733 (2008). https://doi.org/10.1016/j.cclet.2008.03.021
111. K. Zhang, W. Zuo, Z. Wang, J. Liu, T. Li et al., A simple route to $CoFe_2O_4$ nanoparticles with shape and size control and their tunable peroxidase-like activity. RSC Adv. **5**(14), 10632–10640 (2015). https://doi.org/10.1039/C4RA15675G
112. H.-P. Feng, L. Tang, G.-M. Zeng, Y. Zhou, Y.-C. Deng et al., Core-shell nanomaterials: applications in energy storage and conversion. Adv. Colloids Interface Sci. **267**, 26–46 (2019). https://doi.org/10.1016/j.cis.2019.03.001
113. A. Ángeles-Pascual, J.R. Piñón-Hernández, M. Estevez-González, U. Pal, S. Velumani et al., Structure, magnetic and cytotoxic behaviour of solvothermally grown Fe_3O_4@Au core-shell nanoparticles. Mater. Charact. **142**, 237–244 (2018). https://doi.org/10.1016/j.matchar.2018.05.041
114. M. Ye, Q. Zhang, Y. Hu, J. Ge, Z. Lu et al., Magnetically recoverable core–shell nanocomposites with enhanced photocatalytic activity. Chem. A Eur. J. **16**(21), 6243–6250 (2010). https://doi.org/10.1002/chem.200903516
115. J. Lu, B. Fu, M.C. Kung, G. Xiao, J.W. Elam et al., Coking- and sintering-resistant palladium catalysts achieved through atomic layer deposition. Science **335**(6073), 1205–1208 (2012). https://doi.org/10.1126/science.1212906
116. H. Su, Q. Tian, C.-A. Hurd Price, L. Xu, K. Qian et al., Nanoporous core@shell particles: design, preparation, applications in bioadsorption and biocatalysis. Nano Today **31**, 100834 (2020). https://doi.org/10.1016/j.nantod.2019.100834
117. O. Adeniyi, S. Sicwetsha, P. Mashazi, Nanomagnet-silica nanoparticles decorated with Au@Pd for enhanced peroxidase-like activity and colorimetric glucose sensing. ACS Appl. Mater. Interfaces **12**(2), 1973–1987 (2020). https://doi.org/10.1021/acsami.9b15123
118. L. Wang, K.G. Neoh, E.-T. Kang, B. Shuter, Multifunctional polyglycerol-grafted Fe_3O_4@SiO_2 nanoparticles for targeting ovarian cancer cells. Biomaterials **32**(8), 2166–2173 (2011). https://doi.org/10.1016/j.Biomaterials2010.11.042
119. Y. Yang, J. Shi, G. Kawamura, M. Nogami, Preparation of Au–Ag, Ag–Au core–shell bimetallic nanoparticles for surface-enhanced Raman scattering. Scr. Mater. **58**(10), 862–865 (2008). https://doi.org/10.1016/j.scriptamat.2008.01.017
120. T. Li, B. Albee, M. Alemayehu, R. Diaz, L. Ingham et al., Comparative toxicity study of Ag, Au, and Ag–Au bimetallic nanoparticles on *Daphnia magna*. Anal. Bioanal. Chem. **398**(2), 689–700 (2010). https://doi.org/10.1007/s00216-010-3915-1
121. Q. Zhang, I. Lee, J.B. Joo, F. Zaera, Y. Yin, Core–shell nanostructured catalysts. Acc. Chem. Res. **46**(8), 1816–1824 (2013). https://doi.org/10.1021/ar300230s
122. C. Zheng, W. Ke, T. Yin, X. An, Intrinsic peroxidase-like activity and the catalytic mechanism of gold@carbon dots nanocomposites. RSC Adv. **6**(42), 35280–35286 (2016). https://doi.org/10.1039/c6ra01917j
123. X. Liu, X. Wang, Q. Han, C. Qi, C. Wang et al., Facile synthesis of IrO_2/rGO nanocomposites with high peroxidase-like activity for sensitive colorimetric detection of low weight biothiols. Talanta **203**, 227–234 (2019). https://doi.org/10.1016/j.talanta.2019.05.070
124. A. Li, Y. Chen, L. Zhang, in *Hybrid Nanozyme: More Than One Plus One*. ed. by X. Yan (Springer, Singapore, 2020), pp. 367–391
125. B.F. Urbano, I. Villenas, B.L. Rivas, C.H. Campos, Cationic polymer–TiO_2 nanocomposite sorbent for arsenate removal. Chem. Eng. J. **268**, 362–370 (2015). https://doi.org/10.1016/j.cej.2015.01.068
126. Y. Zare, Estimation of material and interfacial/interphase properties in clay/polymer nanocomposites by yield strength data. Appl. Clay Sci. **115**, 61–66 (2015). https://doi.org/10.1016/j.clay.2015.07.021
127. Y. Zare, I. Shabani, Polymer/metal nanocomposites for biomedical applications. Mater. Sci. Eng. C **60**, 195–203 (2016). https://doi.org/10.1016/j.msec.2015.11.023
128. Y. Lin, Y. Huang, J. Ren, X. Qu, Incorporating ATP into biomimetic catalysts for realizing exceptional enzymatic performance over a broad temperature range. NPG Asia Mater. **6**(7), e114 (2014). https://doi.org/10.1038/am.2014.42
129. S. Venkateswarlu, M. Yoon, Core–shell ferromagnetic nanorod based on amine polymer composite (Fe_3O_4@DAPF) for fast removal of Pb(II) from aqueous solutions. ACS Appl.

Mater. Interfaces **7**(45), 25362–25372 (2015). https://doi.org/10.1021/acsami.5b07723

130. S. Yousefinejad, H. Rasti, M. Hajebi, M. Kowsari, S. Sadravi et al., Design of C-dots/Fe_3O_4 magnetic nanocomposite as an efficient new nanozyme and its application for determination of H_2O_2 in nanomolar level. Sens. Actuators B-Chem. **247**, 691–696 (2017). https://doi.org/10.1016/j.snb.2017.02.145
131. X. Ma, X. Ren, X. Guo, C. Fu, Q. Wu et al., Multifunctional iron-based metal−organic framework as biodegradable nanozyme for microwave enhancing dynamic therapy. Biomaterials **214**, 119223 (2019). https://doi.org/10.1016/j.Biomaterials2019.119223
132. L. Gao, X. Gao, X. Yan, in *Kinetics and Mechanisms for Nanozymes*. ed. by X. Yan (Springer, Singapore, 2020), pp. 17–39
133. W. Luo, C. Zhu, S. Su, D. Li, Y. He et al., Self-catalyzed, self-limiting growth of glucose oxidase-mimicking gold nanoparticles. ACS Nano **4**(12), 7451–7458 (2010). https://doi.org/10.1021/nn102592h
134. W. Li, B. Chen, H. Zhang, Y. Sun, J. Wang et al., BSA-stabilized Pt nanozyme for peroxidase mimetics and its application on colorimetric detection of mercury(II) ions. Biosens. Bioelectron. **66**, 251–258 (2015). https://doi.org/10.1016/j.bios.2014.11.032
135. L. Jin, Z. Meng, Y. Zhang, S. Cai, Z. Zhang et al., Ultrasmall Pt nanoclusters as robust peroxidase mimics for colorimetric detection of glucose in human serum. ACS Appl. Mater. Interfaces **9**(11), 10027–10033 (2017). https://doi.org/10.1021/acsami.7b01616
136. S.-B. He, F.-Q. Chen, L.-F. Xiu, H.-P. Peng, H.-H. Deng et al., Highly sensitive colorimetric sensor for detection of iodine ions using carboxylated chitosan-coated palladium nanozyme. Anal. Bioanal. Chem. **412**(2), 499–506 (2020). https://doi.org/10.1007/s00216-019-02270-7
137. G.-J. Cao, X. Jiang, H. Zhang, T.R. Croley, J.-J. Yin, Mimicking horseradish peroxidase and oxidase using ruthenium nanomaterials. RSC Adv. **7**(82), 52210–52217 (2017). https://doi.org/10.1039/C7RA10370K
138. L. Hu, Y. Yuan, L. Zhang, J. Zhao, S. Majeed et al., Copper nanoclusters as peroxidase mimetics and their applications to H_2O_2 and glucose detection. Anal. Chim. Acta **762**, 83–86 (2013). https://doi.org/10.1016/j.aca.2012.11.056
139. S. He, L. Yang, P. Balasubramanian, S. Li, H. Peng et al., Osmium nanozyme as peroxidase mimic with high performance and negligible interference of O_2. J. Mater. Chem. A **8**(47), 25226–25234 (2020). https://doi.org/10.1039/D0TA09247A
140. G. Jin, J. Liu, C. Wang, W. Gu, G. Ran et al., Ir nanoparticles with multi-enzyme activities and its application in the selective oxidation of aromatic alcohols. Appl. Catal. B-Environ. **267**, 118725 (2020). https://doi.org/10.1016/j.apcatb.2020.118725
141. T.G. Choleva, V.A. Gatselou, G.Z. Tsogas, D.L. Giokas, Intrinsic peroxidase-like activity of rhodium nanoparticles, and their application to the colorimetric determination of hydrogen peroxide and glucose. Microchim. Acta **185**(1), 22 (2017). https://doi.org/10.1007/s00604-017-2582-8
142. M. Wang, M. Chang, Q. Chen, D. Wang, C. Li et al., Au_2Pt-PEG-Ce6 nanoformulation with dual nanozyme activities for synergistic chemodynamic therapy/phototherapy. Biomaterials **252**, 120093 (2020). https://doi.org/10.1016/j.Biomaterials2020.120093
143. C.-X. Zhang, Y.-C. Gao, H.-W. Li, Y. Wu, Gold–platinum bimetallic nanoclusters for oxidase-like catalysis. ACS Appl. Nano Mater. **3**(9), 9318–9328 (2020). https://doi.org/10.1021/acsanm.0c01965
144. K. Shah, S. Bhagat, D. Varade, S. Singh, Novel synthesis of polyoxyethylene cholesteryl ether coated Fe–Pt nanoalloys: a multifunctional and cytocompatible bimetallic alloy exhibiting intrinsic chemical catalysis and biological enzyme-like activities. Colloids Surf. A-Physicochem. Eng. Asp. **553**, 50–57 (2018). https://doi.org/10.1016/j.colsurfa.2018.05.034
145. J. Ge, J.-H. Yu, H. Yang, D. Yang, R. Cai, Human serum albumin templated MnO_2 nanosheets as an efficient biomimetic oxidase for biomolecule sensing. J. Mater. Chem. B **8**(48), 11090–11095 (2020). https://doi.org/10.1039/D0TB01766C
146. J. Wang, H. Tao, T. Lu, Y. Wu, Adsorption enhanced the oxidase-mimicking catalytic activity of octahedral-shape Mn_3O_4 nanoparticles as a novel colorimetric chemosensor for ultrasensitive and selective detection of arsenic. J. Colloids Interface Sci. **584**, 114–124 (2021). https://doi.org/10.1016/j.jcis.2020.09.107
147. A. Dhall, A. Burns, J. Dowding, S. Das, S. Seal et al., Characterizing the phosphatase mimetic activity of cerium oxide nanoparticles and distinguishing its active site from that for catalase mimetic activity using anionic inhibitors. Environ. Sci. Nano **4**(8), 1742–1749 (2017). https://doi.org/10.1039/C7EN00394C
148. L. Huang, W. Zhang, K. Chen, W. Zhu, X. Liu et al., Facet-selective response of trigger molecule to CeO_2 110 for up-regulating oxidase-like activity. Chem. Eng. J. **330**, 746–752 (2017). https://doi.org/10.1016/j.cej.2017.08.026
149. X. Liu, L. Yan, H. Ren, Y. Cai, C. Liu et al., Facile synthesis of magnetic hierarchical flower-like Co_3O_4 spheres: mechanism, excellent tetra-enzyme mimics and their colorimetric biosensing applications. Biosens. Bioelectron. **165**, 112342 (2020). https://doi.org/10.1016/j.bios.2020.112342
150. D. Wei, X. Zhang, B. Chen, K. Zeng, Using bimetallic Au@Pt nanozymes as a visual tag and as an enzyme mimic in enhanced sensitive lateral-flow immunoassays: application for the detection of streptomycin. Anal. Chim. Acta **1126**, 106–113 (2020). https://doi.org/10.1016/j.aca.2020.06.009
151. F. Wei, X. Cui, Z. Wang, C. Dong, J. Li et al., Recoverable peroxidase-like Fe_3O_4@MoS_2-Ag nanozyme with enhanced antibacterial ability. Chem. Eng. J. **408**, 127240 (2021). https://doi.org/10.1016/j.cej.2020.127240
152. R. Zhang, N. Lu, J. Zhang, R. Yan, J. Li et al., Ultrasensitive aptamer-based protein assays based on one-dimensional core–shell nanozymes. Biosens. Bioelectron. **150**, 111881 (2020). https://doi.org/10.1016/j.bios.2019.111881

 https://doi.org/10.1007/s40820-021-00674-8

153. Y. Wang, H. Li, L. Guo, Q. Jiang, F. Liu, A cobalt-doped iron oxide nanozyme as a highly active peroxidase for renal tumor catalytic therapy. RSC Adv. **9**(33), 18815–18822 (2019). https://doi.org/10.1039/C8RA05487H

154. S. Bhagat, N.V. Srikanth Vallabani, V. Shutthanandan, M. Bowden, A.S. Karakoti et al., Gold core/ceria shell-based redox active nanozyme mimicking the biological multienzyme complex phenomenon. J. Colloids Interface Sci. **513**, 831–842 (2018). https://doi.org/10.1016/j.jcis.2017.11.064

155. Z. Wang, L. Chen, D. Wang, Z. Ding, X. Zhang et al., High-performance photocathodic bioanalysis based on core–shell structured Cu_2O@TiO_2 nanowire arrays with air–liquid–solid joint interfaces. CCS Chem. (2021). https://doi.org/10.31635/ccschem.021.202100842

156. J. Wang, P. Ni, C. Chen, Y. Jiang, C. Zhang et al., Colorimetric determination of the activity of alkaline phosphatase by exploiting the oxidase-like activity of palladium cube@CeO_2 core–shell nanoparticles. Microchim. Acta **187**(2), 115 (2020). https://doi.org/10.1007/s00604-019-4070-9

157. V.-K. Tran, P.K. Gupta, Y. Park, S.E. Son, W. Hur et al., Functionalized bimetallic IrPt alloy nanoparticles: multienzyme mimics for colorimetric and fluorometric detection of hydrogen peroxide and glucose. J. Taiwan Inst. Chem. Eng. **120**, 336–343 (2021). https://doi.org/10.1016/j.jtice.2021.03.029

158. W. Yang, J. Li, M. Wang, X. Sun, Y. Liu et al., A colorimetric strategy for ascorbic acid sensing based on the peroxidase-like activity of core–shell Fe_3O_4/CoFe-LDH hybrid. Colloids Surf. B-Biointerfaces **188**, 110742 (2020). https://doi.org/10.1016/j.colsurfb.2019.110742

159. S.-B. He, L. Yang, X.-L. Lin, L.-M. Chen, H.-P. Peng et al., Heparin-platinum nanozymes with enhanced oxidase-like activity for the colorimetric sensing of isoniazid. Talanta **211**, 120707 (2020). https://doi.org/10.1016/j.talanta.2019.120707

160. L. Liu, J. Du, W.-E. Liu, Y. Guo, G. Wu et al., Enhanced His@AuNCs oxidase-like activity by reduced graphene oxide and its application for colorimetric and electrochemical detection of nitrite. Anal. Bioanal. Chem. **411**(10), 2189–2200 (2019). https://doi.org/10.1007/s00216-019-01655-y

161. C.H. Tonial, M.F.F. Rodrigues, M.A. Bosse, I.M.O. Sousa, J.D. de Lima et al., Technical and economic evaluation of cultivation and obtaining of *Varronia curassavica* Jacq. Essent. Oil. Ind. Crop Prod. **154**, 12 (2020). https://doi.org/10.1016/j.indcrop.2020.112650

162. O.M. Ighodaro, O.A. Akinloye, First line defence antioxidants-superoxide dismutase (SOD), catalase (CAT) and glutathione peroxidase (GPX): their fundamental role in the entire antioxidant defence grid. Alex J. Med. **54**(4), 287–293 (2018). https://doi.org/10.1016/j.ajme.2017.09.001

163. F.M. Wang, E.G. Ju, Y.J. Guan, J.S. Ren, X.G. Qu, Light-mediated reversible modulation of ROS level in living cells by using an activity-controllable nanozyme. Small **13**(25), 6 (2017). https://doi.org/10.1002/smll.201603051

164. S. Bhagat, N.V.S. Vallabani, V. Shutthanandan, M. Bowden, A.S. Karakoti et al., Gold core/ceria shell-based redox active nanozyme mimicking the biological multienzyme complex phenomenon. J. Colloids Interface Sci. **513**, 831–842 (2018). https://doi.org/10.1016/j.jcis.2017.11.064

165. R. Singh, S. Singh, Redox-dependent catalase mimetic cerium oxide-based nanozyme protect human hepatic cells from 3-AT induced acatalasemia. Colloids Surf. B-Biointerfaces **175**, 625–635 (2019). https://doi.org/10.1016/j.colsurfb.2018.12.042

166. Y.-C. Ma, Y.-H. Zhu, X.-F. Tang, L.-F. Hang, W. Jiang et al., Au nanoparticles with enzyme-mimicking activity-ornamented ZIF-8 for highly efficient photodynamic therapy. Biomater. Sci. **7**(7), 2740–2748 (2019). https://doi.org/10.1039/C9BM00333A

167. J. Li, W. Liu, X. Wu, X. Gao, Mechanism of pH-switchable peroxidase and catalase-like activities of gold, silver, platinum and palladium. Biomaterials **48**, 37–44 (2015). https://doi.org/10.1016/j.Biomaterials2015.01.012

168. I. Celardo, J.Z. Pedersen, E. Traversa, L. Ghibelli, Pharmacological potential of cerium oxide nanoparticles. Nanoscale **3**(4), 1411–1420 (2011). https://doi.org/10.1039/C0NR00875C

169. C. Xu, X. Qu, Cerium oxide nanoparticle: a remarkably versatile rare earth nanomaterial for biological applications. NPG Asia Mater. **6**(3), e90 (2014). https://doi.org/10.1038/am.2013.88

170. S. Guo, Y. Han, L. Guo, Mechanistic study of catalase- and superoxide dismutation-mimic activities of cobalt oxide nanozyme from first-principles microkinetic modeling. Catal. Surv. Asia **24**(1), 70–85 (2020). https://doi.org/10.1007/s10563-019-09290-4

171. Z. Wang, X. Shen, X. Gao, Y. Zhao, Simultaneous enzyme mimicking and chemical reduction mechanisms for nanoceria as a bio-antioxidant: a catalytic model bridging computations and experiments for nanozymes. Nanoscale **11**(28), 13289–13299 (2019). https://doi.org/10.1039/c9nr03473k

172. M.A. Komkova, E.E. Karyakina, A.A. Karyakin, Catalytically synthesized Prussian blue nanoparticles defeating natural enzyme peroxidase. J. Am. Chem. Soc. **140**(36), 11302–11307 (2018). https://doi.org/10.1021/jacs.8b05223

173. H. Lück, in *Peroxidase*. ed. by H.-U. Bergmeyer (Academic Press, London, 1965), pp. 895–897

174. M. Behbahani, H. Mohabatkar, M. Nosrati, Analysis and comparison of lignin peroxidases between fungi and bacteria using three different modes of Chou's general pseudo amino acid composition. J. Theor. Biol. **411**, 1–5 (2016). https://doi.org/10.1016/j.jtbi.2016.09.001

175. A.O. Falade, U.U. Nwodo, B.C. Iweriebor, E. Green, L.V. Mabinya et al., Lignin peroxidase functionalities and prospective applications. MicrobiologyOpen **6**(1), e00394 (2017). https://doi.org/10.1002/mbo3.394

176. M. Khanmohammadi, M.B. Dastjerdi, A. Ai, A. Ahmadi, A. Godarzi et al., Horseradish peroxidase-catalyzed hydrogelation for biomedical applications. Biomater. Sci. **6**(6), 1286–1298 (2018). https://doi.org/10.1039/C8BM00056E

177. J. Duarte Baumer, A. Valério, S.M.A.G.U. de Souza, G.S. Erzinger, A. Furigo et al., Toxicity of enzymatically decolored textile dyes solution by horseradish peroxidase. J.

Hazard. Mater. **360**, 82–88 (2018). https://doi.org/10.1016/j.jhazmat.2018.07.102

178. R.A. Lawrence, R.F. Burk, Glutathione peroxidase activity in selenium-deficient rat liver. Biochem. Biophys. Res. Commun. **71**(4), 952–958 (1976). https://doi.org/10.1016/0006-291X(76)90747-6
179. H. Rekik, N. Zaraî Jaouadi, K. Bouacem, B. Zenati, S. Kourdali et al., Physical and enzymatic properties of a new manganese peroxidase from the white-rot fungus *Trametes pubescens* strain i8 for lignin biodegradation and textile-dyes biodecolorization. Int. J. Biol. Macromol. **125**, 514–525 (2019). https://doi.org/10.1016/j.ijbiomac.2018.12.053
180. M. Debnath, M. Dolai, K. Pal, A. Dutta, H.M. Lee et al., Two dinuclear oxidovanadium(V) complexes of N_2O_2 donor amine-bis(phenolate) ligands with bromo-peroxidase activities: kinetic, catalytic and computational studies. Inorg. Chim. Acta **480**, 149–158 (2018). https://doi.org/10.1016/j.ica.2018.04.044
181. X.Y. Wang, L. Qin, M. Zhou, Z.P. Lou, H. Wei, Nanozyme sensor arrays for detecting versatile analytes from small molecules to proteins and cells. Anal. Chem. **90**(19), 11696–11702 (2018). https://doi.org/10.1021/acs.analchem.8b03374
182. R. Walther, A.K. Winther, A.S. Fruergaard, W. van den Akker, L. Sorensen et al., Identification and directed development of non-organic catalysts with apparent pan-enzymatic mimicry into nanozymes for efficient prodrug conversion. Angew. Chem. Int. Ed. **58**(1), 278–282 (2019). https://doi.org/10.1002/anie.201812668
183. Z. Yang, C. Wang, X. Lu, Conducting polymer-based peroxidase mimics: synthesis, synergistic enhanced properties and applications. Sci. China Mater. **61**(5), 653–670 (2018). https://doi.org/10.1007/s40843-018-9235-3
184. H.-Q. Zheng, C.-Y. Liu, X.-Y. Zeng, J. Chen, J. Lü et al., MOF-808: a metal–organic framework with intrinsic peroxidase-like catalytic activity at neutral pH for colorimetric biosensing. Inorg. Chem. **57**(15), 9096–9104 (2018). https://doi.org/10.1021/acs.inorgchem.8b01097
185. B. Garg, T. Bisht, Carbon nanodots as peroxidase nanozymes for biosensing. Molecules **21**(12), 16 (2016). https://doi.org/10.3390/molecules21121653
186. X. Zhang, G. Li, G. Chen, D. Wu, X. Zhou et al., Single-atom nanozymes: a rising star for biosensing and biomedicine. Coord. Chem. Rev. **418**, 213376 (2020). https://doi.org/10.1016/j.ccr.2020.213376
187. N. Wang, L. Zhu, D. Wang, M. Wang, Z. Lin et al., Sono-assisted preparation of highly-efficient peroxidase-like Fe_3O_4 magnetic nanoparticles for catalytic removal of organic pollutants with H_2O_2. Ultrason. Sonochem. **17**(3), 526–533 (2010). https://doi.org/10.1016/j.ultsonch.2009.11.001
188. M.A. Voinov, J.O.S. Pagán, E. Morrison, T.I. Smirnova, A.I. Smirnov, Surface-mediated production of hydroxyl radicals as a mechanism of iron oxide nanoparticle biotoxicity. J. Am. Chem. Soc. **133**(1), 35–41 (2011). https://doi.org/10.1021/ja104683w
189. R. André, F. Natálio, M. Humanes, J. Leppin, K. Heinze et al., V_2O_5 Nanowires with an intrinsic peroxidase-like activity. Adv. Funct. Mater. **21**(3), 501–509 (2011). https://doi.org/10.1002/adfm.201001302
190. Y. Ding, B. Yang, H. Liu, Z. Liu, X. Zhang et al., FePt-Au ternary metallic nanoparticles with the enhanced peroxidase-like activity for ultrafast colorimetric detection of H_2O_2. Sensor. Actuators B-Chem. **259**, 775–783 (2018). https://doi.org/10.1016/j.snb.2017.12.115
191. J. Mu, Y. Wang, M. Zhao, L. Zhang, Intrinsic peroxidase-like activity and catalase-like activity of Co_3O_4 nanoparticles. Chem. Commun. **48**(19), 2540–2542 (2012). https://doi.org/10.1039/C2CC17013B
192. Y. Chong, Q. Liu, C. Ge, Advances in oxidase-mimicking nanozymes: classification, activity regulation and biomedical applications. Nano Today **37**, 101076 (2021). https://doi.org/10.1016/j.nantod.2021.101076
193. A.L. Hu, H.H. Deng, X.Q. Zheng, Y.Y. Wu, X.L. Lin et al., Self-cascade reaction catalyzed by CuO nanoparticle-based dual-functional enzyme mimics. Biosens. Bioelectron. **97**, 21–25 (2017). https://doi.org/10.1016/j.bios.2017.05.037
194. A.A. Vernekar, T. Das, S. Ghosh, G. Mugesh, A remarkably efficient $MnFe_2O_4$-based oxidase nanozyme. Chemistry **11**(1), 72–76 (2016). https://doi.org/10.1002/asia.201500942
195. X. Xu, S. Wu, D. Guo, X. Niu, Construction of a recyclable oxidase-mimicking Fe_3O_4@MnO_x-based colorimetric sensor array for quantifying and identifying chlorophenols. Anal. Chim. Acta **1107**, 203–212 (2020). https://doi.org/10.1016/j.aca.2020.02.024
196. X. Zhang, Y. Huang, Evaluation of the antioxidant activity of phenols and tannic acid determination with Mn_3O_4 nano-octahedrons as an oxidase mimic. Anal. Methods **7**(20), 8640–8646 (2015). https://doi.org/10.1039/C5AY01732G
197. H. Cheng, S. Lin, F. Muhammad, Y.-W. Lin, H. Wei, Rationally modulate the oxidase-like activity of nanoceria for self-regulated bioassays. ACS Sens. **1**(11), 1336–1343 (2016). https://doi.org/10.1021/acssensors.6b00500
198. R. Ragg, F. Natalio, M.N. Tahir, H. Janssen, A. Kashyap et al., Molybdenum trioxide nanoparticles with intrinsic sulfite oxidase activity. ACS Nano **8**(5), 5182–5189 (2014). https://doi.org/10.1021/nn501235j
199. M. Comotti, C. Della-Pina, E. Falletta, M. Rossi, Aerobic oxidation of glucose with gold catalyst: hydrogen peroxide as intermediate and reagent. Adv. Synth. Catal. **348**(3), 313–316 (2006). https://doi.org/10.1002/adsc.200505389
200. H. Zhang, T. Watanabe, M. Okumura, M. Haruta, N. Toshima, Catalytically highly active top gold atom on palladium nanocluster. Nat. Mater. **11**(1), 49–52 (2012). https://doi.org/10.1038/nmat3143
201. X. Zhang, X. Jiang, T.R. Croley, M.D. Boudreau, W. He et al., Ferroxidase-like and antibacterial activity of PtCu alloy nanoparticles. J. Environ. Sci. Health Pt. C **37**(2), 99–115 (2019). https://doi.org/10.1080/10590501.2019.1602991
202. Y. Liu, H. Wu, Y. Chong, W.G. Wamer, Q. Xia et al., Platinum nanoparticles: efficient and stable catechol oxidase mimetics. ACS Appl. Mater. Interfaces **7**(35), 19709–19717 (2015). https://doi.org/10.1021/acsami.5b05180

 https://doi.org/10.1007/s40820-021-00674-8

203. J. Liu, X. Jiang, L. Wang, Z. Hu, T. Wen et al., Ferroxidase-like activity of Au nanorod/Pt nanodot structures and implications for cellular oxidative stress. Nano Res. **8**(12), 4024–4037 (2015). https://doi.org/10.1007/s12274-015-0904-x
204. M. Chen, Z. Wang, J. Shu, X. Jiang, W. Wang et al., Mimicking a natural enzyme system: cytochrome c oxidase-like activity of Cu_2O nanoparticles by receiving electrons from cytochrome c. Inorg. Chem. **56**(16), 9400–9403 (2017). https://doi.org/10.1021/acs.inorgchem.7b01393
205. Y. Zhang, Y. Jin, H. Cui, X. Yan, K. Fan, Nanozyme-based catalytic Theranostics. RSC Adv. **10**(1), 10–20 (2020). https://doi.org/10.1039/C9RA09021E
206. H. Bayr, Reactive oxygen species. Crit. Care Med. **33**(12), S498–S501 (2005). https://doi.org/10.1097/01.CCM.0000186787.64500.12
207. G. Wu, V. Berka, P.J. Derry, K. Mendoza, E. Kakadiaris et al., Critical comparison of the superoxide dismutase-like activity of carbon antioxidant nanozymes by direct superoxide consumption kinetic measurements. ACS Nano **13**(10), 11203–11213 (2019). https://doi.org/10.1021/acsnano.9b04229
208. N. Singh, M. Geethika, S.M. Eswarappa, G. Mugesh, Manganese-based nanozymes: multienzyme redox activity and effect on the nitric oxide produced by endothelial nitric oxide synthase. Chem.-Eur. J. **24**(33), 8393–8403 (2018). https://doi.org/10.1002/chem.201800770
209. Y.Y. Huang, Z. Liu, C.Q. Liu, E.G. Ju, Y. Zhang et al., Self-assembly of multi-nanozymes to mimic an intracellular antioxidant defense system. Angew. Chem. Int. Ed. **55**(23), 6646–6650 (2016). https://doi.org/10.1002/anie.201600868
210. C. Korsvik, S. Patil, S. Seal, W.T. Self, Superoxide dismutase mimetic properties exhibited by vacancy engineered ceria nanoparticles. Chem. Commun. **10**, 1056–1058 (2007). https://doi.org/10.1039/B615134E
211. J.-D. Cafun, K.O. Kvashnina, E. Casals, V.F. Puntes, P. Glatzel, Absence of Ce^{3+} sites in chemically active colloidal ceria nanoparticles. ACS Nano **7**(12), 10726–10732 (2013). https://doi.org/10.1021/nn403542p
212. S. Guo, L. Guo, Unraveling the multi-enzyme-like activities of iron oxide nanozyme via a first-principles microkinetic study. J. Phys. Chem. C **123**(50), 30318–30334 (2019). https://doi.org/10.1021/acs.jpcc.9b07802
213. L. Pasquato, F. Rancan, P. Scrimin, F. Mancin, C. Frigeri, Methylimidazole-functionalized gold nanoparticles as catalysts for cleavage of a carboxylic acid ester. Chem. Commun. **22**, 2253–2254 (2000). https://doi.org/10.1039/B005244M
214. R. Bonomi, F. Selvestrel, V. Lombardo, C. Sissi, S. Polizzi et al., Phosphate diester and DNA hydrolysis by a multivalent, nanoparticle-based catalyst. J. Am. Chem. Soc. **130**(47), 15744–15745 (2008). https://doi.org/10.1021/ja801794t
215. P. Pengo, S. Polizzi, L. Pasquato, P. Scrimin, Carboxylate–imidazole cooperativity in dipeptide-functionalized gold nanoparticles with esterase-like activity. J. Am. Chem. Soc. **127**(6), 1616–1617 (2005). https://doi.org/10.1021/ja043547c
216. D. Kisailus, M. Najarian, J.C. Weaver, D.E. Morse, Functionalized gold nanoparticles mimic catalytic activity of a polysiloxane-synthesizing enzyme. Adv. Mater. **17**(10), 1234–1239 (2005). https://doi.org/10.1002/adma.200401109
217. Y. Lin, J. Ren, X. Qu, Nano-gold as artificial enzymes: hidden talents. Adv. Mater. **26**(25), 4200–4217 (2014). https://doi.org/10.1002/adma.201400238
218. M.H. Kuchma, C.B. Komanski, J. Colon, A. Teblum, A.E. Masunov et al., Phosphate ester hydrolysis of biologically relevant molecules by cerium oxide nanoparticles. Nanomed.-Nanotechnol. Biol. Med. **6**(6), 738–744 (2010). https://doi.org/10.1016/j.nano.2010.05.004
219. G. Cheng, J.-L. Zhang, Y.-L. Liu, D.-H. Sun, J.-Z. Ni, Synthesis of novel $Fe_3O_4@SiO_2@CeO_2$ microspheres with mesoporous shell for phosphopeptide capturing and labeling. Chem. Commun. **47**(20), 5732–5734 (2011). https://doi.org/10.1039/C1CC10533G
220. C. Xu, Z. Liu, L. Wu, J. Ren, X. Qu, Nucleoside Triphosphates as promoters to enhance nanoceria enzyme-like activity and for single-nucleotide polymorphism typing. Adv. Funct. Mater. **24**(11), 1624–1630 (2014). https://doi.org/10.1002/adfm.201301649
221. R. Tian, J. Sun, Y. Qi, B. Zhang, S. Guo et al., Influence of VO_2 nanoparticle morphology on the colorimetric assay of H_2O_2 and glucose. Nanomaterials **7**(11), 347 (2017). https://doi.org/10.3390/nano7110347
222. N. Singh, M.A. Savanur, S. Srivastava, P. D'Silva, G. Mugesh, A redox modulatory Mn_3O_4 nanozyme with multi-enzyme activity provides efficient cytoprotection to human cells in a Parkinson's disease model. Angew. Chem. Int. Ed. **129**(45), 14455–14459 (2017). https://doi.org/10.1002/anie.201708573
223. S. Liu, F. Lu, R. Xing, J.-J. Zhu, Structural effects of Fe_3O_4 nanocrystals on peroxidase-like activity. Chem. Eur. J. **17**(2), 620–625 (2011). https://doi.org/10.1002/chem.201001789
224. J. Mu, L. Zhang, M. Zhao, Y. Wang, Catalase mimic property of Co_3O_4 nanomaterials with different morphology and its application as a calcium sensor. ACS Appl. Mater. Interfaces **6**(10), 7090–7098 (2014). https://doi.org/10.1021/am406033q
225. G. Fang, W. Li, X. Shen, J.M. Perez-Aguilar, Y. Chong et al., Differential Pd-nanocrystal facets demonstrate distinct antibacterial activity against Gram-positive and Gram-negative bacteria. Nat. Commun. **9**(1), 129 (2018). https://doi.org/10.1038/s41467-017-02502-3
226. K.N. Han, J.-S. Choi, J. Kwon, Gold nanozyme-based paper chip for colorimetric detection of mercury ions. Sci. Rep. **7**(1), 1–7 (2017). https://doi.org/10.1038/s41598-017-02948-x
227. V. Baldim, F. Bedioui, N. Mignet, I. Margaill, J.F. Berret, The enzyme-like catalytic activity of cerium oxide nanoparticles and its dependency on Ce^{3+} surface area concentration. Nanoscale **10**(15), 6971–6980 (2018). https://doi.org/10.1039/C8NR00325D
228. Y. Liu, Y. Xiang, D. Ding, R. Guo, Structural effects of amphiphilic protein/gold nanoparticle hybrid based nanozyme on peroxidase-like activity and silver-mediated

inhibition. RSC Adv. **6**(113), 112435–112444 (2016). https://doi.org/10.1039/C6RA23773H

229. T. Pirmohamed, J.M. Dowding, S. Singh, B. Wasserman, E. Heckert et al., Nanoceria exhibit redox state-dependent catalase mimetic activity. Chem. Commun. **46**(16), 2736–2738 (2010). https://doi.org/10.1039/B922024K
230. E.G. Heckert, A.S. Karakoti, S. Seal, W.T. Self, The role of cerium redox state in the SOD mimetic activity of nanoceria. Biomaterials **29**(18), 2705–2709 (2008). https://doi.org/10.1016/j.Biomaterials2008.03.014
231. X. Wang, W. Cao, L. Qin, T. Lin, W. Chen et al., Boosting the peroxidase-like activity of nanostructured nickel by inducing its 3+ oxidation state in lanio(3) perovskite and its application for biomedical assays. Theranostics **7**(8), 2277–2286 (2017). https://doi.org/10.7150/thno.19257
232. J. Xi, G. Wei, L. An, Z. Xu, Z. Xu et al., Copper/carbon hybrid nanozyme: tuning catalytic activity by the copper state for antibacterial therapy. Nano Lett. **19**(11), 7645–7654 (2019). https://doi.org/10.1021/acs.nanolett.9b02242
233. X. Fan, B. Cai, R. Du, R. Hübner, M. Georgi et al., Ligand-exchange-mediated fabrication of gold aerogels containing different Au(I) content with peroxidase-like behavior. Chem. Mater. **31**(24), 10094–10099 (2019). https://doi.org/10.1021/acs.chemmater.9b03121
234. M. Sun, H. Qian, J. Liu, Y. Li, S. Pang et al., A flexible conductive film prepared by the oriented stacking of Ag and Au/Ag alloy nanoplates and its chemically roughened surface for explosive SERS detection and cell adhesion. RSC Adv. **7**(12), 7073–7078 (2017). https://doi.org/10.1039/C6RA25956A
235. L. Chen, J.M. Chabu, Y. Liu, Bimetallic AgM (M= Pt, Pd, Au) nanostructures: synthesis and applications for surface-enhanced Raman scattering. RSC Adv. **3**(13), 4391–4399 (2013). https://doi.org/10.1039/C3RA23137B
236. W. He, X. Wu, J. Liu, X. Hu, K. Zhang et al., Design of AgM bimetallic alloy nanostructures (M = Au, Pd, Pt) with tunable morphology and peroxidase-like activity. Chem. Mater. **22**(9), 2988–2994 (2010). https://doi.org/10.1021/cm100393v
237. K. Zhang, X. Hu, J. Liu, J.-J. Yin, S. Hou et al., Formation of PdPt alloy nanodots on gold nanorods: tuning oxidase-like activities via composition. Langmuir **27**(6), 2796–2803 (2011). https://doi.org/10.1021/la104566e
238. Y. Wang, H. Zhao, H. Song, J. Dong, J. Xu, Monodispersed gold nanoparticles entrapped in ordered mesoporous carbon/silica nanocomposites as xanthine oxidase mimic for electrochemical sensing of xanthine. Microchim. Acta **187**(10), 543 (2020). https://doi.org/10.1007/s00604-020-04494-2
239. C. Liu, Y. Yan, X. Zhang, Y. Mao, X. Ren et al., Regulating the pro- and anti-oxidant capabilities of bimetallic nanozymes for the detection of Fe^{2+} and protection of Monascus pigments. Nanoscale **12**(5), 3068–3075 (2020). https://doi.org/10.1039/C9NR10135G
240. X. Xia, J. Zhang, N. Lu, M.J. Kim, K. Ghale et al., Pd–Ir core–shell nanocubes: a type of highly efficient and versatile peroxidase mimic. ACS Nano **9**(10), 9994–10004 (2015). https://doi.org/10.1021/acsnano.5b03525
241. S. Zeng, W. Zhang, N. Liu, H. Su, Inverse CeO_2/CuO catalysts prepared by hydrothermal method for preferential CO oxidation. Catal. Lett. **143**(10), 1018–1024 (2013). https://doi.org/10.1007/s10562-013-1065-8
242. I. Yeriskin, M. Nolan, Effect of La doping on CO adsorption at ceria surfaces. J. Chem. Phys. **131**(24), 244702 (2009). https://doi.org/10.1063/1.3271910
243. J. Qin, J. Lu, M. Cao, C. Hu, Synthesis of porous CuO–CeO_2 nanospheres with an enhanced low-temperature CO oxidation activity. Nanoscale **2**(12), 2739–2743 (2010). https://doi.org/10.1039/C0NR00446D
244. J. Wang, S. Lin, Z. Han, Y. Liu, Glutamine-assisted synthesis of Cu-doped CeO_2 nanowires with an improved low-temperature CO oxidation activity. RSC Adv. **5**(36), 28619–28623 (2015). https://doi.org/10.1039/C4RA16556J
245. S. Zhang, Y. Liu, S. Sun, J. Wang, Q. Li et al., Catalytic patch with redox Cr/CeO(2) nanozyme of noninvasive intervention for brain trauma. Theranostics **11**(6), 2806–2821 (2021). https://doi.org/10.7150/thno.51912
246. D. Jampaiah, T. Srinivasa Reddy, A.E. Kandjani, P.R. Selvakannan, Y.M. Sabri et al., Fe-doped CeO_2 nanorods for enhanced peroxidase-like activity and their application towards glucose detection. J. Mater. Chem. B **4**(22), 3874–3885 (2016). https://doi.org/10.1039/c6tb00422a
247. B. Liu, Z. Huang, J. Liu, Boosting the oxidase mimicking activity of nanoceria by fluoride capping: rivaling protein enzymes and ultrasensitive F-detection. Nanoscale **8**(28), 13562–13567 (2016). https://doi.org/10.1039/C6NR02730J
248. J. Lian, P. Liu, C. Jin, Z. Shi, X. Luo et al., Perylene diimide-functionalized CeO_2 nanocomposite as a peroxidase mimic for colorimetric determination of hydrogen peroxide and glutathione. Microchim. Acta **186**(6), 332 (2019). https://doi.org/10.1007/s00604-019-3439-0
249. M. Parra-Robert, M. Zeng, Y. Shu, G. Fernández-Varo, M. Perramón et al., Mesoporous silica coated CeO_2 nanozymes with combined lipid-lowering and antioxidant activity induce long-term improvement of the metabolic profile in obese Zucker rats. Nanoscale (2021). https://doi.org/10.1039/D1NR00790D
250. X. Meng, I. Zare, X. Yan, K. Fan, Protein-protected metal nanoclusters: an emerging ultra-small nanozyme. WIREs Nanomed. Nanobiotechnol. **12**(3), e1602 (2020). https://doi.org/10.1002/wnan.1602
251. R.S. Aparna, J.S.A. Devi, J. Nebu, S.S. Syamchand, S. George, Rapid response of dopamine towards insitu synthesised copper nanocluster in presence of H_2O_2. J. Photochem. Photobiol. A-Chem. **379**, 63–71 (2019). https://doi.org/10.1016/j.jphotochem.2019.04.043
252. B. Liu, J. Liu, Accelerating peroxidase mimicking nanozymes using DNA. Nanoscale **7**(33), 13831–13835 (2015). https://doi.org/10.1039/C5NR04176G
253. J. Huo, J. Hao, J. Mu, Y. Wang, Surface modification of Co_3O_4 nanoplates as efficient peroxidase nanozymes for biosensing application. ACS Appl. Bio. Mater. **4**(4), 3443–3452 (2021). https://doi.org/10.1021/acsabm.1c00017

 https://doi.org/10.1007/s40820-021-00674-8

254. Y. Yue, H. Wei, J. Guo, Y. Yang, Ceria-based peroxidase-mimicking nanozyme with enhanced activity: a coordination chemistry strategy. Colloid Surf. A-Physicochem. Eng. Asp. **610**, 125715 (2021). https://doi.org/10.1016/j.colsurfa.2020.125715
255. Y. Zhao, Y. Wang, A. Mathur, Y. Wang, V. Maheshwari et al., Fluoride-capped nanoceria as a highly efficient oxidase-mimicking nanozyme: inhibiting product adsorption and increasing oxygen vacancies. Nanoscale **11**(38), 17841–17850 (2019). https://doi.org/10.1039/C9NR05346H
256. G. Darabdhara, B. Sharma, M.R. Das, R. Boukherroub, S. Szunerits, Cu–Ag bimetallic nanoparticles on reduced graphene oxide nanosheets as peroxidase mimic for glucose and ascorbic acid detection. Sensor. Actuators B-Chem. **238**, 842–851 (2017). https://doi.org/10.1016/j.snb.2016.07.106
257. C. Xie, X. Wen, C. Xiao, S. Wei, X. Wu et al., Copper nanoclusters/red globe flower carbon as a fenton-like catalyst for the degradation of amido black 10B. Water Air Soil Pollut. **231**(6), 280 (2020). https://doi.org/10.1007/s11270-020-04539-5
258. H. Su, D.-D. Liu, M. Zhao, W.-L. Hu, S.-S. Xue et al., Dual-enzyme characteristics of polyvinylpyrrolidone-capped iridium nanoparticles and their cellular protective effect against H_2O_2-induced oxidative damage. ACS Appl. Mater. Interfaces **7**(15), 8233–8242 (2015). https://doi.org/10.1021/acsami.5b01271
259. T. Li, P. Hu, J. Li, P. Huang, W. Tong et al., Enhanced peroxidase-like activity of Fe@PCN-224 nanoparticles and their applications for detection of H_2O_2 and glucose. Colloids Surf. A-Physicochem. Eng. Asp. **577**, 456–463 (2019). https://doi.org/10.1016/j.colsurfa.2019.06.012
260. A.P. Nagvenkar, A. Gedanken, $Cu_{0.89}Zn_{0.11}O$, A new peroxidase-mimicking nanozyme with high sensitivity for glucose and antioxidant detection. ACS Appl. Mater. Inter. **8**(34), 22301–22308 (2016). https://doi.org/10.1021/acsami.6b05354
261. Y. Liu, H. Wu, M. Li, J.-J. Yin, Z. Nie, pH dependent catalytic activities of platinum nanoparticles with respect to the decomposition of hydrogen peroxide and scavenging of superoxide and singlet oxygen. Nanoscale **6**(20), 11904–11910 (2014). https://doi.org/10.1039/c4nr03848g
262. W. He, Y.-T. Zhou, W.G. Wamer, M.D. Boudreau, J.-J. Yin, Mechanisms of the pH dependent generation of hydroxyl radicals and oxygen induced by Ag nanoparticles. Biomaterials **33**(30), 7547–7555 (2012). https://doi.org/10.1016/j.Biomaterials2012.06.076
263. B. Unnikrishnan, C.-W. Lien, H.-W. Chu, C.-C. Huang, A review on metal nanozyme-based sensing of heavy metal ions: challenges and future perspectives. J. Hazard. Mater. **401**, 123397 (2021). https://doi.org/10.1016/j.jhazmat.2020.123397
264. Y. Liu, Y. Zheng, D. Ding, R. Guo, Switching peroxidase-mimic activity of protein stabilized platinum nanozymes by sulfide ions: substrate dependence, mechanism, and detection. Langmuir **33**(48), 13811–13820 (2017). https://doi.org/10.1021/acs.langmuir.7b03430
265. C.-F. Peng, Y.-Y. Zhang, L.-Y. Wang, Z.-Y. Jin, G. Shao, Colorimetric assay for the simultaneous detection of Hg^{2+} and Ag^{+} based on inhibiting the peroxidase-like activity of core–shell Au@Pt nanoparticles. Anal. Methods **9**(30), 4363–4370 (2017). https://doi.org/10.1039/C7AY01317E
266. H. Deng, S. He, X. Lin, L. Yang, Z. Lin et al., Target-triggered inhibiting oxidase-mimicking activity of platinum nanoparticles for ultrasensitive colorimetric detection of silver ion. Chin. Chem. Lett. **30**(9), 1659–1662 (2019). https://doi.org/10.1016/j.cclet.2019.05.032
267. Z.-J. Xie, M.-R. Shi, L.-Y. Wang, C.-F. Peng, X.-L. Wei, Colorimetric determination of Pb^{2+} ions based on surface leaching of Au@Pt nanoparticles as peroxidase mimic. Microchim. Acta **187**(4), 255 (2020). https://doi.org/10.1007/s00604-020-04234-6
268. W. Zhang, X. Niu, S. Meng, X. Li, Y. He et al., Histidine-mediated tunable peroxidase-like activity of nanosized Pd for photometric sensing of Ag+. Sens. Actuators B-Chem. **273**, 400–407 (2018). https://doi.org/10.1016/j.snb.2018.06.071
269. Y. Liu, D. Ding, Y. Zhen, R. Guo, Amino acid-mediated 'turn-off/turn-on' nanozyme activity of gold nanoclusters for sensitive and selective detection of copper ions and histidine. Biosens. Bioelectron. **92**, 140–146 (2017). https://doi.org/10.1016/j.bios.2017.01.036
270. L. Han, H. Zhang, F. Li, Bioinspired nanozymes with pH-independent and metal ions-controllable activity: field-programmable logic conversion of sole logic gate system. Part. Part. Syst. Charact. **35**(9), 1800207 (2018)
271. C. Wang, H. Wang, B. Xu, H. Liu, Photo-responsive nanozymes: mechanism, activity regulation, and biomedical applications. VIEW **2**(1), 20200045 (2021). https://doi.org/10.1002/VIW.20200045
272. H. Wang, W. Yang, X. Wang, L. Huang, Y. Zhang et al., A CeO_2@MnO_2 core–shell hollow heterojunction as glucose oxidase-like photoenzyme for photoelectrochemical sensing of glucose. Sens. Actuat. B-Chem. **304**, 127389 (2020). https://doi.org/10.1016/j.snb.2019.127389
273. H. Yang, B. Xu, S. Li, Q. Wu, M. Lu et al., A photoresponsive nanozyme for synergistic catalytic therapy and dual phototherapy. Small **17**(10), 2007090 (2021). https://doi.org/10.1002/smll.202007090
274. Q. Zhang, S. Chen, H. Wang, A surface plasmon-enhanced nanozyme-based fenton process for visible-light-driven aqueous ammonia oxidation. Green Chem. **20**(17), 4067–4074 (2018). https://doi.org/10.1039/C8GC01317A
275. M. Zhu, Y. Dai, Y. Wu, K. Liu, X. Qi et al., Bandgap control of α-Fe_2O_3 nanozymes and their superior visible light promoted peroxidase-like catalytic activity. Nanotechnology **29**(46), 465704 (2018). https://doi.org/10.1088/1361-6528/aaddc2
276. F. Wang, E. Ju, Y. Guan, J. Ren, X. Qu, Light-mediated reversible modulation of ROS level in living cells by using an activity-controllable nanozyme. Small **13**(25), 1603051 (2017). https://doi.org/10.1002/smll.201603051
277. N.V.S. Vallabani, A.S. Karakoti, S. Singh, ATP-mediated intrinsic peroxidase-like activity of Fe_3O_4-based nanozyme:

one step detection of blood glucose at physiological pH. Colloids Surf. B-Biointerfaces **153**, 52–60 (2017). https://doi.org/10.1016/j.colsurfb.2017.02.004

278. H. Jia, D. Yang, X. Han, J. Cai, H. Liu et al., Peroxidase-like activity of the Co_3O_4 nanoparticles used for biodetection and evaluation of antioxidant behavior. Nanoscale **8**(11), 5938–5945 (2016). https://doi.org/10.1039/C6NR00860G
279. P. Gallay, M. Eguílaz, G. Rivas, Designing electrochemical interfaces based on nanohybrids of avidin functionalized-carbon nanotubes and ruthenium nanoparticles as peroxidase-like nanozyme with supramolecular recognition properties for site-specific anchoring of biotinylated residues. Biosens. Bioelectron. **148**, 111764 (2020). https://doi.org/10.1016/j.bios.2019.111764
280. S. Cai, K. Lao, C. Lau, J. Lu, "Turn-On" chemiluminescence sensor for the highly selective and ultrasensitive detection of Hg^{2+} ions based on interstrand cooperative coordination and catalytic formation of gold nanoparticles. Anal. Chem. **83**(24), 9702–9708 (2011). https://doi.org/10.1021/ac202789q
281. Y.-Y. Chen, H.-T. Chang, Y.-C. Shiang, Y.-L. Hung, C.-K. Chiang et al., Colorimetric assay for lead ions based on the leaching of gold nanoparticles. Anal. Chem. **81**(22), 9433–9439 (2009). https://doi.org/10.1021/ac9018268
282. S. Mao, J. Chang, G. Zhou, J. Chen, Nanomaterial-enabled rapid detection of water contaminants. Small **11**(40), 5336–5359 (2015). https://doi.org/10.1002/smll.201500831
283. C.-W. Tseng, H.-Y. Chang, J.-Y. Chang, C.-C. Huang, Detection of mercury ions based on mercury-induced switching of enzyme-like activity of platinum/gold nanoparticles. Nanoscale **4**(21), 6823–6830 (2012). https://doi.org/10.1039/C2NR31716H
284. C.-W. Lien, Y.-T. Tseng, C.-C. Huang, H.-T. Chang, Logic control of enzyme-like gold nanoparticles for selective detection of lead and mercury ions. Anal. Chem. **86**(4), 2065–2072 (2014). https://doi.org/10.1021/ac4036789
285. Y.-S. Wu, F.-F. Huang, Y.-W. Lin, Fluorescent detection of lead in environmental water and urine samples using enzyme mimics of catechin-synthesized Au nanoparticles. ACS Appl. Mater. Interfaces **5**(4), 1503–1509 (2013). https://doi.org/10.1021/am3030454
286. L. Luo, Z. Su, J. Zhuo, L. Huang, Y. Nian et al., Copper-sensitized "turn on" peroxidase-like activity of $MMoO_4$ (M = Co, Ni) flowers for selective detection of aquatic copper ions. ACS Sustain. Chem. Eng. **8**(33), 12568–12576 (2020). https://doi.org/10.1021/acssuschemeng.0c03822
287. L.-L. Wu, L.-Y. Wang, Z.-J. Xie, F. Xue, C.-F. Peng, Colorimetric detection of Hg^{2+} based on inhibiting the peroxidase-like activity of DNA–Ag/Pt nanoclusters. RSC Adv. **6**(79), 75384–75389 (2016). https://doi.org/10.1039/C6RA12597B
288. H. Yang, Y. Xiong, P. Zhang, L. Su, F. Ye, Colorimetric detection of mercury ions using MnO_2 nanorods as enzyme mimics. Anal. Methods **7**(11), 4596–4601 (2015). https://doi.org/10.1039/C5AY00633C
289. X. Shi, W. Gu, C. Zhang, L. Zhao, W. Peng et al., A label-free colorimetric sensor for Pb^{2+} detection based on the acceleration of gold leaching by graphene oxide. Dalton Trans. **44**(10), 4623–4629 (2015). https://doi.org/10.1039/C4DT03883E
290. Y. Zhang, Y. Leng, L. Miao, J. Xin, A. Wu, The colorimetric detection of Pb^{2+} by using sodium thiosulfate and hexadecyl trimethyl ammonium bromide modified gold nanoparticles. Dalton Trans. **42**(15), 5485–5490 (2013). https://doi.org/10.1039/C3DT32532F
291. Z.-J. Xie, M.-R. Shi, L.-Y. Wang, C.-F. Peng, X.-L. Wei, Colorimetric determination of Pb^{2+} ions based on surface leaching of Au@Pt nanoparticles as peroxidase mimic. Microchim. Acta **187**, 1–7 (2020). https://doi.org/10.1007/s00604-020-04234-6
292. L. Gao, X. Yan, Nanozymes: an emerging field bridging nanotechnology and biology. Sci. China Life Sci. **59**(4), 400–402 (2016). https://doi.org/10.1007/s11427-016-5044-3
293. N. Logan, C. McVey, C. Elliott, C. Cao, Amalgamated gold-nanoalloys with enhanced catalytic activity for the detection of mercury ions (Hg^{2+}) in seawater samples. Nano Res. (2020). https://doi.org/10.1007/s12274-020-2731-y
294. D. Ou, D. Sun, X. Lin, Z. Liang, Y. Zhong et al., A dual-aptamer-based biosensor for specific detection of breast cancer biomarker HER2 via flower-like nanozymes and DNA nanostructures. J. Mater. Chem. B **7**(23), 3661–3669 (2019). https://doi.org/10.1039/C9TB00472F
295. S. Yang, M. You, F. Zhang, Q. Wang, P. He, A sensitive electrochemical aptasensing platform based on exonuclease recycling amplification and host-guest recognition for detection of breast cancer biomarker HER2. Sens. Actuators B-Chem. **258**, 796–802 (2018). https://doi.org/10.1016/j.snb.2017.11.119
296. X. Wang, B. Zhang, J. Li, H. Chang, W. Wei, A simple and fast chromogenic reaction based on Ag_3PO_4/Ag nanocomposite for tumor marker detection. Talanta **175**, 229–234 (2017). https://doi.org/10.1016/j.talanta.2017.07.039
297. L. Xiao, A. Zhu, Q. Xu, Y. Chen, J. Xu et al., Colorimetric biosensor for detection of cancer biomarker by Au nanoparticle-decorated Bi_2Se_3 nanosheets. ACS Appl. Mater. Interfaces **9**(8), 6931–6940 (2017). https://doi.org/10.1021/acsami.6b15750
298. X.F. Ruan, D. Liu, X.H. Niu, Y.J. Wang, C.D. Simpson et al., 2D graphene oxide/Fe-MOF nanozyme nest with superior peroxidase-like activity and its application for detection of woodsmoke exposure biomarker. Anal. Chem. **91**(21), 13847–13854 (2019). https://doi.org/10.1021/acs.analchem.9b03321
299. X. Xi, X. Peng, C. Xiong, D. Shi, J. Zhu et al., Iron doped graphitic carbon nitride with peroxidase like activity for colorimetric detection of sarcosine and hydrogen peroxide. Microchim. Acta **187**(7), 383 (2020). https://doi.org/10.1007/s00604-020-04373-w
300. K. Wang, C. Wu, F. Wang, M. Liao, G. Jiang, Bimetallic nanoparticles decorated hollow nanoporous carbon framework as nanozyme biosensor for highly sensitive electrochemical sensing of uric acid. Biosens. Bioelectron. **150**, 111869 (2020). https://doi.org/10.1016/j.bios.2019.111869

 https://doi.org/10.1007/s40820-021-00674-8

301. D. Pedone, M. Moglianetti, M. Lettieri, G. Marrazza, P.P. Pompa, Platinum nanozyme-enabled colorimetric determination of total antioxidant level in saliva. Anal. Chem. **92**(13), 8660–8664 (2020). https://doi.org/10.1021/acs.analchem.0c01824
302. P. Ling, C. Qian, J. Yu, F. Gao, Artificial nanozyme based on platinum nanoparticles anchored metal–organic frameworks with enhanced electrocatalytic activity for detection of telomeres activity. Biosens. Bioelectron. **149**, 111838 (2020). https://doi.org/10.1016/j.bios.2019.111838
303. P.-C. Kuo, C.-W. Lien, J.-Y. Mao, B. Unnikrishnan, H.-T. Chang et al., Detection of urinary spermine by using silver–gold/silver chloride nanozymes. Anal. Chim. Acta **1009**, 89–97 (2018). https://doi.org/10.1016/j.aca.2018.01.018
304. D.M. Morens, G.K. Folkers, A.S. Fauci, The challenge of emerging and re-emerging infectious diseases. Nature **430**(6996), 242–249 (2004). https://doi.org/10.1038/nature02759
305. B. Park, S.-J. Choi, Sensitive immunoassay-based detection of Vibrio parahaemolyticus using capture and labeling particles in a stationary liquid phase lab-on-a-chip. Biosens. Bioelectron. **90**, 269–275 (2017). https://doi.org/10.1016/j.bios.2016.11.071
306. B. Pang, X. Ding, G. Wang, C. Zhao, Y. Xu et al., Rapid and quantitative detection of vibrio parahemolyticus by the mixed-dye-based loop-mediated isothermal amplification assay on a self-priming compartmentalization microfluidic chip. J. Agric. Food Chem. **65**(51), 11312–11319 (2017). https://doi.org/10.1021/acs.jafc.7b03655
307. Z. Zhang, L. Xiao, Y. Lou, M. Jin, C. Liao et al., Development of a multiplex real-time PCR method for simultaneous detection of *Vibrio parahaemolyticus*, *Listeria monocytogenes* and *Salmonella* spp. in raw shrimp. Food Control **51**, 31–36 (2015). https://doi.org/10.1016/j.foodcont.2014.11.007
308. S. Yao, C. Zhao, Y. Liu, H. Nie, G. Xi et al., Colorimetric immunoassay for the detection of *Staphylococcus aureus* by using magnetic carbon dots and sliver nanoclusters as o-phenylenediamine-oxidase mimetics. Food Anal. Methods **13**, 833–838 (2020). https://doi.org/10.1007/s12161-019-01683-5
309. S. Bu, K. Wang, C. Ju, C. Wang, Z. Li et al., Point-of-care assay to detect foodborne pathogenic bacteria using a low-cost disposable medical infusion extension line as readout and MnO_2 nanoflowers. Food Control **98**, 399–404 (2019). https://doi.org/10.1016/j.foodcont.2018.11.053
310. S.R. Ahmed, J.C. Corredor, É. Nagy, S. Neethirajan, Amplified visual immunosensor integrated with nanozyme for ultrasensitive detection of avian influenza virus. NanoTheranostics **1**(3), 338 (2017). https://doi.org/10.7150/ntno.20758
311. S. Oh, J. Kim, V.T. Tran, D.K. Lee, S.R. Ahmed et al., Magnetic nanozyme-linked immunosorbent assay for ultrasensitive influenza a virus detection. ACS Appl. Mater. Interfaces **10**(15), 12534–12543 (2018). https://doi.org/10.1021/acsami.8b02735
312. L. Long, J. Liu, K. Lu, T. Zhang, Y. Xie et al., Highly sensitive and robust peroxidase-like activity of Au–Pt core/shell nanorod-antigen conjugates for measles virus diagnosis. J. Nanobiotechnol. **16**(1), 46 (2018). https://doi.org/10.1186/s12951-018-0371-0
313. T. Zhang, F. Tian, L. Long, J. Liu, X. Wu, Diagnosis of rubella virus using antigen-conjugated Au@Pt nanorods as nanozyme probe [Corrigendum]. Int. J. Nanomed. **14**, 1281–1281 (2019). https://doi.org/10.2147/IJN.S202056
314. L. Zhang, Y. Chen, N. Cheng, Y. Xu, K. Huang et al., Ultrasensitive detection of viable enterobacter sakazakii by a continual cascade nanozyme biosensor. Anal. Chem. **89**(19), 10194–10200 (2017). https://doi.org/10.1021/acs.analchem.7b01266
315. L. Zhang, R. Huang, W. Liu, H. Liu, X. Zhou et al., Rapid and visual detection of *Listeria monocytogenes* based on nanoparticle cluster catalyzed signal amplification. Biosens. Bioelectron. **86**, 1–7 (2016). https://doi.org/10.1016/j.bios.2016.05.100
316. S. Mumtaz, L.-S. Wang, S.Z. Hussain, M. Abdullah, Z. Huma et al., Dopamine coated Fe_3O_4 nanoparticles as enzyme mimics for the sensitive detection of bacteria. Chem. Commun. **53**(91), 12306–12308 (2017). https://doi.org/10.1039/C7CC07149C
317. L. Zhang, Z. Qi, Y. Zou, J. Zhang, W. Xia et al., Engineering DNA–nanozyme interfaces for rapid detection of dental bacteria. ACS Appl. Mater. Interfaces **11**(34), 30640–30647 (2019). https://doi.org/10.1021/acsami.9b10718
318. Q. Han, X. Wang, X. Liu, W. Xiao, S. Cai et al., Controllable fabrication of magnetic core–shell nanocomposites with high peroxide mimetic properties for bacterial detection and antibacterial applications. J. Mater. Chem. B **7**(7), 1124–1132 (2019). https://doi.org/10.1039/C8TB02834F
319. P. Liu, Y. Wang, L. Han, Y. Cai, H. Ren et al., Colorimetric assay of bacterial pathogens based on Co_3O_4 magnetic nanozymes conjugated with specific fusion phage proteins and magnetophoretic chromatography. ACS Appl. Mater. Interfaces **12**(8), 9090–9097 (2020). https://doi.org/10.1021/acsami.9b23101
320. S. Wang, W. Deng, L. Yang, Y. Tan, Q. Xie et al., Copper-based metal–organic framework nanoparticles with peroxidase-like activity for sensitive colorimetric detection of staphylococcus aureus. ACS Appl. Mater. Interfaces **9**(29), 24440–24445 (2017). https://doi.org/10.1021/acsami.7b07307
321. J. Fu, Y. Zhou, X. Huang, W. Zhang, Y. Wu et al., Dramatically enhanced immunochromatographic assay using cascade signal amplification for ultrasensitive detection of escherichia coli O157:H7 in milk. J. Agric. Food Chem. **68**(4), 1118–1125 (2020). https://doi.org/10.1021/acs.jafc.9b07076
322. J. Han, L. Zhang, L. Hu, K. Xing, X. Lu et al., Nanozyme-based lateral flow assay for the sensitive detection of Escherichia coli O157:H7 in milk. J. Dairy Sci. **101**(7), 5770–5779 (2018). https://doi.org/10.3168/jds.2018-14429
323. T. Jiang, Y. Song, T. Wei, H. Li, D. Du et al., Sensitive detection of Escherichia coli O157:H7 using Pt–Au bimetal nanoparticles with peroxidase-like amplification. Biosens.

Bioelectron. **77**, 687–694 (2016). https://doi.org/10.1016/j.bios.2015.10.017

324. N. Cheng, C. Zhu, Y. Wang, D. Du, M.-J. Zhu et al., Nanozyme enhanced colorimetric immunoassay for naked-eye detection of *Salmonella enteritidis*. J. Anal. Test. **3**(1), 99–106 (2019). https://doi.org/10.1007/s41664-018-0079-z
325. Y. Song, J. Qiao, W. Liu, L. Qi, Colorimetric detection of serum doxycycline with D-histidine-functionalized gold nanoclusters as nanozymes. Analyst **145**(10), 3564–3568 (2020). https://doi.org/10.1039/D0AN00297F
326. C. Díez, D. Guillarme, A.S. Spörri, E. Cognard, D. Ortelli et al., Aminoglycoside analysis in food of animal origin with a zwitterionic stationary phase and liquid chromatography–tandem mass spectrometry. Anal. Chim. Acta **882**, 127–139 (2015). https://doi.org/10.1016/j.aca.2015.03.050
327. L. Ma, X. Han, L. Xia, R.-M. Kong, F. Qu, A G-triplex based molecular beacon for label-free fluorescence "turn-on" detection of bleomycin. Analyst **143**(22), 5474–5480 (2018). https://doi.org/10.1039/C8AN01208C
328. Y. Zhang, H.M. He, J. Zhang, F.J. Liu, C. Li et al., HPLC-ELSD determination of kanamycin B in the presence of kanamycin A in fermentation broth. Biomed. Chromatogr. **29**(3), 396–401 (2015). https://doi.org/10.1002/bmc.3289
329. Z. Zhang, Y. Tian, P. Huang, F.-Y. Wu, Using target-specific aptamers to enhance the peroxidase-like activity of gold nanoclusters for colorimetric detection of tetracycline antibiotics. Talanta **208**, 120342 (2020). https://doi.org/10.1016/j.talanta.2019.120342
330. W.S. Kong, X.X. Guo, M. Jing, F.L. Qu, L.M. Lu, Highly sensitive photoelectrochemical detection of bleomycin based on Au/WS_2 nanorod array as signal matrix and Ag/ZnMOF nanozyme as multifunctional amplifier. Biosens. Bioelectron **150**, 7 (2020). https://doi.org/10.1016/j.bios.2019.111875
331. A.P. Nagvenkar, A. Gedanken, $Cu_{0.89}Zn_{0.11}O$, A new peroxidase-mimicking nanozyme with high sensitivity for glucose and antioxidant detection. ACS Appl. Mater. Interfaces **8**(34), 22301–22308 (2016). https://doi.org/10.1021/acsami.6b05354
332. M. Lu, B. Li, L. Guan, K. Li, Y. Lin, Carbon-shielded three-dimensional Co–Mn nanowire array anchored on Ni foam with dual-enzyme mimic performance for selective detection of ascorbic acid. ACS Sustain. Chem. Eng. **7**(18), 15471–15478 (2019). https://doi.org/10.1021/acssuschemeng.9b03095
333. X. Liu, X. Wang, C. Qi, Q. Han, W. Xiao et al., Sensitive colorimetric detection of ascorbic acid using Pt/CeO_2 nanocomposites as peroxidase mimics. Appl. Surf. Sci. **479**, 532–539 (2019). https://doi.org/10.1016/j.apsusc.2019.02.135
334. S. Zhuo, J. Fang, M. Li, J. Wang, C. Zhu et al., Manganese (II)-doped carbon dots as effective oxidase mimics for sensitive colorimetric determination of ascorbic acid. Microchim. Acta **186**(12), 745 (2019). https://doi.org/10.1007/s00604-019-3887-6
335. Q. Yang, L. Li, F. Zhao, Y. Wang, Z. Ye et al., Generation of MnO_2 nanozyme in spherical polyelectrolyte brush for colorimetric detection of glutathione. Mater. Lett. **248**, 89–92 (2019). https://doi.org/10.1016/j.matlet.2019.04.007
336. J. Xi, C. Zhu, Y. Wang, Q. Zhang, L. Fan, Mn_3O_4 microspheres as an oxidase mimic for rapid detection of glutathione. RSC Adv. **9**(29), 16509–16514 (2019). https://doi.org/10.1039/C9RA01227C
337. Q. Wang, G. Hong, Y. Liu, J. Hao, S. Liu, Dual enzyme-like activity of iridium nanoparticles and their applications for the detection of glucose and glutathione. RSC Adv. **10**(42), 25209–25213 (2020). https://doi.org/10.1039/D0RA05342B
338. A.B. Ganganboina, R.-A. Doong, The biomimic oxidase activity of layered V_2O_5 nanozyme for rapid and sensitive nanomolar detection of glutathione. Sens. Actuators B-Chem. **273**, 1179–1186 (2018). https://doi.org/10.1016/j.snb.2018.07.038
339. S. Chen, M. Chi, Y. Zhu, M. Gao, C. Wang et al., A facile synthesis of superparamagnetic Fe_3O_4 nanofibers with superior peroxidase-like catalytic activity for sensitive colorimetric detection of L-cysteine. Appl. Surf. Sci. **440**, 237–244 (2018). https://doi.org/10.1016/j.apsusc.2018.01.152
340. W. Huang, Y. Deng, Y. He, Visual colorimetric sensor array for discrimination of antioxidants in serum using MnO_2 nanosheets triggered multicolor chromogenic system. Biosens. Bioelectron. **91**, 89–94 (2017). https://doi.org/10.1016/j.bios.2016.12.028
341. J. Sun, C. Li, Y. Qi, S. Guo, X. Liang, Optimizing colorimetric assay based on V_2O_5 Nanozymes for sensitive detection of H_2O_2 and glucose. Sensors **16**(4), 584 (2016). https://doi.org/10.3390/s16040584
342. J. Zhang, Z. Chen, H. Wu, F. Wu, C. He et al., An electrochemical bifunctional sensor for the detection of nitrite and hydrogen peroxide based on layer-by-layer multilayer films of cationic phthalocyanine cobalt (ii) and carbon nanotubes. J. Mater. Chem. B **4**(7), 1310–1317 (2016). https://doi.org/10.1039/C5TB01995H
343. F. Mollarasouli, K. Asadpour-Zeynali, S. Campuzano, P. Yáñez-Sedeño, J.M. Pingarrón, Non-enzymatic hydrogen peroxide sensor based on graphene quantum dots-chitosan/methylene blue hybrid nanostructures. Electrochim. Acta **246**, 303–314 (2017). https://doi.org/10.1016/j.electacta.2017.06.003
344. W. Zhang, X. Niu, X. Li, Y. He, H. Song et al., A smartphone-integrated ready-to-use paper-based sensor with mesoporous carbon-dispersed Pd nanoparticles as a highly active peroxidase mimic for H_2O_2 detection. Sens. Actuators B-Chem. **265**, 412–420 (2018). https://doi.org/10.1016/j.snb.2018.03.082
345. Y. Liu, X. Liu, Z. Guo, Z. Hu, Z. Xue et al., Horseradish peroxidase supported on porous graphene as a novel sensing platform for detection of hydrogen peroxide in living cells sensitively. Biosens. Bioelectron. **87**, 101–107 (2017). https://doi.org/10.1016/j.bios.2016.08.015
346. J. Zhu, W. Nie, Q. Wang, J. Li, H. Li et al., In situ growth of copper oxide-graphite carbon nitride nanocomposites with peroxidase-mimicking activity for electrocatalytic and

 https://doi.org/10.1007/s40820-021-00674-8

colorimetric detection of hydrogen peroxide. Carbon **129**, 29–37 (2018). https://doi.org/10.1016/j.carbon.2017.11.096

347. Z.-N. Huang, G.-C. Liu, J. Zou, X.-Y. Jiang, Y.-P. Liu et al., A hybrid composite of recycled popcorn-shaped MnO_2 microsphere and Ox-MWCNTs as a sensitive non-enzymatic amperometric H_2O_2 sensor. Microchem J. **158**, 105215 (2020). https://doi.org/10.1016/j.microc.2020.105215
348. X. Luo, H. Shu, Q. Wan, Z. Wang, N. Yang, Biosensing applications of V_2O_5–CeO_2 mesoporous silica. Electroanalysis **27**(9), 2194–2200 (2015). https://doi.org/10.1002/elan.201500250
349. T. Zhang, Y. Xing, Y. Song, Y. Gu, X. Yan et al., AuPt/MOF–graphene: a synergistic catalyst with surprisingly high peroxidase-like activity and its application for H_2O_2 detection. Anal. Chem. **91**(16), 10589–10595 (2019). https://doi.org/10.1021/acs.analchem.9b01715
350. D. Dai, H. Liu, H. Ma, Z. Huang, C. Gu et al., In-situ synthesis of Cu_2OAu nanocomposites as nanozyme for colorimetric determination of hydrogen peroxide. J. Alloys Compd. **747**, 676–683 (2018). https://doi.org/10.1016/j.jallcom.2018.03.054
351. L. Jiao, W. Xu, H. Yan, Y. Wu, C. Liu et al., Fe–N–C single-atom nanozymes for the intracellular hydrogen peroxide detection. Anal. Chem. **91**(18), 11994–11999 (2019). https://doi.org/10.1021/acs.analchem.9b02901
352. H. Liu, L. Zhu, H. Ma, J. Wen, H. Xu et al., Copper(II)-coated Fe_3O_4 nanoparticles as an efficient enzyme mimic for colorimetric detection of hydrogen peroxide. Microchim. Acta **186**(8), 518 (2019). https://doi.org/10.1007/s00604-019-3599-y
353. Y. Lu, W. Ye, Q. Yang, J. Yu, Q. Wang et al., Three-dimensional hierarchical porous PtCu dendrites: a highly efficient peroxidase nanozyme for colorimetric detection of H_2O_2. Sens. Actuators B-Chem. **230**, 721–730 (2016). https://doi.org/10.1016/j.snb.2016.02.130
354. S. Cai, W. Xiao, H. Duan, X. Liang, C. Wang et al., Single-layer Rh nanosheets with ultrahigh peroxidase-like activity for colorimetric biosensing. Nano Res. **11**(12), 6304–6315 (2018). https://doi.org/10.1007/s12274-018-2154-1
355. T.G. Choleva, V.A. Gatselou, G.Z. Tsogas, D.L. Giokas, Intrinsic peroxidase-like activity of rhodium nanoparticles, and their application to the colorimetric determination of hydrogen peroxide and glucose. Microchim. Acta **185**(1), 1–9 (2018). https://doi.org/10.1007/s00604-017-2582-8
356. R.M. Tripathi, S.J. Chung, Phytosynthesis of palladium nanoclusters: an efficient nanozyme for ultrasensitive and selective detection of reactive oxygen species. Molecules **25**(15), 3349 (2020). https://doi.org/10.3390/molecules25153349
357. X. Jiang, C. Sun, Y. Guo, G. Nie, L. Xu, Peroxidase-like activity of apoferritin paired gold clusters for glucose detection. Biosens. Bioelectron **64**, 165–170 (2015). https://doi.org/10.1016/j.bios.2014.08.078
358. P. Si, P. Kannan, L. Guo, H. Son, D.-H. Kim, Highly stable and sensitive glucose biosensor based on covalently assembled high density Au nanostructures. Biosens. Bioelectron. **26**(9), 3845–3851 (2011). https://doi.org/10.1016/j.bios.2011.02.044
359. Y. Xu, P.E. Pehrsson, L. Chen, R. Zhang, W. Zhao, Double-stranded DNA single-walled carbon nanotube hybrids for optical hydrogen peroxide and glucose sensing. J. Phys. Chem. C **111**(24), 8638–8643 (2007). https://doi.org/10.1021/jp0709611
360. L. Han, C. Li, T. Zhang, Q. Lang, A. Liu, Au@ Ag heterogeneous nanorods as nanozyme interfaces with peroxidase-like activity and their application for one-pot analysis of glucose at nearly neutral pH. ACS Appl. Mater. Interfaces **7**(26), 14463–14470 (2015). https://doi.org/10.1021/acsami.5b03591
361. M.N. Karim, S.R. Anderson, S. Singh, R. Ramanathan, V. Bansal, Nanostructured silver fabric as a free-standing NanoZyme for colorimetric detection of glucose in urine. Biosens. Bioelectron. **110**, 8–15 (2018). https://doi.org/10.1016/j.bios.2018.03.025
362. P.C. Lee, N.S. Li, Y.P. Hsu, C. Peng, H.W. Yang, Direct glucose detection in whole blood by colorimetric assay based on glucose oxidase-conjugated graphene oxide/MnO_2 nanozymes. Analyst **144**(9), 3038–3044 (2019). https://doi.org/10.1039/c8an02440e
363. V.T. Pham, V.K. Truong, M.D. Quinn, S.M. Notley, Y. Guo et al., Graphene induces formation of pores that kill spherical and rod-shaped bacteria. ACS Nano **9**(8), 8458–8467 (2015). https://doi.org/10.1021/acsnano.5b03368
364. L. Tonoyan, G.T. Fleming, P.H. Mc Cay, R. Friel, V. O'Flaherty, Antibacterial potential of an antimicrobial agent inspired by peroxidase-catalyzed systems. Front. Microbiol. **8**, 680 (2017). https://doi.org/10.3389/fmicb.2017.00680
365. Y. Sang, W. Li, H. Liu, L. Zhang, H. Wang et al., Construction of nanozyme-hydrogel for enhanced capture and elimination of bacteria. Adv. Funct. Mater. **29**(22), 1900518 (2019). https://doi.org/10.1002/adfm.201900518
366. X. Yang, J. Yang, L. Wang, B. Ran, Y. Jia et al., Pharmaceutical intermediate-modified gold nanoparticles: against multidrug-resistant bacteria and wound-healing application via an electrospun scaffold. ACS Nano **11**(6), 5737–5745 (2017). https://doi.org/10.1021/acsnano.7b01240
367. T.F. Schäberle, I.M. Hack, Overcoming the current deadlock in antibiotic research. Trends Microbiol. **22**(4), 165–167 (2014). https://doi.org/10.1016/j.tim.2013.12.007
368. S. Shi, S. Wu, Y. Shen, S. Zhang, Y. Xiao et al., Iron oxide nanozyme suppresses intracellular *Salmonella enteritidis* growth and alleviates infection in vivo. Theranostics **8**(22), 6149 (2018). https://doi.org/10.7150/thno.29303
369. M.N. Karim, M. Singh, P. Weerathunge, P. Bian, R. Zheng et al., Visible-light-triggered reactive-oxygen-species-mediated antibacterial activity of peroxidase-mimic CuO nanorods. ACS Appl. Nano Mater. **1**(4), 1694–1704 (2018). https://doi.org/10.1021/acsanm.8b00153
370. S.Z.K. Roudbaneh, S. Kahbasi, M.J. Sohrabi, A. Hasan, A. Salihi et al., Albumin binding, antioxidant and antibacterial effects of cerium oxide nanoparticles. J. Mol. Liq. **296**, 111839 (2019). https://doi.org/10.1016/j.molliq.2019.111839

371. W.C. Hu, M.R. Younis, Y. Zhou, C. Wang, X.H. Xia, In situ fabrication of ultrasmall gold nanoparticles/2D MOFs hybrid as nanozyme for antibacterial therapy. Small (2020). https://doi.org/10.1002/smll.202000553
372. C. Li, Y.R. Sun, X.P. Li, S.H. Fan, Y.M. Liu, Bactericidal effects and accelerated wound healing using Tb_4O_7 nanoparticles with intrinsic oxidase-like activity. J. Nanobiotechnol. **17**, 10 (2019). https://doi.org/10.1186/s12951-019-0487-x
373. H.W. Ji, K. Dong, Z.Q. Yan, C. Ding, Z.W. Chen et al., Bacterial hyaluronidase self-triggered prodrug release for chemo-photothermal synergistic treatment of bacterial infection. Small **12**(45), 6200–6206 (2016). https://doi.org/10.1002/smll.201601729
374. Q. Zhang, Y. Zhou, E. Villarreal, Y. Lin, S. Zou et al., Faceted gold nanorods: nanocuboids, convex nanocuboids, and concave nanocuboids. Nano Lett. **15**(6), 4161–4169 (2015). https://doi.org/10.1021/acs.nanolett.5b01286
375. C. Wiegand, M. Abel, P. Ruth, P. Elsner, U.-C. Hipler, pH influence on antibacterial efficacy of common antiseptic substancess. Skin Pharmacol. Physiol. **28**(3), 147–158 (2015). https://doi.org/10.1159/000367632
376. W. Sheng, Z. Zhuang, M. Gao, J. Zheng, J.G. Chen et al., Correlating hydrogen oxidation and evolution activity on platinum at different pH with measured hydrogen binding energy. Nat. Commun. **6**(1), 1–6 (2015). https://doi.org/10.1038/ncomms6848
377. L. Stefan, F. Denat, D. Monchaud, Insights into how nucleotide supplements enhance the peroxidase-mimicking DNAzyme activity of the G-quadruplex/hemin system. Nucleic Acids Res. **40**(17), 8759–8772 (2012). https://doi.org/10.1093/nar/gks581
378. N.S. Vallabani, A. Vinu, S. Singh, A. Karakoti, Tuning the ATP-triggered pro-oxidant activity of iron oxide-based nanozyme towards an efficient antibacterial strategy. J. Colloids Interface Sci. **567**, 154–164 (2020). https://doi.org/10.1016/j.jcis.2020.01.099
379. B. Chishti, H. Fouad, H.K. Seo, O.Y. Alothman, Z. Ansari et al., ATP foster tuning of nanostructured CeO_2 peroxidase-like activity for promising anti-bacterial performance. New J. Chem. **44**, 11291–11303 (2020). https://doi.org/10.1039/C9NJ05955E
380. L. Gao, K.M. Giglio, J.L. Nelson, H. Sondermann, A.J. Travis, Ferromagnetic nanoparticles with peroxidase-like activity enhance the cleavage of biological macromolecules for biofilm elimination. Nanoscale **6**(5), 2588–2593 (2014). https://doi.org/10.1039/C3NR05422E
381. F. Natalio, R. André, A.F. Hartog, B. Stoll, K.P. Jochum et al., Vanadium pentoxide nanoparticles mimic vanadium haloperoxidases and thwart biofilm formation. Nat. Nanotechnol. **7**(8), 530–535 (2012). https://doi.org/10.1038/nnano.2012.91
382. Z. Wang, K. Dong, Z. Liu, Y. Zhang, Z. Chen et al., Activation of biologically relevant levels of reactive oxygen species by Au/g–C_3N_4 hybrid nanozyme for bacteria killing and wound disinfection. Biomaterials **113**, 145–157 (2017). https://doi.org/10.1016/j.Biomaterials2016.10.041
383. L. Ferrucci, E. Fabbri, Inflammageing: chronic inflammation in ageing, cardiovascular disease, and frailty. Nat. Rev. Cardiol. **15**(9), 505–522 (2018). https://doi.org/10.1038/s41569-018-0064-2
384. H. Guo, J.B. Callaway, J.P. Ting, Inflammasomes: mechanism of action, role in disease, and therapeutics. Nat. Med. **21**(7), 677–687 (2015). https://doi.org/10.1038/nm.3893
385. S.J. Kim, T.H. Chung, Cold atmospheric plasma jet-generated RONS and their selective effects on normal and carcinoma cells. Sci. Rep. **6**(1), 20332 (2016). https://doi.org/10.1038/srep20332
386. D. Ni, D. Jiang, C.J. Kutyreff, J. Lai, Y. Yan et al., Molybdenum-based nanoclusters act as antioxidants and ameliorate acute kidney injury in mice. Nat. Commun. **9**(1), 1–11 (2018). https://doi.org/10.1038/s41467-018-07890-8
387. M.D. Okusa, M.H. Rosner, J.A. Kellum, C. Ronco, Therapeutic targets of human AKI: harmonizing human and animal AKI. J. Am. Soc. Nephrol. **27**(1), 44–48 (2016). https://doi.org/10.1681/ASN.2015030233
388. M. Ma, Z. Liu, N. Gao, Z. Pi, X. Du et al., Self-protecting biomimetic nanozyme for selective and synergistic clearance of peripheral amyloid-β in an Alzheimer's disease model. J. Am. Chem. Soc. **142**(52), 21702–21711 (2020). https://doi.org/10.1021/jacs.0c08395
389. F. Li, Y. Qiu, F. Xia, H. Sun, H. Liao et al., Dual detoxification and inflammatory regulation by ceria nanozymes for drug-induced liver injury therapy. Nano Today **35**, 100925 (2020). https://doi.org/10.1016/j.nantod.2020.100925
390. R. Yan, S. Sun, J. Yang, W. Long, J. Wang et al., Nanozyme-based bandage with single-atom catalysis for brain trauma. ACS Nano **13**(10), 11552–11560 (2019). https://doi.org/10.1021/acsnano.9b05075
391. L. Zhang, Y. Zhang, Z. Wang, F. Cao, Y. Sang et al., Constructing metal–organic framework nanodots as bio-inspired artificial superoxide dismutase for alleviating endotoxemia. Mater. Horizons **6**(8), 1682–1687 (2019). https://doi.org/10.1039/C9MH00339H
392. T.F. Liu, B.W. Xiao, F. Xiang, J.L. Tan, Z. Chen et al., Ultrasmall copper-based nanoparticles for reactive oxygen species scavenging and alleviation of inflammation related diseases. Nat. Commun. **11**(1), 16 (2020). https://doi.org/10.1038/s41467-020-16544-7
393. C. Wu, X. Han, W. Feng, Z. Liu, L. Chen et al., Multi-enzymatic activities of ultrasmall ruthenium oxide for anti-inflammation and neuroprotection. Chem. Eng. J. **411**, 128543 (2021). https://doi.org/10.1016/j.cej.2021.128543
394. S. Zhao, Y. Li, Q. Liu, S. Li, Y. Cheng et al., An orally administered CeO_2@montmorillonite nanozyme targets inflammation for inflammatory bowel disease therapy. Adv. Funct. Mater. **30**(45), 2004692 (2020). https://doi.org/10.1002/adfm.202004692
395. C. Liu, Z. Du, M. Ma, Y. Sun, J. Ren et al., Carbon monoxide controllable targeted gas therapy for synergistic anti-inflammation. iScience **23**(9), 101483 (2020). https://doi.org/10.1016/j.isci.2020.101483

 https://doi.org/10.1007/s40820-021-00674-8

396. Z.H. Miao, S.S. Jiang, M.L. Ding, S.Y. Sun, Y. Ma et al., Ultrasmall rhodium nanozyme with RONS scavenging and photothermal activities for anti-inflammation and antitumor theranostics of colon diseases. Nano Lett. **20**(5), 3079–3089 (2020). https://doi.org/10.1021/acs.nanolett.9b05035
397. C.N. Bernstein, M. Fried, J. Krabshuis, H. Cohen, R. Eliakim et al., World gastroenterology organization practice guidelines for the diagnosis and management of IBD in 2010. Inflamm. Bowel Dis. **16**(1), 112–124 (2010)
398. S.-B. Wang, C. Zhang, Z.-X. Chen, J.-J. Ye, S.-Y. Peng et al., A versatile carbon monoxide nanogenerator for enhanced tumor therapy and anti-inflammation. ACS Nano **13**(5), 5523–5532 (2019). https://doi.org/10.1021/acsnano.9b00345
399. M. Popova, L.S. Lazarus, S. Ayad, A.D. Benninghoff, L.M. Berreau, Visible-light-activated quinolone carbon-monoxide-releasing molecule: prodrug and albumin-assisted delivery enables anticancer and potent anti-inflammatory effects. J. Am. Chem. Soc. **140**(30), 9721–9729 (2018). https://doi.org/10.1021/jacs.8b06011
400. X. Ji, K. Damera, Y. Zheng, B. Yu, L.E. Otterbein et al., Toward carbon monoxide-based therapeutics: critical drug delivery and developability issues. J. Pharm. Sci. **105**(2), 406–416 (2016). https://doi.org/10.1016/j.xphs.2015.10.018
401. X. Mu, H. He, J. Wang, W. Long, Q. Li et al., Carbogenic nanozyme with ultrahigh reactive nitrogen species selectivity for traumatic brain injury. Nano Lett. **19**(7), 4527–4534 (2019). https://doi.org/10.1021/acs.nanolett.9b01333
402. S. Zhang, Zhang, Catalytic patch with redox Cr/CeO_2 nanozyme of noninvasive intervention for brain trauma. Theranostics **11**(6), 2806 (2021). https://doi.org/10.7150/thno.51912
403. H. Sung, J. Ferlay, R.L. Siegel, M. Laversanne, I. Soerjomataram et al., Global cancer statistics 2020: GLOBOCAN estimates of incidence and mortality worldwide for 36 cancers in 185 countries. CA-Cancer J. Clin. **7**(3), 209–249 (2021). https://doi.org/10.3322/caac.21660
404. P. Zhao, Z. Jin, Q. Chen, T. Yang, D. Chen et al., Local generation of hydrogen for enhanced photothermal therapy. Nat. Commun. **9**(1), 1–12 (2018). https://doi.org/10.1038/s41467-018-06630-2
405. H. Lin, S. Gao, C. Dai, Y. Chen, J. Shi, A two-dimensional biodegradable niobium carbide (MXene) for photothermal tumor eradication in NIR-I and NIR-II biowindows. J. Am. Chem. Soc. **139**(45), 16235–16247 (2017). https://doi.org/10.1021/jacs.7b07818
406. T. Whiteside, The tumor microenvironment and its role in promoting tumor growth. Oncogene **27**(45), 5904–5912 (2008). https://doi.org/10.1038/onc.2008.271
407. Q. Cheng, W. Yu, J. Ye, M. Liu, W. Liu et al., Nanotherapeutics interfere with cellular redox homeostasis for highly improved photodynamic therapy. Biomaterials **224**, 119500 (2019). https://doi.org/10.1016/j.Biomaterials2019.119500
408. P. Zhu, Y. Chen, J. Shi, Nanoenzyme-augmented cancer sonodynamic therapy by catalytic tumor oxygenation. ACS Nano **12**(4), 3780–3795 (2018). https://doi.org/10.1021/acsnano.8b00999
409. S. Gao, H. Lin, H. Zhang, H. Yao, Y. Chen et al., Nanocatalytic tumor therapy by biomimetic dual inorganic nanozyme-catalyzed cascade reaction. Adv. Sci. **6**(3), 1801733 (2019). https://doi.org/10.1002/advs.201801733
410. Z. Wang, Y. Zhang, E. Ju, Z. Liu, F. Cao et al., Biomimetic nanoflowers by self-assembly of nanozymes to induce intracellular oxidative damage against hypoxic tumors. Nat. Commun. **9**(1), 1–14 (2018). https://doi.org/10.1038/s41467-018-05798-x
411. S. Li, L. Shang, B. Xu, S. Wang, K. Gu et al., A nanozyme with photo-enhanced dual enzyme-like activities for deep pancreatic cancer therapy. Angew. Chem. Int. Ed. **58**(36), 12624–12631 (2019). https://doi.org/10.1002/anie.201904751
412. P. Kreuzaler, C.J. Watson, Killing a cancer: What are the alternatives? Nat. Rev. Cancer **12**(6), 411–424 (2012). https://doi.org/10.1038/nrc3264
413. S.S. Said, S. Campbell, T. Hoare, Externally addressable smart drug delivery vehicles: current technologies and future directions. Chem. Mater. **31**(14), 4971–4989 (2019). https://doi.org/10.1021/acs.chemmater.9b01798
414. X. Yang, Y. Yang, F. Gao, J.-J. Wei, C.-G. Qian et al., Biomimetic hybrid nanozymes with self-supplied H+ and accelerated O_2 generation for enhanced starvation and photodynamic therapy against hypoxic tumors. Nano Lett. **19**(7), 4334–4342 (2019). https://doi.org/10.1021/acs.nanolett.9b00934
415. Z. Xu, P. Sun, J. Zhang, X. Lu, L. Fan et al., High-efficiency platinum–carbon nanozyme for photodynamic and catalytic synergistic tumor therapy. Chem. Eng. J. **399**, 125797 (2020). https://doi.org/10.1016/j.cej.2020.125797
416. Y. Hu, X. Wang, P. Zhao, H. Wang, W. Gu et al., Nanozyme-catalyzed oxygen release from calcium peroxide nanoparticles for accelerated hypoxia relief and image-guided super-efficient photodynamic therapy. Biomater. Sci. **8**(10), 2931–2938 (2020). https://doi.org/10.1039/D0BM00187B
417. D.-W. Zheng, B. Li, C.-X. Li, J.-X. Fan, Q. Lei et al., Carbon-dot-decorated carbon nitride nanoparticles for enhanced photodynamic therapy against hypoxic tumor via water splitting. ACS Nano **10**(9), 8715–8722 (2016). https://doi.org/10.1021/acsnano.6b04156
418. X. Cai, Y. Luo, Y. Song, D. Liu, H. Yan et al., Integrating in situ formation of nanozymes with three-dimensional dendritic mesoporous silica nanospheres for hypoxia-overcoming photodynamic therapy. Nanoscale **10**(48), 22937–22945 (2018). https://doi.org/10.1039/C8NR07679K
419. Z. Yang, J. Wang, S. Ai, J. Sun, X. Mai et al., Self-generating oxygen enhanced mitochondrion-targeted photodynamic therapy for tumor treatment with hypoxia scavenging. Theranostics **9**(23), 6809 (2019). https://doi.org/10.7150/thno.36988
420. J. Zielonka, J. Joseph, A. Sikora, M. Hardy, O. Ouari et al., Mitochondria-targeted triphenylphosphonium-based compounds: syntheses, mechanisms of action, and therapeutic and diagnostic applications. Chem. Rev. **117**(15), 10043–10120 (2017). https://doi.org/10.1021/acs.chemrev.7b00042
421. Z. Tang, Y. Liu, M. He, W. Bu, Chemodynamic therapy: tumour microenvironment-mediated fenton and fenton-like

reactions. Angew. Chem. Int. Ed. **58**(4), 946–956 (2019). https://doi.org/10.1002/anie.201805664

422. M. Huo, L. Wang, Y. Chen, J. Shi, Tumor-selective catalytic nanomedicine by nanocatalyst delivery. Nat. Commun. **8**(1), 357 (2017). https://doi.org/10.1038/s41467-017-00424-8
423. C. Zhang, W. Bu, D. Ni, S. Zhang, Q. Li et al., Synthesis of iron nanometallic glasses and their application in cancer therapy by a localized fenton reaction. Angew. Chem. Int. Ed. **128**(6), 2141–2146 (2016). https://doi.org/10.1002/anie.201510031
424. J. Li, K. Yi, Y. Lei, Z. Qing, Z. Zou et al., Al centre-powered graphitic nanozyme with high catalytic efficiency for pH-independent chemodynamic therapy of cancer. Chem. Commun. **56**, 6285–6288 (2020). https://doi.org/10.1039/D0CC01331E
425. L. Wang, M. Huo, Y. Chen, J. Shi, Iron-engineered mesoporous silica nanocatalyst with biodegradable and catalytic framework for tumor-specific therapy. Biomaterials **163**, 1–13 (2018). https://doi.org/10.1016/j.Biomaterials2018.02.018
426. S. Fu, R. Yang, L. Zhang, W. Liu, G. Du et al., Biomimetic CoO@ AuPt nanozyme responsive to multiple tumor microenvironmental clues for augmenting chemodynamic therapy. Biomaterials **257**, 120279 (2020). https://doi.org/10.1016/j.Biomaterials2020.120279
427. F. Gong, L. Cheng, N. Yang, O. Betzer, L. Feng et al., Ultrasmall oxygen-deficient bimetallic oxide MnWOX nanoparticles for depletion of endogenous gsh and enhanced sonodynamic cancer therapy. Adv. Mater. **31**(23), 1900730 (2019). https://doi.org/10.1002/adma.201900730
428. X. Han, J. Huang, X. Jing, D. Yang, H. Lin et al., Oxygen-deficient black titania for synergistic/enhanced sonodynamic and photoinduced cancer therapy at near infrared-ii biowindow. ACS Nano **12**(5), 4545–4555 (2018). https://doi.org/10.1021/acsnano.8b00899
429. X. Pan, L. Bai, H. Wang, Q. Wu, H. Wang et al., Metal–organic-framework-derived carbon nanostructure augmented sonodynamic cancer therapy. Adv. Mater. **30**(23), 1800180 (2018). https://doi.org/10.1002/adma.201800180
430. P. Huang, X. Qian, Y. Chen, L. Yu, H. Lin et al., Metalloporphyrin-Encapsulated biodegradable nanosystems for highly efficient magnetic resonance imaging-guided sonodynamic cancer therapy. J. Am. Chem. Soc. **139**(3), 1275–1284 (2017). https://doi.org/10.1021/jacs.6b11846
431. A. Ma, H. Chen, Y. Cui, Z. Luo, R. Liang et al., Metalloporphyrin complex-based nanosonosensitizers for deep-tissue tumor theranostics by noninvasive sonodynamic therapy. Small **15**(5), 1804028 (2019). https://doi.org/10.1002/smll.201804028
432. X. Wang, X. Zhong, L. Bai, J. Xu, F. Gong et al., Ultrafine titanium monoxide (TiO_{1+x}) nanorods for enhanced sonodynamic therapy. J. Am. Chem. Soc. **142**(14), 6527–6537 (2020). https://doi.org/10.1021/jacs.9b10228
433. X. Zhong, X. Wang, L. Cheng, Y.A. Tang, G. Zhan et al., GSH-Depleted PtCu3 nanocages for chemodynamic-enhanced sonodynamic cancer therapy. Adv. Funct. Mater. **30**(4), 1907954 (2020). https://doi.org/10.1002/adfm.201907954
434. H.S. Jung, P. Verwilst, A. Sharma, J. Shin, J.L. Sessler et al., Organic molecule-based photothermal agents: an expanding photothermal therapy universe. Chem. Soc. Rev. **47**(7), 2280–2297 (2018). https://doi.org/10.1039/c7cs00522a
435. W. Tang, W. Fan, W. Zhang, Z. Yang, L. Li et al., Wet/Sonochemical synthesis of enzymatic two-dimensional MnO_2 nanosheets for synergistic catalysis-enhanced photoTheranostics Adv. Mater. **31**(19), 1900401 (2019). https://doi.org/10.1002/adma.201900401
436. S. Kang, Y.-G. Gil, D.-H. Min, H. Jang, Nonrecurring circuit nanozymatic enhancement of hypoxic pancreatic cancer phototherapy using speckled Ru–Te hollow nanorods. ACS Nano **14**(4), 4383–4394 (2020). https://doi.org/10.1021/acsnano.9b09974
437. X. Zhu, Y. Gong, Y. Liu, C. Yang, S. Wu et al., Ru@ CeO_2 yolk shell nanozymes: oxygen supply in situ enhanced dual chemotherapy combined with photothermal therapy for orthotopic/subcutaneous colorectal cancer. Biomaterials **242**, 119923 (2020). https://doi.org/10.1016/j.Biomaterials2020.119923
438. N.S. Abadeer, C.J. Murphy, Recent progress in cancer thermal therapy using gold nanoparticles. J. Phys. Chem. C. **120**(9), 4691–4716 (2016). https://doi.org/10.1021/acs.jpcc.5b11232
439. W. Fan, B. Yung, P. Huang, X. Chen, Nanotechnology for multimodal synergistic cancer therapy. Chem. Rev. **117**(22), 13566–13638 (2017). https://doi.org/10.1021/acs.chemrev.7b00258
440. L. Li, H. Liu, J. Bian, X. Zhang, Y. Fu et al., Ag/Pd bimetal nanozyme with enhanced catalytic and photothermal effects for ROS/hyperthermia/chemotherapy triple-modality antitumor therapy. Chem. Eng. J. **397**, 125438 (2020). https://doi.org/10.1016/j.cej.2020.125438
441. S. Liang, X. Deng, Y. Chang, C. Sun, S. Shao et al., Intelligent hollow Pt-CuS janus architecture for synergistic catalysis-enhanced sonodynamic and photothermal cancer therapy. Nano Lett. **19**(6), 4134–4145 (2019). https://doi.org/10.1021/acs.nanolett.9b01595
442. Q. Chen, S. He, F. Zhang, F. Cui, J. Liu et al., A versatile Pt–Ce_6 nanoplatform as catalase nanozyme and NIR-II photothermal agent for enhanced PDT/PTT tumor therapy. Sci. China Mater. **64**, 510–530 (2021). https://doi.org/10.1007/s40843-020-1431-5
443. Y. Yang, D.-M. Zhu, Y. Liu, B. Jiang, W. Jiang et al., Platinum–carbon-integrated nanozymes for enhanced tumor photodynamic and photothermal therapy. Nanoscale **12**, 13548–13557 (2020). https://doi.org/10.1039/D0NR02800B
444. S. Farkona, E.P. Diamandis, I.M. Blasutig, Cancer immunotherapy: the beginning of the end of cancer? BMC Med. **14**(1), 73 (2016). https://doi.org/10.1186/s12916-016-0623-5
445. M. Hao, B. Chen, X. Zhao, N. Zhao, F.-J. Xu, Organic/inorganic nanocomposites for cancer immunotherapy. Mater. Chem. Front. **4**(9), 2571–2609 (2020). https://doi.org/10.1039/D0QM00323A

 https://doi.org/10.1007/s40820-021-00674-8

446. G. Yang, L. Xu, Y. Chao, J. Xu, X. Sun et al., Hollow MnO_2 as a tumor-microenvironment-responsive biodegradable nano-platform for combination therapy favoring antitumor immune responses. Nat. Commun. **8**(1), 902 (2017). https://doi.org/10.1038/s41467-017-01050-0

447. Y. Xia, L. Rao, H. Yao, Z. Wang, P. Ning et al., Engineering macrophages for cancer immunotherapy and drug delivery. Adv. Mater. **32**(40), 2002054 (2020). https://doi.org/10.1002/adma.202002054

448. M. Song, T. Liu, C. Shi, X. Zhang, X. Chen, bioconjugated manganese dioxide nanoparticles enhance chemotherapy response by priming tumor-associated macrophages toward M1-like phenotype and attenuating tumor hypoxia. ACS Nano **10**(1), 633–647 (2016). https://doi.org/10.1021/acsnano.5b06779

449. B. Xu, Y. Cui, W. Wang, S. Li, C. Lyu et al., Immunomodulation-enhanced nanozyme-based tumor catalytic therapy. Adv. Mater. **32**(33), 2003563 (2020). https://doi.org/10.1002/adma.202003563